COHERENT CONTROL OF OPTICAL PROCESSES IN A RESONANT MEDIUM

A Thesis

by

CHRISTOPHER MICHAEL O'BRIEN

Submitted to the Office of Graduate Studies of
Texas A&M University
in partial fulfillment of the requirements for the degree of

DOCTOR OF PHILOSOPHY

December 2011

Major Subject: Physics

COHERENT CONTROL OF OPTICAL PROCESSES IN A RESONANT MEDIUM

A Thesis

by

CHRISTOPHER MICHAEL O'BRIEN

Submitted to the Office of Graduate Studies of
Texas A&M University
in partial fulfillment of the requirements for the degree of

DOCTOR OF PHILOSOPHY

Approved by:

Chair of Committee,	Olga Kocharovskaya
Committee Members,	George R. Welch
	Philip Hemmer
	Alexi V. Sokolov
Head of Department,	Edward S. Fry

December 2011

Major Subject: Physics

ABSTRACT

Coherent Control of Optical Processes in a Resonant Medium. (December 2011)
Christopher Michael O'Brien, B.S., Texas A&M University
Chair of Advisory Committee: Dr. Olga Kocharovskaya

The resonant absorption, emission, and scattering of light are the fundamental optical processes that have been used both to probe matter and to manipulate light itself. In the last decade there has been essential progress in coherent control of both linear and nonlinear optical responses based on resonant excitation of atomic coherence in multilevel quantum systems. Some interesting and useful phenomena, resulting from coherent control of absorption and the group index, such as electromagnetically induced transparency, lasing without inversion, and ultra-slow group velocity of light have been widely studied. This work is focused on coherent control of refractive index and resonant fluorescence in multilevel medium.

We suggest two promising schemes for resonant enhancement of the refractive index with eliminated absorption and propose their implementation in transition element doped crystals with excited state absorption and in a cell of Rb atoms at natural abundance. We show how to use one of these schemes for spatial variation of the refractive index via its periodic resonant increase/decrease, remarkably keeping at the same time zero absorption/gain. It opens the way to production of transparent photonic structures (such as distributed Bragg reflectors, holey fibers, or photonic crystals) in a homogeneous resonant atomic media such as dielectrics with homogeneously distributed impurities, atomic, or molecular gases. These optically produced photonic structures could easily be controlled (including switching on/off, changing amplitude and period of modulation) and would be highly selective in frequency, naturally limited by the width of the optical resonance.

We also derive the optical fluorescence spectra of a three-level medium driven by two coherent fields at the adjacent transitions in a general case when all three transitions are allowed. We show that coherent driving can efficiently control the distribution of intensities between the fluorescent channels. In particular, the total intensity of fluorescence at the transition which is not driven by the optical fields may essentially exceed the fluorescence intensity at the driven transitions under the condition of two-photon resonance. This counter-intuitive effect is due to depletion of the intermediate state via atomic interference.

ACKNOWLEDGMENTS

For the inspiration and guidance they have supplied I would like to thank all of my collaborators, Petr Anisimov, Yuri Rostovtsev, Shaoyan Gao, and Alexey Kalachev. I would also like to acknowledge and thank my committee members Alexei Sokolov, George Welch, and Phil Hemmer for their support. As well as pledge my deep admiration for my advisor Olga Kocharovskaya who first developed my interest in Quantum Optics, and who's patience and dedication made this dissertation possible.

TABLE OF CONTENTS

Page

Page

LIST OF TABLES

LIST OF FIGURES

FIGURE Page

FIGURE Page

FIGURE Page

1. INTRODUCTION: STATE OF THE ART AND FORMULATION OF THE PROBLEMS

1.1 Optical coherence effects

The resonant absorption, emission and scattering of light are the fundamental processes that have been used both to probe matter and to manipulate light itself. In the last two decades there has been essential progress in coherent control of both linear and nonlinear optical responses based on resonant excitation of atomic coherence (the coherent superposition of atomic energy states) in multilevel quantum systems. Atomic coherence results in multiple interfering absorption paths for the radiation interacting with the resonant transitions. This interference greatly modifies both linear and nonlinear atomic responses leading to many interesting and useful phenomena such as electromagnetically induced transparency (EIT), lasing without inversion, slow and stored light, etc.

The simplest system in which these effects can be observed is a three-level lambda system, shown in Fig. 1.1, interacting with two laser fields (probe and control) in such a way that the laser driven transitions a$\leftrightarrow$b and a$\leftrightarrow$c are dipole allowed while the third transition c$\leftrightarrow$b, typically hyperfine or Zeeman, is dipole forbidden. When the decay rate of atomic coherence at the forbidden transition is slower than at the allowed transition the interference leads to dramatic modifications of the optical response of the system. In particular, absorption of a probe field tuned to the resonance with the a$\leftrightarrow$b transition can be canceled leading to an initially opaque medium being rendered transparent for the probe field. This phenomenon of EIT was theoretically predicted by Kocharovskaya [1] and experimentally discovered by Harris [2].

This thesis follows the style of *Physical Review A*.

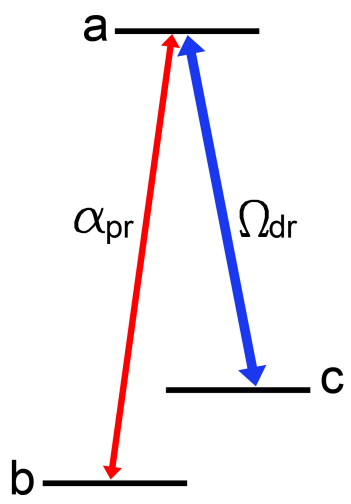

Fig. 1.1. Energy level diagram for the resonant lambda system.

Suppression of the resonant absorption also provides the possibility for lasing without inversion. Lasing without inversion (LWI) was predicted by Kocharovskaya [3], concurrently with Harris [4] and followed by a proposal of Scully [5]. If there is no absorption of the field and the medium becomes transparent even a small amount of population is incoherently pumped into the excited state can lead to laser action, population inversion is no longer needed. There have been several reviews of the subject [6–8], and it has been experimentally verified [9]. LWI could be used to construct lasers at the fast decaying transitions where it is difficult or impossible to produce population inversion such as X-ray transitions in atoms or a Gamma Ray transitions in nuclei [10].

EIT appears in a narrow range of frequency detunings from the two-photon resonance condition. A narrow transparency resonance is accompanied by sharp dispersion leading to the possibility of manipulating the group velocity of a light pulse propagating in the medium, i.e. to reduce it by many orders of magnitude [11] or even bring the pulse to a complete stop [12–14], or to imprint the the quantum

state carried by pulse photons into a superposition of long-lived spin states of atoms and to later retrieve it with (ideally) no losses [15, 16], thus realizing the first steps toward optically carried quantum information storage and processing and quantum computing. While most EIT experiments are done in gases, it has also been experimentally verified in solids, with one experiment showing EIT in room temperature Ruby [17]. The theory of EIT has also been extended to include the unavoidable inhomogeneous broadening experienced in solids both at the optical and low-frequency transition [18].

Both EIT and LWI are based on coherent control of resonant absorption, while slow light uses coherent control of the group index. This work is focused on the possibilities to control the refractive index near atomic resonance while eliminating resonant absorption. The goals are to realize a resonant enhancement of refractive index and its periodic spatial and/or temporal variation with eliminated resonant absorption. We are also interested in controlling resonant fluorescence by coherent optical driving of adjacent transitions in multilevel atomic systems.

Optically generated coherence can be used for the enhancement of refractive index. The idea to use a coherent preparation of a medium for elimination of resonant absorption as pioneered by Scully [19]. He proposed a scheme with a partially populated upper level and a initially prepared coherence between the ground state sublevels. The maximum refractive index in this system occurs at the frequency tuned between sublevels where absorption is compensated by inversionless gain. This work was generalized in [20], to include the density dependent near dipole-dipole interactions. Following this proposal a number of other three and four level schemes involving resonant driving at one or two atomic transitions and probing of the adjacent transition in which resonant enhancement of refractive index is accompanied by vanishing absorption were suggested [21]. $\chi \sim 1$ without absorption was expected in high density ($N\lambda^3 \approx 50$) alkali gas. One scheme, namely, the so called double dark resonance scheme allows for the elimination of the gain region though under a

rather exotic and narrow range of parameters [22]. A proof of principal experiment was done in Rb vapors, with a density of 10^{12} cm^{-3}, which showed resonance index enhancement with vanishing absorption, although the magnitude of index enhancement in this experiment was quite low, of an order of $\Delta n = 10^{-4}$ [23]. Unfortunately, refractive index enhancement with vanishing absorption was unavoidably accompanied by a region of gain in all of these schemes, which would lead to instability in the case of high index.

More recently, Yavuz suggested a interesting new scheme for coherent control and index enhancement. He considered a resonant four level system involving two Raman transitions optically pumped into the ground state and driven by two far off-resonant control fields forming two Λ systems with the same probe field [24]. The dispersive and absorption characteristics in such a system, as functions of two-photon detuning, essentially interchange so that the maximum resonant refractive index is accompanied by vanishing absorption. Similar to the previous proposals involving resonant driving the effect was attributed to interference and an index on the order of 10 for alkali vapor cells with densities (10^{17} cm^{-3}) was predicted. At the same time, similar to most earlier suggestions, gain appears at the frequencies in the vicinity of vanishing absorption.

The possibility to control the fluorescence properties of three level systems by coherent driving have been widely studied for the last two decades [25–29]. A number of interesting effects have been predicted and studied in resonant fluorescence spectra, such as as fluorescence inhibition [30, 31], line narrowing [28, 30, 32] and production of squeezed states [33, 34].

It has also been shown that the fluorescence of non-driven transitions can be modified in three level media [35] where the fluorescence intensity from the non-driven transition can be made larger than the fluorescence intensity of the driven transitions under special conditions. This occurs because the generated coherence

can block one photon fluorescence at the pumped transition while allowing absorption at the combinational frequency leading to a larger population in the un-driven level.

1.2 Application of controlling the index of refraction

Tightly focused laser radiation allows for the selective addressing of small regions of a medium. In microscopy, it is used to image tiny objects such as biological cells, organic molecules or NV centers in the dilute diamond. In lithography, it is used for production of miniature semiconductor integral circuits. In information processing, it is used to provide multiple parallel optical channels. For all of these applications, a key issue is the spatial resolution which is defined by the minimum spot size the laser radiation can be focused to. This focal spot size is fundamentally limited by the wavelength of light in the medium, λ, which depends on the refractive index n as following: $\lambda = \lambda_{\text{vac}}/n$. Thus, high refractive index (RI) is very important for achieving high spatial resolution in all of these applications. Materials with enhanced RI on demand would also be important for phase shifters, interferometers, and magnetic Faraday rotators. While those are examples of what can be done with large changes, even the use of optical control to provide small changes in the RI in a media may have many useful applications. For example a small shift in the RI for a specific frequency, say $\Delta n > 10^{-3}$ would be enough to allow for proper phase matching of non-linear processes such as parametric down conversion to create entangled pairs of single photons. Even a controllable small shift in the RI could be used in optical quantum memory schemes based on changing the RI [36].

Index of refraction characterizes the response of a medium to electromagnetic radiation and hence it is strongly enhanced near the atomic resonance. However, if a medium is in thermal equilibrium the enhancement of RI near the atomic resonance is accompanied by an enhancement of absorption. Such that, when the maximal contribution from the atomic resonance to the RI is reached, the contribution to the absorption is the same. As a result, a 2π phase shift and e-fold absorption take

place at the same distance in a medium, which prevents usage of the obtained RI in transmission experiments. In a inverted medium, high RI in the vicinity of the atomic resonance is accompanied by high gain. However, even higher gain is present at exact resonance which makes such a system unstable and again non-suitable for high index applications.

So far relatively high refractive indexes with vanishing absorption have been found mainly in far off-resonant solids, namely, well inside the energy band gaps of some semiconductors corresponding to IR range of frequency. The RI in these materials gets larger when the frequency approaches or exceeds the band gap however it is accompanied by strong absorption. Some high RI materials are listed in Table 1.1.

High refractive index need not be our only goal. The same process can be used to create lower RI. With a large decrease in the RI, indexes near zero may be possible. Near zero RI would imply that the wavelength fills the entire media which would be an interesting way to test collective effects in a media, since even a non-dense media would see a vast number of atoms inside of a cubic wavelength. Changing the sign of the electric index of refraction is also possible, when the magnetic index of refraction is also negative, this would lead to optical meta materials.

It is worth while to also point out that in all of the previous proposals the RI was uniform in space. None of those proposals was suitable for achieving spatial modulation of refractive index with zero absorption. Currently the periodic modulation of RI is achieved in combinational materials, namely, one, two, or three dimensional periodic heterostructure made of two dielectric materials with different refractive indexes, such as distributed Bragg reflectors (DBR), holey fibers, or photonic band gap crystals (PGB). Such structures find many applications, including reflective coatings, distributed feedback lasers, and optical cavities. Different technologies such as photo-lithography, etching, drilling, and self-assembling are used for construction of such structures. Our goal is to look for the schemes of coherent control which would allow for periodic modulation of RI with zero absorption. It can lead to production

Table 1.1
High refractive index materials

Material	λ (nm)	n	Band Gap (eV)
Ge	2000	4.10 [37]	0.66 [38]
Si	1000	3.57 [39]	1.12 [38]
Si	370	6.86-2.05i [39]	1.12 [38]
$Y_3Al_5O_{12}$	813	1.82 [40]	6.45 [41]
$Y_3Al_5O_{12}$	405	1.86 [42]	6.45 [41]
$Y_3Al_5O_{12}$	193	1.9 [43]	6.45 [41]
MgO	193	1.96 [43]	7.6 [43]
$MgAl_2O_4$	193	1.87 [43]	7.75 [43]

of transparent photonic structures in a homogeneous resonant atomic media such as dielectrics with homogeneously distributed impurities, atomic, or molecular gases simply by illuminating these materials with standing waves of a laser field. Such optically produced photonic structures could easily be optically controlled (including switching on/off, changing amplitude and period of modulation) and would be highly selective in frequency, naturally limited by the width of the optical resonance.

1.3 Using two Λ schemes for refractive index control

The simplest model of a medium is as a collection of two level atomic systems, where refractive index as characterized by the linear response is strongly enhanced near resonance. However, it is accompanied by either resonant absorption or gain preventing the use of high refractive index. A mixture of two two-level atomic species could provide overlapping absorption and gain if the difference in resonance frequencies is on the scale of the linewidth and one of the atomic species is inverted. A proper overlap could result in high refractive index with vanishing absorption for a weak field properly tuned between two atomic resonances. However the difficulties associated with the practical implementation of such a combined system (finding

proper species, providing for an even mixture, and providing population inversion for one species while avoiding spatial fluctuations of density and population exchange, etc.) would hardly be surmountable as discussed in [21].

Our idea [44] is to use coherent effects in a mixture of different species to induce strong and overlapping electromagnetic responses to provide high refractive index at vanishing absorption. This is done by implementing a separate far detuned lambda scheme in each species. As discussed in Section 2, each of these far detuned lambda schemes will then behave as an effective two level scheme. The superposition of these resonances in a medium then can lead to a optically controlled RI with no absorption or gain as discussed in Section 3. This double Λ scheme can then be implemented either in a gas containing two different isotopes of the same element or in a doped crystal where the dopant has two different isotopes or sits at two distinct crystal sites in the lattice.

1.4 Using excited state absorption for refractive index control

We suggest a second model for using the resonant feature for RI control that relies on excited state absorption (ESA) as a natural combination of two two-level transitions (one inverted and one non inverted) [45]. A ladder scheme with a populated intermediate level and closely matched transitions will have the two level absorption and two level gain we need. By applying a strong control field, coherent control can be used to modify the properties of either the upper absorption transition by implementing a far detuned Λ scheme, or the lower gain transition by implementing a far detuned V scheme. Either way we can control the properties of one of the transitions, such that the gain can be used to compensate the absorption so that we can make use of the resonant RI while maintaining vanishing absorption and no regions of gain as discussed in Section 4.

1.5 Refractive index in gases and solids

Previous experimental studies of RI enhancement in Rb gas [23, 46] have shown RI changes of $\Delta n < 10^{-4}$. Any hot gas has a maximum susceptibility that will be limited by the collisional broadening since as the density increases so does the linewidth implying a maximum change in the refractive index for most gases will be between .1 and 1, as we discuss in Section 3.

Potentially higher resonant refractive indexes could be obtained in solids (in particular, in rare-earth and/or transition metal ions doped dielectric crystals or stoichiometric crystals including such ions) [47]. A scheme for refractive index enhancement in rare earth doped crystals has been proposed [45].

Some of the benefits of solids are clear, there are much higher densities than in atomic vapor, and no collisional broadening. At the same time there are new challenges with solids where large inhomogeneous broadening and spatial density fluctuations can present new problems. Application of coherently driven multilevel schemes to solids were considered in a number of papers and very high indexes of an order of 10-100 were expected [48, 49]. However the same problem with instability due to the nearby gain regions was inherent to these proposals. Besides so far inhomogeneous broadening one of the main limiting factors for refractive index enhancements in solids has been ignored, leading to impossible claims.

We therefore suggest schemes for the control of RI that can be implemented either in gases and solids; with an example gas scheme given in Section 3, and an example crystal scheme given in Section 4.

1.6 Optically controllable photonic structures

We extend our scheme for RI control using ESA to give the possibility to modulate the refractive index in time or space. This can be accomplished by coherently controlling the upper absorption transition such that its amplitude, position, and linewidth

exactly match the lower gain transition. In which case the medium becomes completely transparent, but we show that if the populated energy level is modulated in space or time, say by another control field using the ac-Stark shift; that the RI is also modulated in space or time. This means for the first time photonic structures can be optically created in a homogeneous media.

It allows for optical modulation of refractive index while keeping transparency of the medium and suppressing the development of instabilities associated with the presence of gain. Combination of enhanced and reduced indexes in the neighboring regions of a medium would allow for high index contrast and for production of coherently controllable waveguides or distributed Bragg reflectors [50] as discussed in Section 5.

1.7 Controlling resonant fluorescence

Coherent control can also be used to manipulate the fluorescence of a media. Previously, coherent control of resonance fluorescence has been studied at transitions directly coupled to one of two applied fields. Fluorescence at the third transition that is not coupled directly to the fields has usually not been considered since these transitions in atoms are electro-dipole forbidden due to the selection rules. The situation may be different for example, in atomic gases when one of the three transitions is magneto-dipole allowed hyperfine or Zeeman transition driven by a radio frequency field or in molecular gases when the driven transition is chosen between different vibrational or rotational levels. All three transitions may be allowed between the energy levels of transition element ions doped into the dielectric crystals due to admixture of the crystal field, or between the dimensional quantization levels in asymmetric quantum wells. In these cases, studying the fluorescence at the transition not coupled to the fields could provide important spectroscopic information.

In Section 6 we derive and compare the fluorescence spectra from three-level atomic systems, with all three transitions allowed and coherently coupled with two

fields in the cascade and lambda configurations [51]. We show that the total fluorescence intensity at the transition which is not coupled to the fields (which we call for simplicity two-photon fluorescence though it is actually one-photon fluorescence at the combinational frequency) may essentially dominate each of the two one-photon (i.e. directly excited) channels. Which corresponds to a recently discovered counter-intuitive effect, called the "valve" effect, which was predicted and experimentally observed in scattering of Mössbauer gamma-ray radiation under the condition of resonant radio frequency, RF, driving of the split excited nuclear state [52, 53].

2. EFFECTIVE TWO LEVEL ATOM USING A FAR DETUNED LAMBDA SCHEME

2.1 Introduction

Our main tool for controlling the refractive index of a material will be using coherent control to produce effective two level responses from three level atoms with properties we can control. We can produce an effective two level atom by using coherent control, specifically using a far detuned lambda scheme as described in Fig. 2.1. The role of the far-detuned driving field is to shift the position of an upper level by the magnitude of one-photon detuning Δ making an effective two-level transition for the probe field close to one-photon resonance, under the condition of two-photon resonance. When the two-photon coherence lives much longer than the optical polarization the resonant response to the probe field at the effective two-level transition, produced by the driving field, may be as strong as in the case of a probe field resonant with the original transition in 3-level system even though the driving field may remain relatively weak; its Rabi frequency Ω does not exceed the one-photon detuning: $\Omega \ll \Delta$.

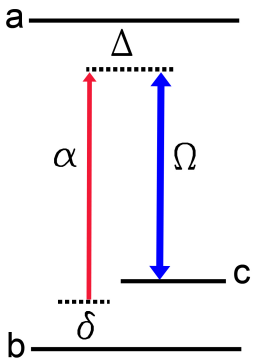

Fig. 2.1. A far detuned three-level Λ scheme as described in the text.

A simple physically intuitive picture is presented in the decaying dressed state basis which was developed by Anisimov [54]. In a typical dressed state picture, we take the density matrix Hamiltonian including only the strong field terms, ignoring the weaker probe field. Then perform a transformation that diagonalizes the Hamiltonian, which gives us the eigenvalues and eigenvectors that define the dressed states. The problem with this method is it does not consider the decoherence rate or population decay rates, which are integral to all coherence effects, since coherence between energy levels can not exist if all of the decoherence rates are too large. The decaying dressed state method takes a more practical approach, first you solve for the exact solution to the density matrix system, then for the transition of interest you expand the solution using partial fractions into the a series of Lorentzians. Each of these Lorentzian terms represents an effective transition, so putting them all together gives you a dressed state picture of the system that includes all of the decay terms. The decaying dressed state basis is a way to interpret the behavior of coherent systems that are exactly solvable. In the decaying dressed states basis the whole system can be represented as a series of effective two-level schemes with position, width, and amplitude of the resonances determined by the driving field. It allows for a simple, analytic, and intuitive understanding of the susceptibility for the total system. Thus a variety of absorption, amplification, and dispersion profiles may be engineered.

2.2 Three-level coherently driven system: density matrix formalism

We consider a three-level system with one excited state and two ground state sub-levels labeled $|\mathrm{a}\rangle$, $|\mathrm{b}\rangle$ and $|\mathrm{c}\rangle$, correspondingly (see Fig. 2.1). The system is driven by a coherent field with frequency ω_{dr} and Rabi frequency Ω, while being probed by a weak field with frequency ω_{pr} and Rabi frequency α. All-fields are far off-resonance with atomic transitions so that one-photon contributions are negligible, implying the driving field detuning $\Delta \gg \Omega$. The frequencies of the fields are chosen in such a way that they result in a two-photon transition in the three-level system

involving one photon from the probe field and one photon from the driving field. The three-level system is initially prepared in one of the two ground state sublevels via optical pumping. If the population is in state $|\mathrm{b}\rangle$ than the scheme exhibits two-photon absorption while if the population is in state $|\mathrm{c}\rangle$ then the scheme provides two-photon gain for the probe field.

The index of refraction and absorption coefficient can be found if the complex susceptibility is known. The complex susceptibility itself can be calculated if the optical coherence excited by a weak probe field is known.

In all of the cases that we wish to discuss we will assume population decay from the excited state will be to the ground states, so population is conserved in the system. Therefore the only way to properly treat such systems is to use the density matrix formalism. Thus we are using the density matrix formalism to calculate the optical coherence induced by a weak probe field applied to a$\leftrightarrow$b transition in a three-level system driven off-resonance by a field applied to an adjacent transition a$\leftrightarrow$c.

We begin with the master equation:

$$\dot{\hat{\rho}} = -\frac{i}{\hbar}\left[\hat{H}, \hat{\rho}\right] - \hat{\Gamma}, \tag{2.1}$$

where we define the density matrix as:

$$\hat{\rho} = \begin{pmatrix} \rho_{\mathrm{aa}} & \rho_{\mathrm{ab}} & \rho_{\mathrm{ac}} \\ \rho_{\mathrm{ba}} & \rho_{\mathrm{bb}} & \rho_{\mathrm{cb}} \\ \rho_{\mathrm{ca}} & \rho_{\mathrm{cb}} & \rho_{\mathrm{cc}} \end{pmatrix}; \tag{2.2}$$

the diagonal terms of the density matrix give the percentage of the atoms that are in that energy state, while the off diagonal terms define the strength of the coherence

between the energy levels. The Hamiltonian for our lambda scheme with applied electric fields $\mathrm{E_{dr}cos}\omega_{\mathrm{dr}}t$ and $\mathrm{E_{pr}cos}\omega_{\mathrm{pr}}t$ is defined by:

$$\hat{H} = \hbar \begin{pmatrix} \omega_{\mathrm{a}} & -2\alpha cos\omega_{\mathrm{pr}}t & -2\Omega cos\omega_{\mathrm{dr}}t \\ -2\alpha^{*} cos\omega_{\mathrm{pr}}t & \omega_{\mathrm{b}} & 0 \\ -2\Omega^{*} cos\omega_{\mathrm{dr}}t & 0 & \omega_{\mathrm{c}} \end{pmatrix}, \tag{2.3}$$

where in the Hamiltonian we have introduced the Rabi frequencies for the probe field α and the driving field Ω that are defined by the product of the dipole moment for the transition and the applied electric field as:

$$\alpha = \frac{d_{\mathrm{ab}}\mathrm{E_{pr}}}{2\hbar}, \tag{2.4}$$

$$\Omega = \frac{d_{\mathrm{ac}}\mathrm{E_{dr}}}{2\hbar}, \tag{2.5}$$

where d_{ij} is the dipole moment for transition i$\leftrightarrow$j. This formalism allows for phenomenologically including population decay rates $\gamma_{\mathrm{r}}^{\mathrm{ij}}$ from level i$\leftrightarrow$j, coherence decay rates γ_{ij} for transition i$\leftrightarrow$j, and incoherent pumping rates r_{ij} from level $|\mathrm{i}\rangle$ to $|\mathrm{j}\rangle$ by the subtraction of $\hat{\Gamma}$. The off diagonal terms are given by $\Gamma_{\mathrm{ij}} = \gamma_{ij}$ and the diagonal terms are given by:

$$\Gamma_{\mathrm{aa}} = \gamma_{\mathrm{r}}^{\mathrm{ac}}\rho_{\mathrm{aa}} + \gamma_{\mathrm{r}}^{\mathrm{ab}}\rho_{\mathrm{aa}} - r_{\mathrm{ba}}\rho_{\mathrm{bb}} - r_{\mathrm{ca}}\rho_{\mathrm{cc}}, \tag{2.6}$$

$$\Gamma_{\mathrm{bb}} = -\gamma_{\mathrm{r}}^{\mathrm{ab}}\rho_{\mathrm{aa}} - \gamma_{\mathrm{r}}^{\mathrm{cb}}\rho_{\mathrm{cc}} + r_{\mathrm{ba}}\rho_{\mathrm{bb}} + r_{\mathrm{cb}}\rho_{\mathrm{bb}}, \tag{2.7}$$

$$\Gamma_{\mathrm{cc}} = \gamma_{\mathrm{r}}^{\mathrm{cb}}\rho_{\mathrm{cc}} - \gamma_{\mathrm{r}}^{\mathrm{ab}}\rho_{\mathrm{aa}} + r_{\mathrm{ca}}\rho_{\mathrm{cc}}. \tag{2.8}$$

We can then write out the 9 equations given by Eq. (2.1), this can be reduced to five equations by noting that ρ_{ji} is equal to the Hermitian conjugate of ρ_{ij} and that population is conserved in the closed system, so we can always eliminate one of the

population equations by assuming $\rho_{\rm bb} = 1-\rho_{\rm aa}-\rho_{\rm cc}$. Therefore we have the following equations:

$$\begin{aligned}\dot{\rho}_{\rm aa} &= i\left(e^{i\omega_{\rm pr}t}+e^{-i\omega_{\rm pr}t}\right)\left(\alpha\rho_{\rm ba}-\alpha^*\rho_{\rm ab}\right)+i\left(e^{i\omega_{\rm dr}t}+e^{-i\omega_{\rm dr}t}\right)\left(\Omega\rho_{\rm ca}-\Omega^*\rho_{\rm ac}\right) \\ &\quad -\gamma_{\rm r}^{\rm ac}\rho_{\rm aa}-\gamma_{\rm r}^{\rm ab}\rho_{\rm aa}+r_{\rm ba}\rho_{\rm bb}+r_{\rm ca}\rho_{\rm cc},\end{aligned} \tag{2.9}$$

$$\dot{\rho}_{\rm cc} = i\left(e^{i\omega_{\rm dr}t}+e^{-i\omega_{\rm dr}t}\right)\left(\Omega\rho_{\rm ca}-\Omega^*\rho_{\rm ac}\right)-\gamma_{\rm r}^{\rm cb}\rho_{\rm cc}+\gamma_{\rm r}^{\rm ab}\rho_{\rm aa}-r_{\rm ca}\rho_{\rm cc}, \tag{2.10}$$

$$\begin{aligned}\dot{\rho}_{\rm ab} &= -i(\omega_{\rm a}-\omega_{\rm b})\rho_{\rm ab}-\gamma_{\rm ab}\rho_{\rm ab}-i\alpha\left(e^{i\omega_{\rm pr}t}+e^{-i\omega_{\rm pr}t}\right)\left(\rho_{\rm aa}-\rho_{\rm bb}\right) \\ &\quad +i\Omega\left(e^{i\omega_{\rm dr}t}+e^{-i\omega_{\rm dr}t}\right)\rho_{\rm cb},\end{aligned} \tag{2.11}$$

$$\begin{aligned}\dot{\rho}_{\rm ac} &= -i(\omega_{\rm a}-\omega_{\rm c})\rho_{\rm ac}-\gamma_{\rm ac}\rho_{\rm ac}+i\alpha\left(e^{i\omega_{\rm pr}t}+e^{-i\omega_{\rm pr}t}\right)\rho_{\rm cb} \\ &\quad -i\Omega\left(e^{i\omega_{\rm dr}t}+e^{-i\omega_{\rm dr}t}\right)\left(\rho_{\rm aa}-\rho_{\rm cc}\right),\end{aligned} \tag{2.12}$$

$$\begin{aligned}\dot{\rho}_{\rm cb} &= -i(\omega_{\rm c}-\omega_{\rm b})\rho_{\rm cb}-\gamma_{\rm cb}\rho_{\rm cb}-i\alpha\left(e^{i\omega_{\rm pr}t}+e^{-i\omega_{\rm pr}t}\right)\rho_{\rm ca} \\ &\quad +i\Omega^*\left(e^{i\omega_{\rm dr}t}+e^{-i\omega_{\rm dr}t}\right)\rho_{\rm ab}.\end{aligned} \tag{2.13}$$

Now were going to assume either continuous wave lasers or significantly long pulses such that the pulse duration $\tau_{\rm pulse} \gg 1/\gamma_{\rm ab}$. Therefore we can assume slowly varying wave packets such that the only significant temporal dependence of the coherences is the oscillation frequency of the field, so we can define the coherences as:

$$\rho_{\rm ab} = \sigma_{\rm ab}e^{-i\omega_{\rm pr}t}, \tag{2.14}$$

$$\rho_{\rm ac} = \sigma_{\rm ac}e^{-i\omega_{\rm dr}t}, \tag{2.15}$$

$$\rho_{\rm cb} = \sigma_{\rm cb}e^{-i(\omega_{\rm pr}-\omega_{\rm dr})t}, \tag{2.16}$$

where $\sigma_{\rm ij}$ is the slowly varying coherence amplitude for transition i$\leftrightarrow$j. Since we are considering optical fields all of our one photon detunings will still be much smaller than our transition frequencies therefore we use the rotating wave approximation i.e., we only keep the terms with frequency components that go like the difference in transition frequencies, neglecting the second components of each term whose frequency

dependence goes as the addition of transition frequencies. Substituting Eqs. (2.14-2.16) into Eqs. (2.9-2.13) we get the equations for the slowly varying terms:

$$\dot{\rho}_{aa} = i\left(\alpha\sigma_{ba} - \alpha^*\sigma_{ab}\right) + i\left(\Omega\sigma_{ca} - \Omega^*\sigma_{ac}\right) - \gamma_r^{ac}\rho_{aa} - \gamma_r^{ab}\rho_{aa} + r_{ba}\rho_{bb} + r_{ca}\rho_{cc}, \tag{2.17}$$

$$\dot{\rho}_{cc} = i\left(\Omega\sigma_{ca} - \Omega^*\sigma_{ac}\right) - \gamma_r^{cb}\rho_{cc} + \gamma_r^{ab}\rho_{aa} - r_{ca}\rho_{cc}, \tag{2.18}$$

$$\dot{\sigma}_{ab} = -i(\Delta + \delta)\sigma_{ab} - \gamma_{ab}\sigma_{ab} - i\alpha(\rho_{aa} - \rho_{bb}) + i\Omega\sigma_{cb}, \tag{2.19}$$

$$\dot{\sigma}_{ac} = -i\Delta\sigma_{ac} - \gamma_{ac}\sigma_{ac} + i\alpha\sigma_{cb} - i\Omega(\rho_{aa} - \rho_{cc}), \tag{2.20}$$

$$\dot{\sigma}_{cb} = -i\delta\sigma_{cb} - \gamma_{cb}\sigma_{cb} - i\alpha\sigma_{ca} + i\Omega^*\sigma_{ab}, \tag{2.21}$$

where the one photon detuning of the driving field is defined as $\Delta = \omega_{ac} - \omega_{dr}$ and the two photon detuning of the probe field is defined as $\delta = \omega_{ab} - \Delta - \omega_{pr}$; where $\omega_{ij} = \omega_i - \omega_j$.

For simplicity we assume fixed populations. Which implies either that the driving fields do not disturb an initial population distribution due to sufficiently short interaction time $t_{int}\Omega^2/\Delta \ll 1$ or sufficiently strong optical pumping through some additional levels (not indicated in the Fig. 2.1); or that we are in a steady state regime where the populations are fixed to a value, which can be solved for using a rate equations approach. Therefore we can take the population terms to be constant $\rho_{ii} = \sigma_{ii}$ for each energy level $|i\rangle$. We will also assume a relatively weak probe field i.e, $\alpha << \Omega, \gamma_{ab}$; therefore, we can neglect terms that are proportional to the square of the probe field in the expression. Finally, we assume the time derivative of all of the slowly varying coherence amplitudes can be neglected i.e., $\dot{\sigma}_{ij} = 0$ for all transitions

i↔j. Together these three assumptions give a system of three equations to solve for the coherence:

$$0 = (\Delta + \delta)\sigma_{ab} - i\gamma_{ab}\sigma_{ab} + \alpha(\sigma_{aa} - \sigma_{bb}) - \Omega\sigma_{cb}, \tag{2.22}$$

$$0 = \Delta\sigma_{ca} + i\gamma_{ca}\sigma_{ca} + \Omega^*(\sigma_{aa} - \sigma_{cc}), \tag{2.23}$$

$$0 = \delta\sigma_{cb} - i\gamma_{cb}\sigma_{cb} + \alpha\sigma_{ca} - \Omega^*\sigma_{ab}. \tag{2.24}$$

Which we can solve for the analytic expression for the a↔b coherence:

$$\sigma_{ab} = \frac{\alpha(\sigma_{bb} - \sigma_{aa})(\delta - i\gamma_{cb})}{(\Delta + \delta - i\gamma_{ab})(\delta - i\gamma_{cb}) - |\Omega|^2} + \frac{|\Omega|^2}{\Delta + i\gamma_{ac}} \frac{\alpha(\sigma_{aa} - \sigma_{cc})}{(\Delta + \delta - i\gamma_{ab})(\delta - i\gamma_{cb}) - |\Omega|^2}. \tag{2.25}$$

2.3 Electric susceptibility

The linear electric susceptibility is the proportionality constant between the average induced polarization and the applied electric field:

$$\vec{P} = \chi\epsilon_0\vec{E}, \tag{2.26}$$

where ϵ_0 is the permittivity of free space. We can then solve for the average induced polarization by finding the expectation value for the dipole moments:

$$\vec{P} = \mathrm{N} < \hat{d} >= \mathrm{N} \cdot \mathrm{Tr}(\hat{\rho}\hat{d}), \tag{2.27}$$

where N is the number of ions per unit volume which we will takes as having units ions/cm^3. The dipole matrix $\hat{d}$ has non zero elements only for electro-dipole allowed transitions and for non-zero elements, it has the value of the dipole moment for the transition. In the case of our far detuned lambda scheme we take a↔b and a↔c to

be dipole allowed and transition c↔b to not be dipole allowed; we can then take the dipole matrix to be:

$$\hat{d} = \begin{Bmatrix} 0 & \vec{d}_{\rm ab} & \vec{d}_{\rm ac} \\ \vec{d}_{\rm ba} & 0 & 0 \\ \vec{d}_{\rm ca} & 0 & 0 \end{Bmatrix} \tag{2.28}$$

Then we can take the trace:

$$\begin{aligned} {\rm Tr}(\hat{\rho}\hat{d}) &= \vec{d}_{\rm ab}\rho_{\rm ba} + \vec{d}_{\rm ac}\rho_{\rm ca} + \vec{d}_{\rm ba}\rho_{\rm ab} + \vec{d}_{\rm ca}\rho_{\rm ac} \\ &= \vec{d}_{\rm ab}\sigma_{\rm ba}e^{i\omega_{\rm pr}t} + \vec{d}_{\rm ac}\sigma_{\rm ca}e^{i\omega_{\rm dr}t} + \vec{d}_{\rm ba}\sigma_{\rm ab}e^{-i\omega_{\rm pr}t} + \vec{d}_{\rm ca}\sigma_{\rm ac}e^{-i\omega_{\rm dr}t} \\ &= 2\vec{d}_{\rm ba}\sigma_{\rm ab}cos\omega_{\rm pr}t + 2\vec{d}_{\rm ca}\sigma_{\rm ac}cos\omega_{\rm dr}t, \end{aligned} \tag{2.29}$$

where the second line comes from Eq. (2.14) and Eq. (2.15); the third line of Eq. (2.29) is due to $\sigma_{\rm ij} = \sigma^*_{\rm ji}$, $d_{\rm ij} = d^*_{\rm ji}$ and the need for the expectation value of the trace to be real. Since were looking for the susceptibility of the probe field when $\omega_{\rm pr}$ and $\omega_{\rm dr}$ are different we can neglect the contribution from the c↔b transition. Therefore the probe field susceptibility is given by:

$$\chi = \frac{2Nd_{\rm ba}\sigma_{\rm ab}}{\epsilon_0 {\rm E}_{\rm pr}}, \tag{2.30}$$

where the vector signs have been removed because we assume the induced dipole is in the same direction as the applied field and the time dependence of both cancels out. We can then use Eq. (2.4) to put the susceptibility in the same terms as our coherence expression:

$$\chi = \frac{N\epsilon_0|d_{ab}|^2}{\hbar}\frac{\sigma_{ab}}{\alpha}. \tag{2.31}$$

We can then make Eq. (2.33) a more straight forward expression by using the definition for the Einstein coefficient for two level spontaneous emission:

$$\gamma_{\rm r}^{\rm ab} = \frac{2|d_{ab}|^2(2\pi)^2}{3\epsilon_0\hbar\lambda_{\rm pr}^3}. \tag{2.32}$$

Therefore we get the expression for χ in terms of the solution of the Bloch equations that we will be using throughout this work,

$$\chi = \frac{3}{8\pi^2} N \lambda_{\rm pr}^3 \gamma_{\rm r}^{\rm ab} \frac{\sigma_{\rm ab}}{\alpha}; \tag{2.33}$$

where in this equation $\gamma_{\rm r}^{\rm ab}$ is the radiative decay rate of the probed transition, N is the density of atoms, $\lambda_{\rm pr}$ is the wavelength of the probe, $\sigma_{\rm ab}$ is the coherence of the probed transition given by Eq. (2.25), and α is the Rabi frequency of the probe field. Using Eq. (2.25) in Eq. (2.33) we have the resonant susceptibility of the three level far detuned lambda system:

$$\chi = \frac{3N\lambda_{\rm pr}^3\gamma_{\rm r}^{\rm ab}}{8\pi^2}\{\frac{(\sigma_{\rm bb}-\sigma_{\rm aa})(\delta - i\gamma_{\rm cb})}{(\Delta+\delta-i\gamma_{\rm ab})(\delta-i\gamma_{\rm cb})-|\Omega|^2} + \frac{|\Omega|^2}{\Delta+i\gamma_{\rm ac}}\frac{(\sigma_{\rm aa}-\sigma_{\rm cc})}{(\Delta+\delta-i\gamma_{\rm ab})(\delta-i\gamma_{\rm cb})-|\Omega|^2}\}. \tag{2.34}$$

2.4 Optical field propagation

The complex susceptibility given by Eq. (2.34) represents the response of the system to an applied field. This response then gives the induced polarization which acts as a source for Maxwell's equations:

$$\vec{\bigtriangledown}\cdot\vec{D} = \rho_f, \tag{2.35}$$

$$\vec{\bigtriangledown}\cdot\vec{B} = 0, \tag{2.36}$$

$$\vec{\bigtriangledown}\times\vec{E} = -\frac{\delta\vec{B}}{\delta t}, \tag{2.37}$$

$$\vec{\bigtriangledown}\times\vec{H} = \vec{J}_f + \frac{\delta\vec{D}}{\delta t}. \tag{2.38}$$

In this work we will assume that the free current $\vec{J}_f$ and the free charge ρ_f are both zero. $\vec{B}$ and $\vec{E}$ are the magnetic and electric fields. The electric displacement field $\vec{D}$ is given by the electric field and the polarization:

$$\vec{D} = \epsilon_0 \vec{E} + \vec{P} = \epsilon_0 (1 + \chi + \chi_{\text{bg}}) \vec{E}. \tag{2.39}$$

Here χ is the resonant susceptibility of the medium given by Eq. (2.34) while χ_{bg} is the susceptibility due to the host medium so for gases $\chi_{\text{bg}} = 0$ and for crystals $\chi_{\text{bg}} > 0$. In fact we can define a background refractive index, for when there is no resonance present by $n_{\text{bg}} = \sqrt{1 + \chi_{\text{bg}}}$, which for simplicity we will assume is real. We will also assume that our medium does not support magnetization, therefore the magnetizing field $\vec{H} = \vec{B}/\mu_0$. Using Maxwell's equations we can derive a wave equation for the electric field, by taking the curl of Eq. (2.37) and some convenient vector identities:

$$\vec{\bigtriangledown} \times (\vec{\bigtriangledown} \times \vec{E}) = \vec{\bigtriangledown}(\vec{\bigtriangledown} \cdot \vec{E}) - \bigtriangledown^2 \vec{E} = \vec{\bigtriangledown} \times (-\frac{\delta \vec{B}}{\delta t}) = -\mu_0 \frac{\delta}{\delta t} (\vec{\bigtriangledown} \times \vec{H}). \tag{2.40}$$

Now we can substitute in Eq. (2.38):

$$\vec{\bigtriangledown}(\vec{\bigtriangledown} \cdot \vec{E}) - \bigtriangledown^2 \vec{E} = -\mu_0 \frac{\delta^2 \vec{D}}{\delta t^2} = -\mu_0 \frac{\delta^2}{\delta t^2} (n_{\text{bg}}^2 + \chi) \vec{E}. \tag{2.41}$$

When the susceptibility is spatially uniform in the medium then $\vec{\bigtriangledown} \cdot \vec{E} = 0$, giving the wave equation:

$$\bigtriangledown^2 - \frac{1}{c^2} \frac{\delta^2}{\delta t^2} (n_{\text{bg}}^2 + \chi) \vec{E} = 0. \tag{2.42}$$

In Section 5 we will be creating a susceptibility that is modulated in space such that χ is a function of z. In this case we can not dismiss $\vec{\bigtriangledown} \cdot \vec{E}$, instead we need to start from Eq. (2.35):

$$\vec{\bigtriangledown} \cdot (n_{\mathrm{bg}}^2 + \chi(\mathrm{z}))\vec{E} = 0, \tag{2.43}$$

$$\vec{\bigtriangledown} \cdot \vec{E} = -\frac{1}{n_{\mathrm{bg}}^2}\vec{\bigtriangledown} \cdot (\chi(\mathrm{z})\vec{E}) = -\frac{1}{n_{\mathrm{bg}}^2}\left(\chi(\mathrm{z})\vec{\bigtriangledown} \cdot \vec{E} + \vec{E} \cdot \vec{\bigtriangledown}\chi\right), \tag{2.44}$$

$$\vec{\bigtriangledown} \cdot \vec{E} = -\frac{\vec{E} \cdot \vec{\bigtriangledown}\chi}{n_{\mathrm{bg}}^2 + \chi}. \tag{2.45}$$

We take the electric field to be a plane wave:

$$\vec{E} = \hat{\mathrm{z}}\mathrm{E}_{\mathrm{pr}}(\mathrm{z}) \cos \omega_{\mathrm{pr}} t, \tag{2.46}$$

where $\hat{\mathrm{z}}$ is a unit vector in the z-direction; then since the susceptibility only varies in the z-direction we have:

$$\begin{aligned} -\vec{\bigtriangledown}(\vec{\bigtriangledown} \cdot \vec{E}) &= \hat{\mathrm{z}}\frac{\delta}{\delta}\left[\frac{\vec{E} \cdot \vec{\bigtriangledown}\chi}{n_{\mathrm{bg}^2+\chi}}\right] \\ &= \frac{\hat{\mathrm{z}}}{n_{\mathrm{bg}}^2 + \chi}\left[\frac{\delta \mathrm{E}_{\mathrm{pr}}(\mathrm{z})}{\delta \mathrm{z}}\frac{\delta\chi}{\delta \mathrm{z}} + \mathrm{E}_{\mathrm{pr}}(\mathrm{z})\frac{\delta^2\chi}{\delta \mathrm{z}^2} - \frac{\mathrm{E}_{\mathrm{pr}}(\mathrm{z})}{n_{\mathrm{bg}}^2 + \chi}\left(\frac{\delta\chi}{\delta \mathrm{z}}\right)^2\right] \end{aligned} \tag{2.47}$$

Each of the terms in Eq. (2.47) needs to be compared to $(\omega_{\mathrm{pr}}/c)^2$. Which shows that for small modulations of refractive index, this term can be neglected; say we have a 10% modulation of the RI over a single wavelength as does the electric field then the first of these terms goes as:

$$\frac{1}{n_{\mathrm{bg}}^2}\left(\frac{\delta E}{\delta \mathrm{z}}\right)\left(\frac{\delta\chi}{\delta \mathrm{z}}\right) \simeq \frac{1}{n_{\mathrm{bg}}\lambda_{\mathrm{pr}}^2}\left(\frac{\Delta n}{n_{\mathrm{bg}}}\right) \simeq \frac{.1}{n_{\mathrm{bg}}\lambda_{\mathrm{pr}}^2} \ll \frac{\omega_{\mathrm{pr}}^2}{c^2} = \left(\frac{2\pi}{\lambda_{\mathrm{pr}}}\right)^2, \tag{2.48}$$

is about three orders of magnitude smaller. The second term gives:

$$\frac{1}{n_{\rm bg}^2}\left(\frac{\delta^2\chi}{\delta {\rm z}^2}\right) \simeq \frac{1}{n_{\rm bg}\lambda_{\rm pr}^2}\left(\frac{\Delta n}{n_{\rm bg}}\right) \simeq \frac{.1}{n_{\rm bg}\lambda_{\rm pr}^2} \ll \frac{\omega_{\rm pr}^2}{c^2} = \left(\frac{2\pi}{\lambda_{\rm pr}}\right)^2, \tag{2.49}$$

again about three orders of magnitude smaller. The last of these terms goes as:

$$\frac{1}{n_{\rm bg}^4}\left(\frac{\delta\chi}{\delta {\rm z}}\right)^2 \simeq \frac{1}{\lambda_{\rm pr}^2}\left(\frac{\Delta n}{n_{\rm bg}}\right)^2 \simeq \frac{.01}{n_{\rm bg}^2\lambda_{\rm pr}} \ll \frac{\omega_{\rm pr}^2}{c^2} = \left(\frac{2\pi}{\lambda_{\rm pr}}\right)^2, \tag{2.50}$$

is 4 orders of magnitude smaller. Therefore there are 3 orders of magnitude difference between the $\vec{\bigtriangledown}\cdot\vec{E}$ term and the other terms in the equation, so it can safely be neglected. Although for modulations over very small spacial periods the term given by Eq. (2.49) may bear consideration.

By assuming that $n_{\rm bg}$ is constant over the frequencies of interest and that the complex susceptibility $\chi = \chi' - i\chi''$, only slowly varies in time we can simplify Eq. (2.42):

$$\left[\frac{\delta^2}{\delta {\rm z}^2} + \frac{\omega_{\rm pr}^2}{c^2}(n_{\rm bg}^2 + \chi' - i\chi'')\right] {\rm E_{pr}(z)} = 0 \tag{2.51}$$

Now if we note that $\omega_{\rm pr} = 2\pi/\lambda_{\rm pr}$, the solution of the wave equation is given by:

$${\rm E_{pr}(z)} = {\rm E_{pr}} e^{-i\frac{2\pi\sqrt{n_{\rm bg}^2+\chi'}}{\lambda_{\rm pr}}\sqrt{1-i\frac{\chi''}{n_{\rm bg}^2+\chi'}}{\rm z}}. \tag{2.52}$$

In this work we will always be dealing with situations when $\chi'' \ll n_{\rm bg}^2 + \chi'$ so the square root can be replaced with the first terms of its Taylor series:

$$\sqrt{1 - i\frac{\chi''}{n_{\rm bg}^2+\chi'}} = 1 - \frac{i}{2}\frac{\chi''}{n_{\rm bg}^2+\chi'} = 1 - \frac{i\chi''}{2n^2}, \tag{2.53}$$

where we have defined the RI as $n = \sqrt{n_{\rm bg}^2 + \chi'}$. Now the solution to the wave equation is given by:

$${\rm E_{pr}(z)} = {\rm E_{pr}} e^{\frac{-2\pi i n}{\lambda_{\rm pr}}{\rm z}} e^{-\frac{\pi\chi''}{\lambda_{\rm pr} n}{\rm z}}. \tag{2.54}$$

Now we can clearly identify in Eq. (2.54) that imaginary part of the susceptibility causes the field to either experience absorption or gain in the medium depending on the sign of χ''. The term is exponential such that e-fold absorption happens to the applied field in a distance of $n\chi''\lambda_{\rm pr}/\pi$ inside the media. While the real part of the susceptibility χ' modifies the refractive index which gives the amount of phase shift of the field as it propagates through the media.

2.5 Local field effects

So far we have implied that the electric field given by Maxwell's equations and that used for the optical Bloch equations is the same. This neglects near dipole-dipole effects (NDD) that appear in dense media [55]. In fact this is inconsistent because the optical Bloch equations are equations for the atom that experiences the local electric field, while Maxwell's equations and the wave equation we derived in the previous section are for the macroscopic field. Therefore in the Bloch equations given by Eqs. (2.24-2.25), assuming a isotropic homogeneous material we should use the microscopic local field given by the Lorentz-Lorenz relation [56]:

$$\mathrm{E_L} = \mathrm{E} + \frac{1}{3\epsilon_0}\mathrm{P}. \tag{2.55}$$

Since this implies that the polarization, which we use the optical Bloch equations to solve for, then goes into these equations, to find the susceptibility we now need to solve the coupled Maxwell-Bloch equations as a self consistent set of equations. This can lead to many interesting effects, primarily an enhancement in the susceptibility. In the lasing without inversion approach to refractive index enhancement in gas pioneered by Scully [19] there has been studies showing that the refractive index enhancement will be increased by the local field effects [55, 57].

We studied this effect for our resonant enhancement of RI scheme in both gases and solids by numerically solving the self-consistent equations. We find that when

the resonant susceptibility is much smaller than the background refractive index $\chi \ll n_{\rm bg}^2$ that the only non-negligible effect due to the local fields is to increase the susceptibility by the local field correction factor:

$$l = \frac{n_{\rm bg}^2 + 2}{3}; \tag{2.56}$$

therefore, for gases this term can be neglected while for the solid systems that we will consider in Sections 4 and 5 it can be quite significant. Of course when the enhanced susceptibilities approach 1, there can be more interesting effects but we will not consider those in this work.

There are two other considerations due to NDD effects that may be considered. For one there is a frequency shift of the lines called the Lorentz local-field shift [58]. This will give an excitation dependent shift in the detunings, but since in most cases it will be quite small; and frequency shifts do not have an overall effect on theory, so we will neglect it in this work. In solids there will also be an enhancement effect on the control field Rabi frequencies, though it would be disingenuous to claim this decreases the control field intensities needed to reach a given Rabi frequency, since the Eswald-Oseen extinction theorem implies that the field entering the crystal will lose intensity while passing through the vacuum and dielectric interface also by a factor l [59, 60].

2.6 Effect of inhomogeneous broadening

We derived the expression for the susceptibility Eq. (2.34) under the assumption of homogeneous broadening, when values of the Rabi frequency Ω and one-photon detuning Δ are well defined by intensity and frequency of the driving field. In the case of inhomogeneous broadening of the probed transition the frequency of the driving field defines only the mean value of one-photon detuning Δ_0 while variance is defined by inhomogeneous broadening. Namely, $\Delta = \Delta_0 + \Delta_{\rm inh}$ with $\langle \Delta_{\rm inh}^2 \rangle - \langle \Delta_{\rm inh} \rangle^2 =$

$\left(\gamma_{\rm ab}^{\rm inh}\right)^2$, where $\langle\cdots\rangle$ is averaging over the inhomogeneous profile. For the case of inhomogeneous broadening of the c↔b transition we only have a mean value of the two photon detuning δ_0 while the varying detuning is given by $\delta = \delta_0 + \delta_{\rm inh}$ with $\langle\delta_{\rm inh}^2\rangle - \langle\delta_{\rm inh}\rangle^2 = \left(\gamma_{\rm cb}^{\rm inh}\right)^2$. Therefore, the two-photon transition probability, frequency, and width are also not well defined. For coherence effects in resonant lambda systems such as EIT, it was shown [18] that inhomogeneous broadening can cause a significant change in the theory derived for homogeneous broadening. Therefore it is important to consider, but we demonstrate for our case of a far detuned scheme, inhomogeneous broadened systems will behave similarly to homogeneously broadened systems.

The inhomogeneous profile in both solids and gases will be Gaussian, but in order to easily deal with the analytic expressions we will approximate with a Lorentzian profile. If we start with the coherence given by Eq. (3.2) or Eq. (3.3), we can integrate over the Lorentzian distributions of the one and two photon detunings:

$$\sigma_{\rm ab}^{\rm inh} = \int_{-\infty}^{\infty} d\Delta_{\rm inh} \frac{\gamma_{\rm ab}^{\rm inh}/\pi}{\Delta_{\rm inh}^2 + (\gamma_{\rm ab}^{\rm inh})^2} \int_{-\infty}^{\infty} d\delta_{\rm inh} \frac{\gamma_{\rm cb}^{\rm inh}/\pi}{\delta_{\rm inh}^2 + (\gamma_{\rm cb}^{\rm inh})^2} \sigma_{\rm ab}(\Delta_{\rm inh}, \delta_{\rm inh}). \qquad (2.57)$$

In the limit, $\Delta_0 > \gamma_{\rm ab}, \gamma_{\rm cb}, \Omega$; these integrals can be solved analytically which shows that the inhomogeneous profile can be taken into consideration in all the equations we derive simply by replacing the homogeneous linewidths with the total linewidth that includes the inhomogeneous broadening i.e., $\gamma_{\rm ab} \to \gamma_{\rm ab} + \gamma_{\rm ab}^{\rm inh} + \gamma_{\rm cb}^{\rm inh}$ and $\gamma_{\rm cb} \to \gamma_{\rm cb} + \gamma_{\rm cb}^{\rm inh}$. Except we also have to replace $\gamma_{\rm ac} \to \gamma_{\rm ac} - \gamma_{\rm ab}^{\rm inh}$. It is important to keep in mind this is not a change in the linewidth of the a↔c transition, just in how the decoherence of this transition comes into Eq. (2.34). One can see that the quantity that matters is the total linewidth.

Numerical treatments of inhomogeneous broadening for the far detuned lambda scheme also confirm that by including the total linewidth into the homogeneously broadened theory, we retrieve the correct amplitude, linewidth, and position of the two photon feature. Of course a numerical treatment shows that the lineshape will be distorted from the theory for cases with inhomogeneous broadening on the same order

or larger as the homogeneous since the inhomogeneous broadening has a Gaussian shape.

2.7 Dressed-state analysis: an effective two-level system

The susceptibility in a Λ-configuration is inversely proportional to a quadratic polynomial in terms of the two-photon detuning δ, see Eq. (2.25). Zeros of this polynomial correspond to the two resonant contributions to the optical coherence as it has been previously discussed [54]. The two zeros of the denominator are given by:

$$\delta_{\pm} = -\frac{\Delta}{2} + \frac{i}{2}(\gamma_{\rm ab} + \gamma_{\rm cb}) \pm \frac{\Delta}{2}\sqrt{1 - \frac{2i(\gamma_{\rm ab} - \gamma_{\rm cb})}{\Delta} - \frac{(\gamma_{\rm ab} - \gamma_{\rm cb})^2}{\Delta^2} + \frac{4\Omega^2}{\Delta^2}}. \quad (2.58)$$

Since were assuming $\Delta \gg \Omega, \gamma_{\rm ij}$; we can then approximate the square root by its Taylor series. Defining the small parameter as x:

$$x = \frac{2i(\gamma_{\rm ab} - \gamma_{\rm cb})}{\Delta} + \frac{(\gamma_{\rm ab} - \gamma_{\rm cb})^2}{\Delta^2} - \frac{4|\Omega|^2}{\Delta^2}, \quad (2.59)$$

the square root becomes:

$$\begin{aligned}\sqrt{1-x} = 1 - \frac{1}{2}x - \frac{1}{8}x^2 - \frac{1}{16}x^3 - \frac{5}{128}x^4 - \frac{7}{256}x^5 - \frac{21}{1024}x^6 \\ - \frac{33}{2048}x^7 - \frac{429}{32768}x^8 - \frac{715}{65536}x^9 - \frac{2431}{262144}x^{10} + \ldots .\end{aligned} \quad (2.60)$$

The reason we keep so many terms is to keep the final expression as exact as possible, we can later simplify. Let us define two expressions to simplify x:

$$\xi = \frac{|\Omega|^2}{\Delta^2}, \quad (2.61)$$

$$g = \frac{\gamma_{\rm ab} - \gamma_{\rm cb}}{\Delta}. \quad (2.62)$$

Therefore x is then given by:

$$x = 2ig + g^2 - 4\xi. \tag{2.63}$$

Only keeping terms in the series that go up to ξ^6 and droping terms that go as g^2 gives us:

$$\begin{aligned}\sqrt{1-x} \simeq 1 - ig(1 - 2\xi + 6\xi^2 - 20\xi^3 + 70\xi^4 - 252\xi^5 + 924\xi^6 + \dots) \\ + 2\xi(1 - \xi + 2\xi^2 - 5\xi^3 + 14\xi^4 - 42\xi^5 + \dots).\end{aligned} \tag{2.64}$$

Therefore we can express the two poles as:

$$\delta_+ = \frac{|\Omega|^2}{\Delta}(1 - \xi\Delta^*) + i\gamma_{\rm cb}(1 - \xi\gamma^*) + i\gamma_{\rm ab}\xi\gamma^*, \tag{2.65}$$

$$\delta_- = -\Delta - \frac{|\Omega|^2}{\Delta}(1 - \xi\Delta^*) + i\gamma_{\rm ab}(1 - \xi\gamma^*) + i\gamma_{\rm cb}\xi\gamma^*; \tag{2.66}$$

where in the gas case $\Delta^* = \gamma^* = 1$, we now have different expressions for the two defined as:

$$\gamma^* = \left(1 - 3\xi + 10\xi^2 - 35\xi^3 + 126\xi^4 - 462\xi^5 + \dots\right), \tag{2.67}$$

$$\Delta^* = \left(1 - 2\xi + 5\xi^2 - 14\xi^3 + 42\xi^4 + \dots\right). \tag{2.68}$$

To get higher accuracy all we have to do is to keep expanding the series for γ^* and Δ^* to higher multiples of ξ, so all the expressions remain correct as long as these are calculated to the accuracy needed. Each of these poles correspond to a Lorentzian

response which can be found using using partial fractions. The amplitude of each Lorentzian is given by the original amplitude as a function of the poles:

$$A_+ = \frac{A(\delta_+)}{\delta_+ - \delta_-}, \tag{2.69}$$

$$A_- = \frac{-A(\delta_-)}{\delta_+ - \delta_-}, \tag{2.70}$$

with:

$$\delta_+ - \delta_- = \Delta\left[1 + 2\xi(1 - \xi\Delta^*) - ig(1 - 2\xi\gamma^*)\right]. \tag{2.71}$$

To simplify the analysis from here we will break Eq. (2.34) into its two terms $\chi = \chi_1 + \chi_2$ where term 1 is due to the population difference for transition a$\leftrightarrow$b and term 2 is due to the population difference for transition a$\leftrightarrow$c:

$$\chi_1 = \frac{3N\lambda_{\mathrm{pr}}^3\gamma_{\mathrm{r}}^{\mathrm{ab}}}{8\pi^2}\frac{(\sigma_{\mathrm{bb}} - \sigma_{\mathrm{aa}})(\delta - i\gamma_{\mathrm{ab}})}{(\Delta + \delta - i\gamma_{\mathrm{ab}})(\delta - i\gamma_{\mathrm{ab}}) - |\Omega|^2}, \tag{2.72}$$

$$\chi_2 = \frac{3N\lambda_{\mathrm{pr}}^3\gamma_{\mathrm{r}}^{\mathrm{ab}}}{8\pi^2}\frac{|\Omega|^2}{\Delta + i\gamma_{\mathrm{ac}}}\frac{(\sigma_{\mathrm{aa}} - \sigma_{\mathrm{cc}})}{(\Delta + \delta - i\gamma_{\mathrm{ab}})(\delta - i\gamma_{\mathrm{ab}}) - |\Omega|^2}. \tag{2.73}$$

Each of these two susceptibilities can then be expressed as two Lorentzians each due to one of the poles of the denominator. In this dressed state basis one term is due to the original probed transition which we will label the one photon term (1ph) and the other is due to the two photon resonance (2ph) from b$\leftrightarrow$c so each term i $\in \{1, 2\}$ will go as:

$$\chi_{\mathrm{i}} = \frac{\mathrm{A}_{\mathrm{i}}^{\mathrm{1ph}}}{\delta - \delta_{\mathrm{i}}^{\mathrm{1ph}} - i\gamma_{\mathrm{i}}^{\mathrm{1ph}}} + \frac{\mathrm{A}_{\mathrm{i}}^{\mathrm{2ph}}}{\delta - \delta_{\mathrm{i}}^{\mathrm{2ph}} - i\gamma_{\mathrm{i}}^{\mathrm{2ph}}}; \tag{2.74}$$

where the 2 photon expression comes from δ_+ and the one photon feature from δ_-. Therefore, $\gamma_{\mathrm{i}}^{\mathrm{1ph}}$ is given by the imaginary part of Eq. (2.66) and $\delta_{\mathrm{i}}^{\mathrm{1ph}}$ is given by the

real part of Eq. (2.66). While $\gamma_{\rm i}^{\rm 2ph}$ and $\delta_{\rm i}^{\rm 2ph}$ are derived similarly from Eq. (2.65). Therefore we have:

$$\delta_{\rm i}^{\rm 1ph} = -\Delta - \frac{|\Omega|^2}{\Delta}(1-\xi\Delta^*) \tag{2.75}$$

$$\gamma_{\rm i}^{\rm 1ph} = \gamma_{ab}(1-\xi\gamma^*) + \gamma_{cb}\xi\gamma^* \tag{2.76}$$

$$\delta_{\rm i}^{\rm 2ph} = -\Delta - \frac{|\Omega|^2}{\Delta}(1-\xi\Delta^*) \tag{2.77}$$

$$\gamma_{\rm i}^{\rm 2ph} = \gamma_{ab}(1-\xi\gamma^*) + \gamma_{cb}\xi\gamma^* \tag{2.78}$$

For the amplitudes we have to use the numerator of $\chi_{\rm i}$ as A in Eq. (2.70) to solve for $\rm A_i^{1ph}$ and in Eq. (2.69) to find $\rm A_i^{2ph}$.

$$A_1^{\rm 2ph} = \frac{3N\lambda_{\rm pr}^3\gamma_{\rm r}^{\rm ab}}{8\pi^2}\frac{\xi(\sigma_{\rm bb}-\sigma_{\rm aa})(1-\xi\Delta^*+ig\xi\gamma^*)}{1+2\xi(1-\xi\Delta^*)-ig(1-2\xi\gamma^*)}, \tag{2.79}$$

$$A_1^{\rm 1ph} = \frac{3N\lambda_{\rm pr}^3\gamma_{\rm r}^{\rm ab}}{8\pi^2}\frac{(\sigma_{\rm bb}-\sigma_{\rm aa})(1+\xi-\xi^2\Delta^*-ig(1-\xi\gamma^*)}{1+2\xi(1-\xi\Delta^*)-ig(1-2\xi\gamma^*)}, \tag{2.80}$$

$$A_2^{\rm 2ph} = \frac{3N\lambda_{\rm pr}^3\gamma_{\rm r}^{\rm ab}}{8\pi^2}\frac{1}{1+i\gamma_{\rm ac}/\Delta}\frac{-\xi(\sigma_{\rm aa}-\sigma_{\rm cc})}{1+2\xi(1-\xi\Delta^*)-ig(1-2\xi\gamma^*)}, \tag{2.81}$$

$$A_2^{\rm 1ph} = \frac{3N\lambda_{\rm pr}^3\gamma_{\rm r}^{\rm ab}}{8\pi^2}\frac{1}{1+i\gamma_{\rm ac}/\Delta}\frac{\xi(\sigma_{\rm aa}-\sigma_{\rm cc})}{1+2\xi(1-\xi\Delta^*)-ig(1-2\xi\gamma^*)}. \tag{2.82}$$

In the limit that $\Delta \gg \gamma_{\rm ab}, \gamma_{\rm ac}, \Omega$ a simple analytic expression is given for both contributions to the susceptibility:

$$\chi_1 = \frac{3N\lambda_{\rm pr}^3\gamma_{\rm r}^{\rm ab}}{8\pi^2}\{\frac{1-\xi}{\delta-\Delta(1-\xi)-i[\gamma_{\rm ab}(1-\xi)+\gamma_{\rm cb}\xi]} + \frac{\xi}{\delta-\Delta\xi-i[\gamma_{\rm cb}(1-\xi)+\gamma_{\rm ab}\xi]}\}, \tag{2.83}$$

$$\chi_2 = \frac{3N\lambda_{\rm pr}^3\gamma_{\rm r}^{\rm ab}}{8\pi^2}\{\frac{\xi}{\delta-\Delta(1-\xi)-i[\gamma_{\rm ab}(1-\xi)+\gamma_{\rm cb}\xi]} + \frac{-\xi}{\delta-\Delta\xi-i[\gamma_{\rm cb}(1-\xi)+\gamma_{\rm ab}\xi]}\}. \tag{2.84}$$

In this work $\omega_{\rm pr}$ is tuned to the vicinity of two-photon resonance ($\delta \ll \Delta$) therefore the contribution from the one photon-resonance of system 2 can always be neglected, while the one photon contribution of system 1 can be neglected when $\gamma_{\rm ab}/\Delta_1 \ll \xi_1$.

2.8 Behavior of the system

It has been shown in the previous section that the two photon resonant feature is equivalent to an effective two level atomic system with the amplitude, frequency, and width of the transition controlled by the driving field. Furthermore, the electromagnetic response of this effective system can be as strong as the resonant response of an actual two level system. The original probed transition had a susceptibility amplitude of:

$$\mathrm{A}_{\rm original} = \frac{3N\lambda_{\rm pr}^3}{8\pi^2}\frac{\gamma_{\rm r}^{\rm ab}}{\gamma_{\rm ab}}. \tag{2.85}$$

While the amplitude of the two photon effective two level atom is:

$$\mathrm{A}_{\rm 2ph} = \frac{3N\lambda_{\rm pr}^3}{8\pi^2}\frac{\gamma_{\rm r}^{\rm ab}\xi}{\gamma_{\rm cb}(1-\xi)\gamma_{\rm ab}\xi} = \frac{\xi\gamma_{\rm ab}\mathrm{A}_{\rm original}}{\gamma_{\rm cb}(1-\xi)+\gamma_{\rm ab}\xi}. \tag{2.86}$$

It is clear that for the 2-photon feature to be close the same strength as the original transition we require $\xi \gg \gamma_{\rm cb}/\gamma_{\rm ab}$. Although, the amplitude will be half of the original amplitude with $\xi = \gamma_{\rm cb}/\gamma_{\rm ab}$. Therefore, when the low frequency coherence decays slower than the optical one $\gamma_{\rm ab} \gg \gamma_{\rm cb}$, the contribution from the two-photon resonance can be nearly as large as the contribution from the one-photon resonance.

As the amplitude of the 2-photon feature is smaller, it also has a narrower linewidth, with the effective linewidth given by:

$$\gamma_{\rm eff} = \gamma_{\rm cb}(1-\xi) + \gamma_{\rm ab}\xi. \tag{2.87}$$

Therefore the effective linewidth of our 2-photon feature can not be made larger than the original transition linewidth but can be decreased by the choice of ξ. While the shift from the resonance frequency of the original transition is given by:

$$\omega_{\text{eff}} - \omega_{\text{ab}} = \Delta + \frac{|\Omega|^2}{\Delta}. \tag{2.88}$$

Therefore our effective two level system has a frequency shifted by the one photon detuning and the ac-Stark shift, such that by choosing Δ we have control over the transition frequency. Together our choice of ξ and Δ gives us complete control of the properties of our effective two level system, within the restraints put on these two values by the physical system.

2.9 Conclusion

We have shown how a far detuned lambda system near two photon resonance acts as an effective two level atom. The applied control field splits the original resonant Lorentzian feature (seen by the probe field) into a one photon and two photon feature. The choice of the control field Rabi frequency and one photon detuning allows us to control the transition frequency, line width, and amplitude of both of the Lorentzians. In particular when the control field is strong compared to the original line width and the low frequency coherence decay rate is much smaller than the original line width, the two photon feature can approach an amplitude of half of the original transition amplitude.

We would like to reiterate that using the decaying dressed state basis [54] is essential to getting the full understanding of our effective two level system. Using the dressed state basis alone does not incorporate the effect of decoherence and therefore can lead to errors if used to estimate transition amplitudes and frequencies, and can not determine the transition line width at all. The results in this section are not limited to the far-detuned Λ scheme. We will show in Section 4 that an effective

two level atomic system can also be produced in a far-detuned V scheme. Having a way to make effective two level atomic systems will be key to our schemes for the enhancement and manipulation of refractive index at vanishing absorption that will be discussed in the following sections.

3. RESONANT ENHANCEMENT OF REFRACTIVE INDEX BY USING TWO Λ SCHEMES

3.1 Introduction

A mixture of two level atomic species will provide overlapping absorption and gain if the difference in resonance frequencies is on the scale of the linewidth and one of the atomic species is inverted. A proper overlap could result in high refractive index with vanishing absorption for a weak field properly tuned between two atomic resonances. However the difficulties associated with the practical implementation of such a combined system (finding proper species, providing for an even mixture, and providing population inversion for one species while avoiding spatial fluctuations of density and population exchange, etc.) would hardly be surmountable [21].

We consider here an idea, to use coherent effects in a mixture of different species to induce strong and overlapping electromagnetic responses to provide high refractive index with vanishing absorption. The use of a coherent preparation of a medium for elimination of absorption and index enhancement was pioneered by Scully [19], which was further generalized in [20] by including the density dependent near dipole-dipole interactions.

Only recently, a new scheme for coherent control and index enhancement was suggested [24]. This scheme is based on a resonant four level system involving two Raman transitions optically pumped into the ground state and driven by two far off-resonant control fields forming two Λ systems with the same probe field. The dispersive and absorption characteristics in such a system as functions of two-photon detuning essentially interchange so that the maximum resonant refractive index is accompanied by vanishing absorption. Similar to the previous proposals involving resonant driving the effect was attributed to interference and an index on the order of 10 for alkali vapors with densities (10^{17} cm^{-3}) was predicted. Although there was undesirable gain in the vicinity of vanishing absorption.

In this work [44], we have studied the physical mechanisms responsible for index enhancement in the case of far off-resonant driving and its limitations. In the following section, a simpler system is considered. It represents itself as a mixture of two three-level atomic species each driven by a corresponding far-detuned coherent field at one atomic transition and probed by the same weak field at a adjacent transition in the vicinity of two-photon resonance. This idea could be implemented in many different mediums, for example in a gas of two different isotopes of the same species, in a doped crystal with two different isotopes, or a doped crystal where the dopant sits at non-equivalent sites in the crystal. We will consider an implementation in gas where we shown that a proper treatment of collisional broadening implies that any given mixture has a maximum possible index enhancement. The experimental realization of the proposed system in a cell of Rb atoms with natural abundance (72% ^{85}Rb and 28% ^{87}Rb) is analyzed. The same system was used by a proof of principal experiment which showed an enhancement of $\Delta n = 2.2 \cdot 10^{-7}$ [46]. An upper limit due to the dipole-dipole broadening at the high atomic density of the refractive index enhancement in such a system is estimated as $\Delta n \simeq 10^{-1}$.

3.2 Mixture of two coherently driven atomic systems

We consider a mixture of two atomic species with the density of atoms for each species N_{s1} and N_{s2} being free parameters. Each of them is represented as a three-level system, labeled by si $\in$ {s1, s2}, with one excited state and two ground state sub-levels labeled $|a_i\rangle$, $|b_i\rangle$ and $|c_i\rangle$, correspondingly (see Fig. 3.1). The system, driven by a pair of coherent fields with frequencies ω_{si} and Rabi frequencies Ω_{si}, is probed by a weak field with frequency ω_{pr} and Rabi frequency α_{si}. The driving field Rabi frequencies $\Omega_{si} = d_{si}^{ac} E_{si}/(2\hbar)$ are defined by the applied electric field E_c and the dipole moment of the a$\leftrightarrow$c transition d_{si}^{ac}. The Rabi frequencies of the probe field $\alpha_{si} = d_{si}^{ab} E_{pr}/(2\hbar)$ in each system may be different because the dipole moment of the probed transition a$\leftrightarrow$b in s1-system can be different from the dipole moment

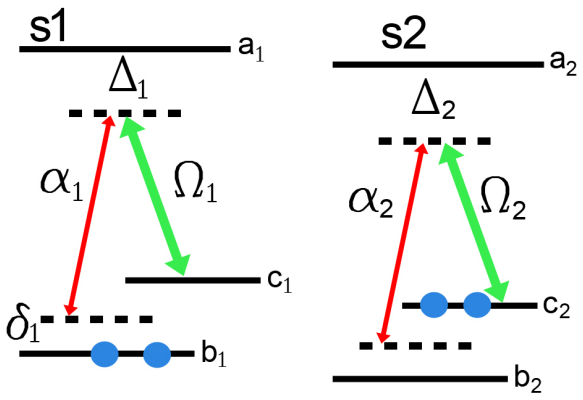

Fig. 3.1. Mixture of two three-level Λ systems. The initially populated level is indicated by the dot.

of the probed transition in s2-system. All-fields are far off-resonance with atomic transitions so that one-photon contributions are negligible, implying $\Delta_{si} >> \Omega_{si}$. The frequencies of the fields are chosen in such a way that they result in one two-photon transition in each three-level system involving one photon from the probe field and one photon from the corresponding driving field. So each three-level system forms a Λ scheme with the same probe and corresponding driving field (see Fig. 3.1). Each three-level system is initially prepared in one of the two ground state sublevels via optical pumping as indicated in Fig. 3.1. So the first scheme exhibits two-photon absorption for the probe field while the second scheme provides two-photon gain, as discussed in Section 2.

The index of refraction and absorption coefficient can be found if the complex susceptibility is known. In our system the total complex susceptibility is equal to the sum of individual contributions from each of the three-level systems. The complex susceptibility itself can be calculated if the optical coherence excited by a weak probe field is known:

$$\chi_{si} = \frac{3}{8\pi^2}\gamma_r^{si} N_{si} \lambda_{pr}^3 \frac{\sigma_{ab}^{si}}{\alpha_{si}}, \tag{3.1}$$

where $\gamma_{\mathrm{r}}^{\mathrm{si}}$ is the radiative decay rate of the probed transition, λ_{pr} is the wavelength of the probe, and $\sigma_{\mathrm{ab}}^{\mathrm{si}}$ is the coherence of the probed transition.

The slowly varying amplitude of the optical coherence induced by a weak probe field $\alpha_{\mathrm{si}} << \Omega_{\mathrm{si}}, \gamma_{\mathrm{ab}}^{\mathrm{si}}$ was calculated in Section 2 and is found to be:

$$\sigma_{\mathrm{ab}}^{\mathrm{s1}} = \frac{\left(\delta_{\mathrm{s1}} - i\gamma_{\mathrm{cb}}^{\mathrm{s1}}\right)\alpha_{\mathrm{s1}}}{\left(\delta_{\mathrm{s1}} + \Delta_{\mathrm{s1}} - i\gamma_{\mathrm{ab}}^{\mathrm{s1}}\right)\left(\delta_{\mathrm{s1}} - i\gamma_{\mathrm{cb}}^{\mathrm{s1}}\right) - \left|\Omega_{\mathrm{s1}}\right|^2}, \tag{3.2}$$

for s1-system presented in Fig. 3.1 (left), while for s2-system presented in Fig. 3.1 (right) it is found to be:

$$\sigma_{\mathrm{ab}}^{\mathrm{s2}} = -\frac{\left|\Omega_{\mathrm{s2}}\right|^2\left(\Delta_{\mathrm{s2}} + i\gamma_{\mathrm{ac}}^{\mathrm{s2}}\right)^{-1}\alpha_{\mathrm{s2}}}{\left(\delta_{\mathrm{s2}} + \Delta_{\mathrm{s2}} - i\gamma_{\mathrm{ab}}^{\mathrm{s2}}\right)\left(\delta_{\mathrm{s2}} - i\gamma_{\mathrm{cb}}^{\mathrm{s2}}\right) - \left|\Omega_{\mathrm{s2}}\right|^2}. \tag{3.3}$$

In these equations, we introduced the following parameters for si-system: $\Delta_{\mathrm{si}} = \omega_{\mathrm{ab}}^{\mathrm{si}} - \omega_{\mathrm{cb}}^{\mathrm{si}} - \omega_{\mathrm{si}}$ and $\delta_{\mathrm{si}} = \omega_{\mathrm{si}} + \omega_{\mathrm{cb}}^{\mathrm{si}} - \omega_{\mathrm{pr}}$ are the one- and the two-photon detunings for si-drive field, respectively. Finally, we can write down the expression for complex susceptibility of the system:

$$\begin{aligned}\chi\left(\omega_{\mathrm{pr}}\right) = &\frac{3\lambda_{\mathrm{pr}}^3}{8\pi^2}\frac{\mathrm{N}_{\mathrm{s1}}\gamma_{\mathrm{r}}^{\mathrm{s1}}\left(\delta_{\mathrm{s1}} - i\gamma_{\mathrm{cb}}^{\mathrm{s1}}\right)}{\left(\delta_{\mathrm{s1}} + \Delta_{\mathrm{s1}} - i\gamma_{\mathrm{ab}}^{\mathrm{s1}}\right)\left(\delta_{\mathrm{s1}} - i\gamma_{\mathrm{cb}}^{\mathrm{s1}}\right) - \left|\Omega_{\mathrm{s1}}\right|^2} \\ &- \frac{3\lambda_{\mathrm{pr}}^3}{8\pi^2}\frac{\mathrm{N}_{\mathrm{s2}}\gamma_{\mathrm{r}}^{\mathrm{s2}}\left|\Omega_{\mathrm{s2}}\right|^2\left(\Delta_{\mathrm{s2}} + i\gamma_{\mathrm{ac}}^{\mathrm{s2}}\right)^{-1}}{\left(\delta_{\mathrm{s2}} + \Delta_{\mathrm{s2}} - i\gamma_{\mathrm{ab}}^{\mathrm{s2}}\right)\left(\delta_{\mathrm{s2}} - i\gamma_{\mathrm{cb}}^{\mathrm{s2}}\right) - \left|\Omega_{\mathrm{s2}}\right|^2}.\end{aligned} \tag{3.4}$$

In the following sections, individual contributions are discussed and physical insights are given.

3.3 Combining effective two-level absorption and gain

The slowly varying amplitude of the optical coherence induced by a weak probe field in a Λ-configuration is inversely proportional to a quadratic polynomial in terms of the two-photon detuning δ_{si}. Zeros of this polynomial correspond to the two main contributions to the optical coherence as has been previously discussed in [54]. For

the case of a far-detuned driving field, $\Delta_{\rm si} \gg \Omega_{\rm si}, \gamma_{\rm ab}^{\rm si}, \gamma_{\rm cb}^{\rm si}$, these resonance contributions are far-detuned as well and associated with one- and two-photon resonances. As shown in Section 2, this is clearly seen for s1 after expanding Eq. (3.2) in terms of the first order of the small parameter $\xi_{\rm s1} = |\Omega_{s1}|^2/\Delta_{\rm s1}^2$:

$$\sigma_{ab}^{\rm s1} = \frac{\alpha_{\rm s1}(1-\xi_{\rm s1})}{\delta_{\rm s1} - \Delta_{\rm s1}(1-\xi_{\rm s1}) - i[\gamma_{ab}^{\rm s1}(1-\xi_{\rm s1}) + \gamma_{cb}^{\rm s1}\xi_{\rm s1}]} + \frac{\alpha_{\rm s1}\xi_{\rm s1}}{\delta_{\rm s1} - \Delta_{\rm s1}\xi_{\rm s1} - i[\gamma_{cb}^{\rm s1}(1-\xi_{\rm s1}) + \gamma_{ab}^{\rm s1}\xi_{\rm s1}]}. \tag{3.5}$$

If $\Delta_{\rm s2} \gg \gamma_{\rm ac}^{\rm s2}$ as well, a similar expression can be found for s2 with the exception that the two photon amplitude is now negative and therefore provides gain due to the population in level $|c_2\rangle$; while the one photon amplitude is different since the feature would no longer be present in the absence of a control field:

$$\sigma_{ab}^{\rm s2} = \frac{\alpha_{\rm s2}\xi_{\rm s2}}{\delta_{\rm s2} - \Delta_{\rm s2}(1-\xi_{\rm s2}) - i[\gamma_{ab}^{\rm s2}(1-\xi_{\rm s2}) + \gamma_{cb}^{\rm s2}\xi_{\rm s1}]} + \frac{-\alpha_{\rm s2}\xi_{\rm s2}}{\delta_{\rm s2} - \Delta_{\rm s2}\xi_{\rm s2} - i[\gamma_{cb}^{\rm s2}(1-\xi_{\rm s2}) + \gamma_{ab}^{\rm s2}\xi_{\rm s2}]}. \tag{3.6}$$

Furthermore, our probe field $\omega_{\rm pr}$ is tuned to the vicinity of two-photon resonance ($\delta_{\rm si} \ll \Delta_{\rm si}$) therefore the contribution from the one photon-resonance of the second system can always be neglected, while the one photon contribution of the first system can be neglected when $\gamma_{\rm ab}^{\rm s1}/\Delta_{\rm s1} \ll \xi_{\rm s1}$. Thus the total susceptibility of the probe field is given by:

$$\chi = \frac{3{\rm N}_{\rm s1}\lambda_{\rm pr}^3\gamma_{\rm r}^{\rm s1}}{8\pi^2}\frac{\xi_{\rm s1}}{\delta_{\rm s1} - \Delta_{\rm s1}\xi_{\rm s1} - i[\gamma_{cb}^{\rm s1}(1-\xi_{\rm s1}) + \gamma_{ab}^{\rm s1}\xi_{\rm s1}]} + \frac{3{\rm N}_{\rm s2}\lambda_{\rm pr}^3\gamma_{\rm r}^{\rm s2}}{8\pi^2}\frac{-\xi_{\rm s2}}{\delta_{\rm s2} - \Delta_{\rm s2}\xi_{\rm s2} - i[\gamma_{cb}^{\rm s2}(1-\xi_{\rm s2}) + \gamma_{ab}^{\rm s2}\xi_{\rm s2}]}, \tag{3.7}$$

where $\gamma_{\rm r}^{\rm si}$ is the radiative decay rate of the a$\leftrightarrow$b for each transition.

When the low frequency coherence decays slower than the optical one $\gamma_{\rm ab}^{\rm si} \gg \gamma_{\rm cb}^{\rm si}$, the contribution from the two-photon resonance can be nearly as large as the con-

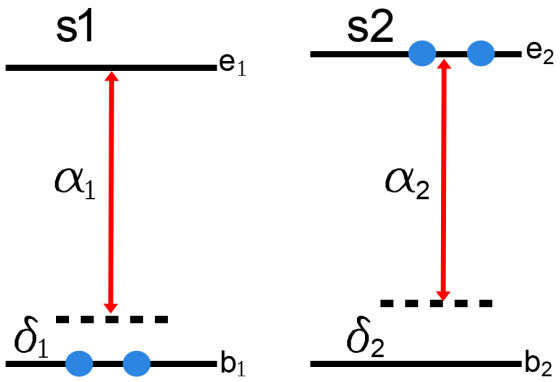

Fig. 3.2. An equivalent representation of a mixture of two three-level sub-system driven by coherent off-resonant fields.

tribution from the one-photon resonance. This would simply require $\xi_{\rm si} \geq \gamma_{\rm cb}^{\rm si}/\gamma_{\rm ab}^{\rm si}$. Hence, both of our three level schemes behave as effective two level schemes with susceptibilities on the same order as the ones for the original transition. The presence of the drive fields allow for the control of the strength, width, and position of the resonances. This, in turn, leads to the manipulation of the atomic responses of the individual systems (see Fig. 3.2). We will use this flexibility combined with appropriate mixing of the species to obtain enhanced refractive index without absorption.

At first, we take an approach similar to [24]. It is based on the absorption and amplification resonances having the same magnitude, width and being separated by the full width at half maximum (FWHM). This arrangement results in the absorption being compensated by nearby gain. Furthermore, at the point of no absorption the maximum(minimum) of the real part of the complex susceptibility associated with the absorption resonance adds up with the maximum(minimum) of the real part of the complex susceptibility associated with the gain resonance. We demonstrate this (see Fig. 3.3) by calculating the atomic response from a mixture of two three-level sub-systems in the case of $\xi_{\rm si} \approx \gamma_{\rm cb}^{\rm si}/\gamma_{\rm ab}^{\rm si}$. Numerical values of the parameters used are listed in the caption to the figure. Although this arrangement provides a high value of refractive index with no absorption, the disadvantage of such an approach

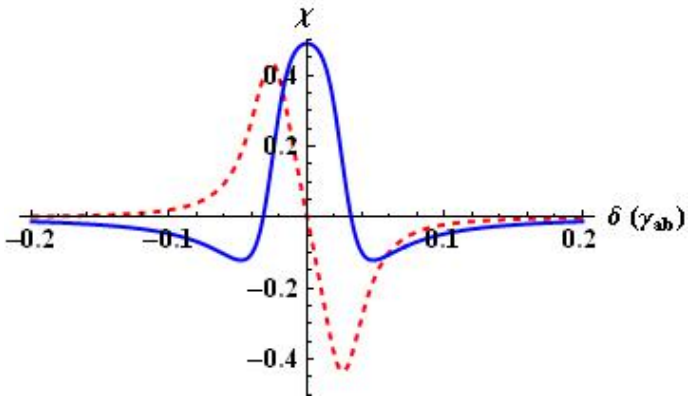

Fig. 3.3. Combined real (solid) and imaginary (dashed) parts of the susceptibility from two three-level systems. Where the x-axis is normalized to $\gamma_{ab}^{s1} = \gamma_{ab}^{s2} = \gamma_{ab}$, and the y-axis is normalized to $\eta = 3N_{s1}\lambda_{pr}^3\gamma_r^{s1}/(8\pi^2) = 3N_{s2}\lambda_{pr}^3\gamma_r^{s2}/(8\pi^2) = 1$. With $\Omega_{s1} = \Omega_{s2} = 2\gamma_{ab}$, $\Delta_{s1} = \Delta_{s2} = 20\gamma_{ab}$, and $\gamma_{cb}^{s1} = \gamma_{cb}^{s2} = 0.016\gamma_{ab}$. Resonances have equal strength and width, but are shifted by FWHM. Obtained maximum at zero absorption is 0.5η.

can easily be seen in Fig. 3.3. Namely, non-compensated gain is present in close proximity to the point of enhanced refractive index.

In order to avoid undesirable gain in the system, we suggest an alternative to the previously outlined approach. This is done at the expense of a reduced enhancement of the refractive index. In this approach a narrower amplification resonance is superimposed on top of a broader absorption resonance. The amplification resonance is positioned at the maximum of the real part of the complex susceptibility associated with the absorption resonance. The magnitude of the amplification resonance is chosen to compensate present absorption in the narrow region without providing gain. For such an arrangement, the amplification resonance provides no contribution to the refractive index enhancement at the point of no absorption. In order to demonstrate the approach, we present the atomic response of the mixture of two three-level systems in Fig. 3.4.

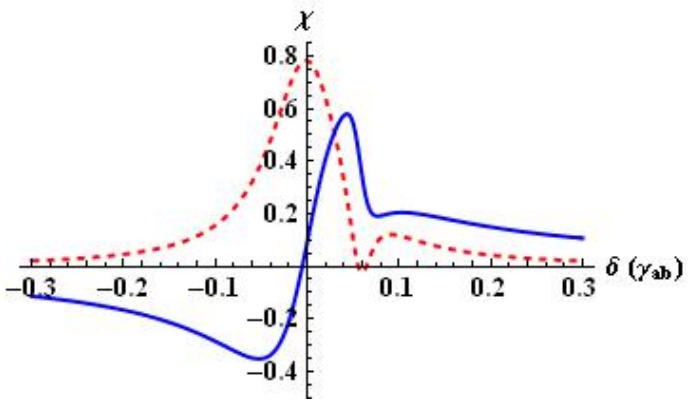

Fig. 3.4. Combined real (solid) and imaginary (dashed) parts of the susceptibility from two three-level systems. With $\Omega_{s1} = 4\gamma_{ab}$ and $\Omega_{s2} = 1.5\gamma_{ab}$, and all other parameters the same as in Fig. 3.3. Amplification is weaker and narrower than absorption. The relative shift is adjusted to get zero absorption and no gain. Obtained maximum at zero absorption is 0.33η.

The main limitation for our effective 2 level transition is to have as high a susceptibility as the original transition, is the need for a strong control field Rabi frequency $|\Omega_{si}|^2 > \Delta_{si}^2\gamma_{cb}^{si}/\gamma_{ab}^{si}$. Therefore we need as small hyperfine decoherence as possible $\gamma_{cb}^{si} \ll \gamma_{ab}^{si}$ in order to limit the needed intensity of the driving fields. At the same time we do not want to increase γ_{ab}^{si} since this would lower the achievable refractive index, so in Section 3.4 we will study γ_{ab}^{si} in hot gas, while in Section 3.5 we will study the behavior of γ_{cb}^{si} in gas.

3.4 Refractive index dependence on the optical linewidth

Electromagnetic response of an atomic system can be increased by improving the $\gamma_r^{si}/\gamma_{ab}$ ratio and by having more atoms per cubic wavelength $N_{si}\lambda_{pr}^3$. The last approach seems to be the easiest but it leads to a decrease of aforementioned ratio due to atomic interaction in dense media. Large estimates for achievable refractive indexes in previous works were due to not considering the effect of increasing density on the

ratio $\gamma_{\rm r}^{\rm si}/\gamma_{\rm ab}$. Past estimates and experiments [23, 46] have been done in hot gas, so in this section we will consider implementation in a gas of two different species, while in Section 4 we will consider an implementation in solids. The main homogeneous broadening mechanism in gases is collisional broadening; according to Lewis [61], the collisional contribution to the linewidth is proportional to concentration N, namely the HWHM is:

$$\Gamma_{\rm coll}^{\rm si} \simeq f_{\rm si} c r_e \lambda_{\rm pr} {\rm N} \sqrt{g_g^{\rm si}/g_e^{\rm si}}, \tag{3.8}$$

with $g_g^{\rm si}$ and $g_e^{\rm si}$ to be the degeneracies of the ground and excited states, respectively; r_e is the classical radius of the electron, and $f_{\rm si}$ is the oscillator strength of the transition. This broadening comes from resonant dipole-dipole interaction between induced optical dipoles. Where in Eq. (3.8) we have used the total population ${\rm N} = {\rm N_{s1}} + {\rm N_{s2}}$, since isotopes of the same atom are identical with regard to collisions. For example take the ^{85}Rb D1 line, Eq. (3.8) gives $\Gamma_{\rm coll} = .365 \cdot 10^{-13} {\rm MHz \cdot cm^3 \cdot N}$ and [62] measured the self broadening as $\Gamma_{\rm coll} = .375(\pm.12) \cdot 10^{-13} {\rm MHz \cdot cm^3 \cdot N}$. For high gas densities there are also collision induced frequency shifts [63] that we will not consider since they will not have much of an effect on our theory.

In a hot gas cell the density will be determined by the temperature of the cell, so both the inhomogeneous Doppler broadening and the homogeneous collisional broadening are dependent on the density. The Doppler contribution is given by the half width at half maximum (HWHM) of the Maxwell distribution for each species,

$$\Gamma_D^{\rm si} = \sqrt{\frac{2kT\ln(2)}{m_{\rm si}c^2}}\omega_0; \tag{3.9}$$

where k is Boltzmann's constant, T is the absolute temperature of the gas, $\rm m_{si}$ is the mass of the atomic species, c is the speed of light, and $\omega_0 = 2\pi c/\lambda_{\rm pr}$ is the transition frequency.

Since we want a large resonant refractive index we are interested in high gas densities, where the susceptibility has saturated due to collisional broadening be-

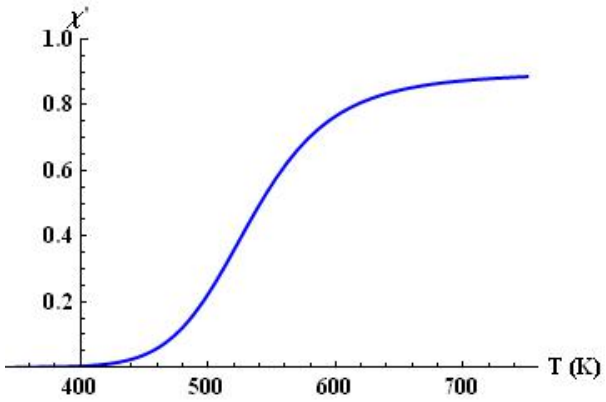

Fig. 3.5. The peak real part of the susceptibility for the D2 line of ^{85}Rb as a function of absolute temperature.

coming much larger than the other broadening mechanisms. The susceptibility of the effective two level system will always be constrained by the original two level susceptibility of the a↔b transition given by:

$$\chi^{si}_{max} = \frac{3}{8\pi^2} \frac{N_{si}\lambda^3_{pr}\gamma^{si}_r}{.5\gamma^{si}_r + \Gamma^{si}_D + \Gamma^{si}_{coll}}. \tag{3.10}$$

Since the linewidth and total atomic response grow linearly with concentration which leads to a saturated value of the maximum susceptibility at high density.

Consider the D2 line of ^{85}Rb with $\Gamma_{coll} = .515 \cdot 10^{-13} cm^3 MHz \cdot N$, when the collisional broadening becomes much larger than the other broadening terms the two level susceptibility saturates at 750K or a density of N$\approx 6 \cdot 10^{17} cm^{-3}$ (see Fig. 3.5). This leads to a maximum real part of the resonant susceptibility of .885 or a refractive index of 1.37. Therefore there is no way to enhance the refractive index of Rubidium past $\Delta n = 4 \cdot 10^{-1}$.

3.5 Ratio of hyperfine decoherence to optical decoherence rate

At low densities the main contribution to the hyperfine decoherence will be due to time of flight in our control beams, since as atoms leave the interaction region we are losing coherence. This decoherence can be described as [64]:

$$\Gamma_{\mathrm{TF}}^{\mathrm{si}} = \frac{\sqrt{2}\ln(2)}{2\pi d}\sqrt{\frac{2kT}{m}}, \tag{3.11}$$

where d is the $1/e$ diameter of the beam. While at high densities the main contribution to the hyperfine broadening is the decay of hyperfine population due to spin-exchange collisions between two atoms. This self broadening, like collisional broadening is linearly proportional to the density. For example for ^{85}Rb we can estimate the decoherence as $\Gamma_{\mathrm{sb}}^{\mathrm{si}} = 2\pi \cdot 2.83 \cdot 10^{-16}\mathrm{N}$ MHz [65].

The time of flight decoherence can be decreased by including a neutral buffer gas. Then as our atomic species is leaving the beam area it will repeatedly collide with the buffer gas atoms leading to a longer path length in the beam. With the background gas the time of flight decoherence will be given by [61]:

$$\Gamma_{\mathrm{TF,\,BG}}^{\mathrm{si}} = \left(\frac{4.81}{d}\right)^2 \mathrm{D}_0 \frac{\mathrm{P}_0}{\mathrm{P}_{\mathrm{BG}}}, \tag{3.12}$$

where D_0 is the diffusion coefficient measured at a reference pressure of P_0, and P_{BG} is the buffer gas. The buffer gas will also broaden both transitions due to collisional broadening, while even at high buffer pressures, collisions with the buffer gas will only have a negligible effect on $\gamma_{\mathrm{cb}}^{\mathrm{si}}$, but will have a noticeable addition to the optical decoherence rate that scales linearly with buffer gas pressure. At high buffer gas pressures this effect can significantly reduce the maximum susceptibility possible.

For example consider the Rb D2 line, we can express the buffer gas contribution to the collisional decoherence is $\Gamma_{\mathrm{BG}}^{\mathrm{si}} = 2\pi \cdot 4.735\mathrm{MHz} \cdot \mathrm{P}_{\mathrm{BG}}$ [66]. $\mathrm{D}_0 = .21\mathrm{cm}^2/\mathrm{s}$ [67] at $\mathrm{P}_0 = 760\mathrm{Torr}$, giving for $d = 1\mathrm{mm}$, $\Gamma_{\mathrm{TF,BG}}^{\mathrm{si}} = 2\pi \cdot .369\mathrm{MHz} \cdot \mathrm{Torr}/\mathrm{P}_{\mathrm{BG}}$. For this

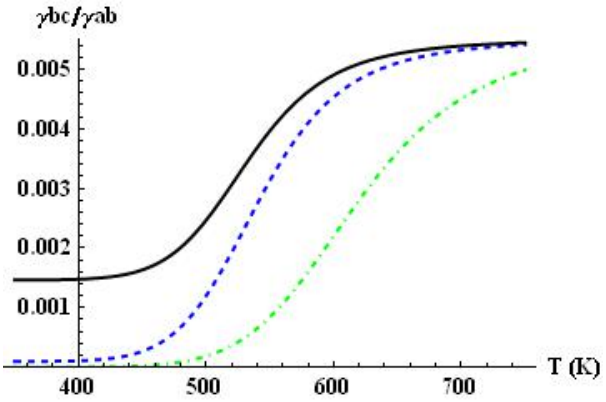

Fig. 3.6. The ratio of hyperfine to optical decoherence rates plotted as a function of temperature for the case where there is no buffer gas (solid), with a Neon buffer gas at 10Torr (dashed), and at 300Torr (dot-dashed).

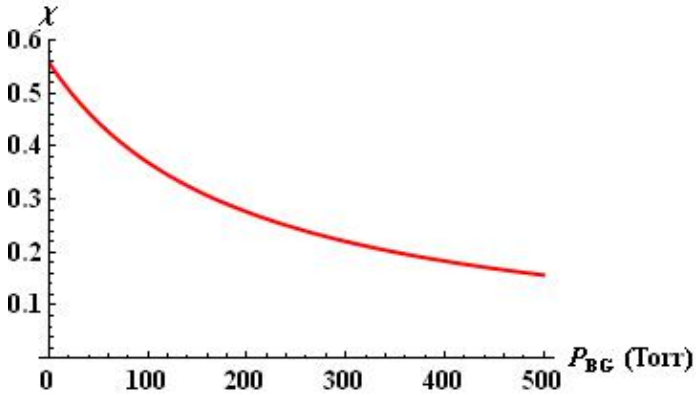

Fig. 3.7. The maximum real part of the 2 level susceptibility for Rb D2 line plotted as a function of the buffer gas pressure. Plotted at a temperature of 550K.

case the effect of the buffer gas on the decoherence ratio is shown in Fig. 3.6. For maximum refractive index enhancement it is better to use a low pressure buffer gas as can be seen in Fig. 3.7.

3.6 Implementation in gas

Alkali metals such as Sodium, Rubidium, Potassium have been good test systems for demonstrating many coherent effects. To demonstrate refractive index enhancement, one needs to find two transitions with frequency differences for the one-photon and two-photon transitions in the GHz range. This is possible if a mixture of isotopes is considered. However only Rubidium has a comparable ratio of naturally occurring isotopes (28% of ^{87}Rb and 72% of ^{85}Rb) and large enough hyperfine splitting. Thus let us consider as a physical example a naturally occurring mixture of Rb vapors.

Rb atoms have two suitable transitions called D1 at 794.8nm and D2 at 780.2nm. The D1 and D2 transitions have common ground levels and differ in the excited state. The excited level structure for the D1 and D2 transitions has a separation less than 0.8GHz thus for one-photon detunings much larger than this separation the value of effective far-detuned dipole moment can be used. Numerical values for π-polarized light are $1.727ea_0$ and $2.44ea_0$ for D1 and D2 transitions correspondingly. A stronger dipole moment guaranties a stronger atomic response and therefore lager susceptibilities. A stronger dipole moment also implies a lower intensity requirement for the control fields to reach the needed Rabi frequency. Therefore the D2 transition seems to be the optimal choice from all the accounts. The natural linewidth of the Rb D2 absorption line is $2\pi \cdot 6.067$ MHz, although the radiative decay rate is $2\pi \cdot 5.12$MHz.

In order to implement refractive index enhancement with vanishing absorption while maintaining no nearby regions of gain in a Rb gas it is necessary to implement system 1 in ^{85}Rb and system 2 in ^{87}Rb. Since at natural abundance the density of ^{85}Rb is nearly three times larger than ^{87}Rb and we need the effective absorption transition to be stronger than the effective gain transition. This choice also determines the one photon detuning for system 1 since if we want the same probe field to address both transitions then the difference in transition frequencies $\omega_{\rm ab}(^{87}\text{Rb}) - \omega_{\rm ab}(^{85}\text{Rb}) = 2\pi \cdot .39$GHz determines the difference in one photon detun-

ings. The ground state of Rb has 2 hyperfine levels separated by $2\pi \cdot 3.036$GHz and $2\pi \cdot 6.835$GHz for 85 and 87 isotope respectively. We assume that the probe field is applied to the lower of the two hyperfine levels and the control fields to the upper. First it tells us that we need $\Delta > 2\pi \cdot 7$GHz in order to avoid one photon resonance, therefore we will take $\Delta_{s2} = 2\pi \cdot 10$GHz, implying $\Delta_{s1} = 2\pi \cdot 10.385$GHz.

Except for the transition frequencies all other properties of interest for ^{85}Rb and ^{87}Rb including the dipole moments and the decoherence rates are essentially the same, when the slight mass difference is neglected. The decoherence rate of the optical transition has four contributions: $\gamma_{ab}^{si} = .5\gamma_r^{si} + \Gamma_{coll}^{si} + \Gamma_D^{si} + \Gamma_{BG}^{si}$. The population decay rate is fairly unaffected by density and is given by $\gamma_r^{si} = 2\pi \cdot 6$MHz. As discussed in section 3.4, we can take the ideal density for Rb to be $N = 6 \cdot 10^{17}\text{cm}^{-3}$; unfortunately, at this density $\gamma_{ab}^{si} = \gamma_{ac}^{si} = 197$GHz which violates our condition to avoid the one photon absorption of $\Delta \gg \gamma_{ab}^{si}, \gamma_{ac}^{si}$, since having such a large one photon detuning would lead to a unachievable Rabi frequency.

Say for our control fields we are limited to focusing a 100mW beam into a diameter of 1mm, this would give us Rabi frequencies of $2\pi \cdot 150$MHz, so we take $\Omega_1 = 2\pi \cdot 150$MHz and $\Omega_2 = 2\pi \cdot 135$MHz. Implying the max control field ratio ξ we can achieve is $2.25 \cdot 10^{-4}$. The decoherence ratio is equal to this ξ at a temperature of $T = 450$K, or a density of $N = 3.3 \cdot 10^{14}\text{cm}^{-3}$ so at natural abundance we have $N_{s1} = .72N$ and $N_{s2} = .28N$. For a fixed ξ, a smaller buffer gas pressure is better so we will take $P_{BG} = 10$Torr. This buffer gas will add $2\pi \cdot 47$MHz to the optical decoherence, and the time of flight broadening is $\Gamma_{hyp,BG}^{si} = 2\pi \cdot 37$kHz. At this density the hyperfine self broadening is $\Gamma_{hf,self}^{si} = 2\pi \cdot 93$kHz, so $\gamma_{cb}^{si} = 2\pi \cdot 130$kHz. The collisional broadening is $\Gamma_{coll}^{si} = 2\pi \cdot 17$MHz, and the Doppler broadening is $\Gamma_D^{si} = 2\pi \cdot 315$MHz, therefore $\gamma_{ab}^{si} = 2\pi \cdot 382$MHz.

With these values for the detunings and Rabi frequencies the susceptibility is plotted in Fig. 3.8. There is a particular frequency where we have vanishing absorption and a significant resonant susceptibility $\text{Re}\chi = .0095$. At the same time we have

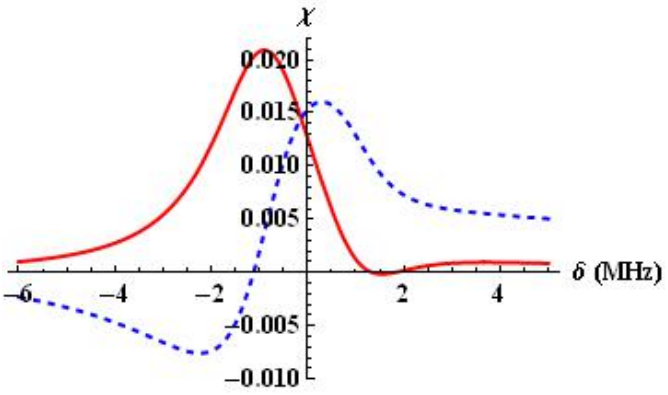

Fig. 3.8. The real (solid) and imaginary (dashed) part of the susceptibility as a function of the detuning, plotted for the scheme without gain and with $\Omega_1 = 2\pi \cdot 150\text{MHz}$ as described in the text.

no regions of nearby gain so that the probe field will remain stable at that frequency. Therefore in a hot Rb gas we have a maximum refractive index enhancement of $\Delta n \approx 4.7 \cdot 10^{-3}$.

When it is possible to use strong control fields we can achieve the maximum possible susceptibility increase. Consider focusing a 10W beam into a 1mm diameter, then the Rabi frequencies are $\Omega_1 = \Omega_2 = 2\pi \cdot 1.5\text{GHz}$. This allows us to use larger one photon detunings to $\Delta_1 = 2\pi \cdot 20\text{GHz}$, $\Delta_2 = 2\pi \cdot 20.27\text{GHz}$. Which gives $\xi = .0055$, allowing for a higher ratio of $\gamma_{\text{ab}}/\gamma_{\text{cb}}$. Taking T = 600K, gives us $\text{N} = 4 \cdot 10^{16}\text{cm}^{-3}$ which leads to $\gamma_{\text{ab}}^{\text{si}} = 2\pi \cdot 4.667\text{GHz}$ and $\gamma_{\text{cb}}^{\text{si}} = 2\pi \cdot 71\text{MHz}$. Then the change in index is $\Delta n = .18$ as shown in Fig. 3.9.

3.7 Experimental realization

A proof of principal experiment to demonstrate resonant enhancement of refractive index in hot Rb gas was performed by Yavuz [46]. He implements the same two lambda systems in ^{85}Rb and ^{87}Rb at natural abundance using the D2 line and a 10 Torr Neon buffer gas as described in the previous section. It demonstrated that a

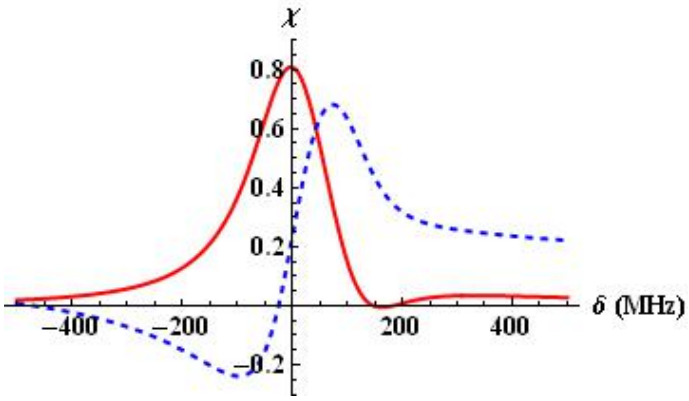

Fig. 3.9. The real (solid) and imaginary (dashed) part of the susceptibility as a function of the detuning, plotted for the scheme with $\Omega_1 = \Omega_2 = 2\pi \cdot 1.5\text{GHz}$ as described in the text.

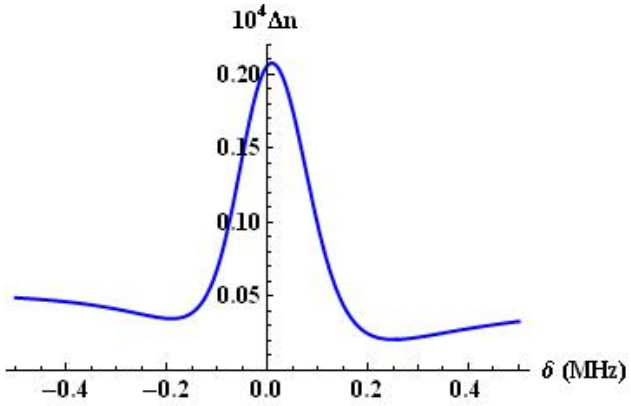

Fig. 3.10. The expected refractive index enhancement for experiment described in [46] plotted as a function of two photon detuning, using the experimental numbers as reported in the text.

probe field can interact with both of the lambda systems, and that the two susceptibilities straight forwardly superimpose. At a temperature of 363K the Rb density of N $= 2.4 \cdot 10^{12}\text{cm}^{-3}$ the optical broadening should be $\gamma_{\text{ab}}^{\text{si}} = 2\pi \cdot$ 334MHz and the hyperfine broadening should be $\gamma_{\text{cb}}^{\text{si}} = 2\pi \cdot 16\text{kHz}$.

The laser power is given as a 100mW focused in a 2.4 diameter spot size, implying that $\Omega_{\text{si}} < 2\pi \cdot 63\text{MHz}$. Based on the experimental results of both the gain and absorption being roughly equal in height and width with a two photon HWHM of 125kHz we can assume that $\Omega_{\text{s1}} = 2\pi \cdot 34\text{MHz}$ and $\Omega_{\text{s2}} = 2\pi \cdot 58\text{MHz}$. The control fields in the experiment are taken such that $\Delta_{\text{s1}} = 2\pi \cdot 15.6\text{GHz}$ and $\Delta_{\text{s2}} = 2\pi \cdot 16\text{GHz}$. With an applied pump field intensity of 1.77W/cm^2, numerical simulations show that for a pump field with a bandwidth of about 500MHz the population difference for both systems would be close to 1 as needed, with the worst being system 2 with $\sigma_{\text{cc}}^{\text{s2}} - \sigma_{\text{aa}}^{\text{s2}} = .93$.

The theoretical curve for the resonant refractive index with these parameters is plotted in Fig. 3.10. The theory predicts a change in index of $\Delta n = 1.7 \cdot 10^{-5}$. The theory also shows that there is a background index due to the one photon feature of n $= 1 + 4 \cdot 10^{-6}$, since $\xi_{\text{s1}} < \gamma_{\text{cb}}^{\text{s1}}/\gamma_{\text{ab}}^{\text{s1}}$, that would not of been directly observed in the experiment.

The reported refractive index change of Δn $= 2 \cdot 10^{-7}$ is two orders of magnitude less than what was possible in the experiment [46] due to issues with the cross pumping of the ^{87}Rb and ^{85}Rb populations. As explained in [46], this could be due to the frequency width of the pump fields being larger than the separation between the hyperfine level of ^{87}Rb and ^{85}Rb which would reduce the population difference between levels $|c_{\text{i}}\rangle$ and $|b_{\text{i}}\rangle$ and thus significantly reduce the RI enhancement.

3.8 Conclusion

We have given a simple model for how to implement refractive index enhancement without absorption while avoiding any nearby regions of gain. This is done by

implementing a far detuned Λ system in two different atomic isotopes mixed in a hot gas. Engineering a larger width for the absorptive resonance allows one to eliminate any amplification region in the vicinity of the enhanced index and vanishing absorption.

We have shown that with reasonable beam intensities this scheme can be implemented in ^{85}Rb and ^{87}Rb at natural abundance for refractive index enhancement on the order of $\Delta n \simeq 5 \cdot 10^{-3}$. Potentially higher resonant refractive indexes with vanishing absorption could be obtained with much stronger beam intensities or in solids.

4. REFRACTIVE INDEX ENHANCEMENT IN MEDIUMS THAT EXPERIENCE EXCITED STATE ABSORPTION

4.1 Introduction

In this section we suggest using excited state absorption (ESA) as a natural implementation of a combination of two two-level transitions (one inverted and one non inverted) [45]. In other words, we consider a ladder scheme with respect to the probe field with the populated intermediate level. So one transition produces gain and the other produces absorption. The tuning of the parameters of one of the transitions is provided by applying a coherent driving field at a adjacent transition. If the absorbing transition is controlled it makes a far-detuned Λ scheme (see Fig. 4.5) and when the gain transition is controlled it forms a far-detuned V system together with this lower transition (see Fig. 4.1(b)). So unlike a combination of two two-level systems, the transition frequencies can be separated by more than a line width. We show that this system leads to high refractive index without absorption for a properly tuned probe field in the absence of any amplification region.

4.2 Ladder system with populated intermediate level

We consider a three-level ladder system with allowed transitions a$\leftrightarrow$b and b$\leftrightarrow$c which have similar but slightly different frequencies. The same probe field is simultaneously applied to both transitions, see Fig. 4.1(a). The intermediate level is to be populated by incoherent pumping through an auxiliary level (not shown in Fig. 4.1(a)). So that a$\leftrightarrow$b is an amplifying while b$\leftrightarrow$c is an absorbing transition. The probe field is considered to be too weak to redistribute energy level populations. We can solve for the susceptibility of the ladder system using the density matrix formalism, taking the rotating wave approximation, and assuming a steady state where the normalized the population of each level is fixed; the solution is given by Eq. (4.1).

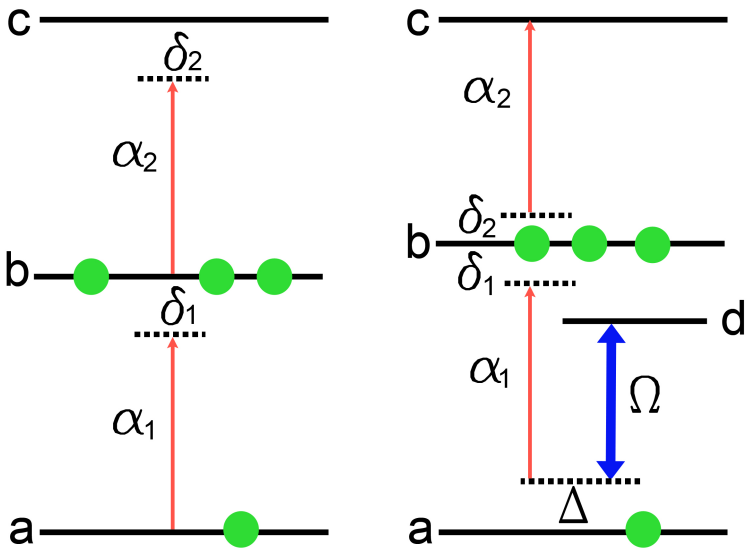

Fig. 4.1. (a) Energy level diagram for the three level ladder scheme where the population is fixed in an intermediate state that experiences ESA. (b) Energy level diagram for a four level system where a control field has been applied to an empty transition forming a V system together with lower transition.

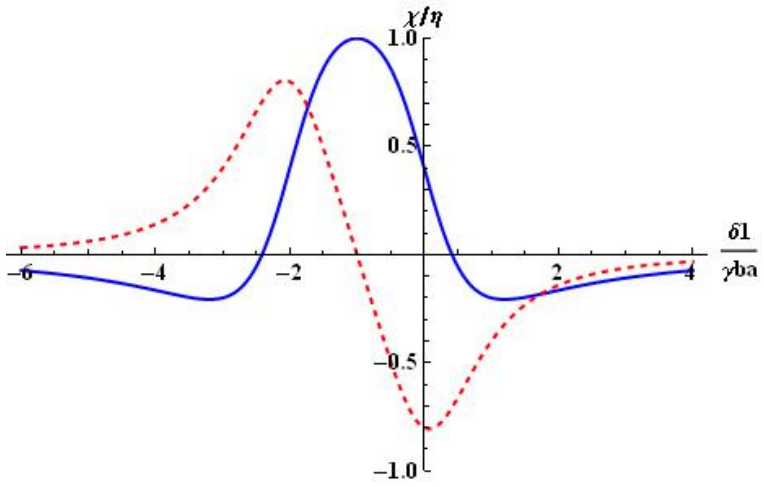

Fig. 4.2. The real (solid line) and imaginary (the dashed line) parts of the susceptibility are normalized to the resonant value of $\chi''_{\rm cb} = 3N\lambda_{\rm pr}^3 l\gamma_{\rm r}^{\rm cb}/(8\pi^2\gamma_{\rm cb}) = 1$, as functions of the detuning, $\delta_1/\gamma_{\rm cb}$. With $\gamma_{\rm cb} = \gamma_{\rm ba}$ and $\gamma_{\rm r}^{\rm cb} = \gamma_{\rm r}^{\rm ba}$.

The total susceptibility of the system represents itself as a sum of susceptibilities originating from b↔c and a↔b transitions accordingly,

$$\chi = \frac{3N\lambda_{\rm pr}^3 l}{8\pi^2}\left\{\frac{\gamma_{\rm r}^{\rm ba}(\sigma_{\rm aa}-\sigma_{\rm bb})}{\delta_1 - i\gamma_{\rm ba}} + \frac{\gamma_{\rm r}^{\rm cb}(\sigma_{\rm bb}-\sigma_{\rm cc})}{\delta_2 - i\gamma_{\rm cb}}\right\}; \tag{4.1}$$

where $\lambda_{\rm pr}$ is the wavelength of the probe field, $\gamma_{\rm ij}$ is the decoherence rate at half width half maximum (HWHM) linewidth between level $|{\rm i}\rangle$ and $|{\rm j}\rangle$, $\gamma_{\rm r}^{\rm ij}$ are the radiative decay rates between level $|{\rm i}\rangle$ and $|{\rm j}\rangle$, N is the number of ions/cm^3, $l = (2 + n_{\rm bg}^2)/3$ is the local field correction factor discussed in Section 2.5, and δ_1, δ_2 are the one photon detunings of the probe field as shown in Fig. 4.1(a). We can plot these in terms of the detuning of the upper system, $\delta_2 = \omega_{\rm cb} - \omega_{\rm pr}$. Because both transitions are probed by the same field the upper detuning is not independent of the lower detuning, $\delta_1 = \delta_2 - \omega_{\rm cb} + \omega_{\rm ba}$. Now we can take the susceptibility in terms of its Cartesian components $\chi = \chi' - i\chi''$, our goal is to maximize χ' while requiring $\chi'' = 0$.

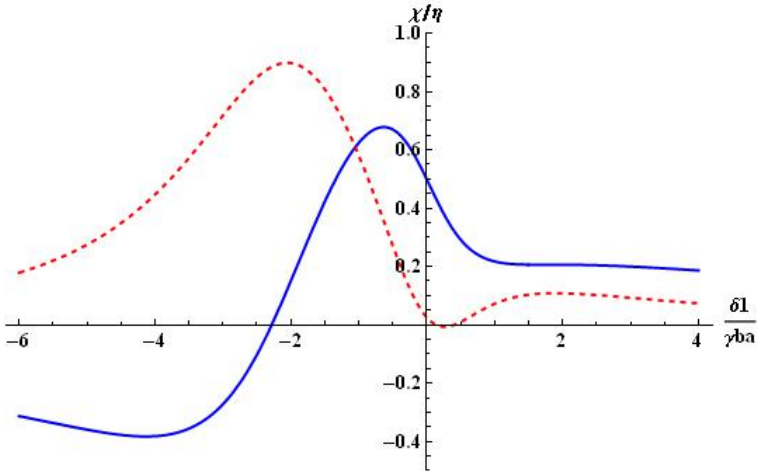

Fig. 4.3. The real (solid line) and imaginary (the dashed line) parts of the susceptibility are normalized to the resonant value of $\chi''_{\rm cb} = 3N\lambda_{\rm pr}^3 l\gamma_{\rm r}^{\rm cb}/(8\pi^2\gamma_{\rm cb}) = 1$, as functions of the detuning, $\delta_1/\gamma_{\rm cb}$. With $\gamma_{\rm cb} = 2\gamma_{\rm ba}$ and $\gamma_{\rm r}^{\rm cb} = 4\gamma_{\rm r}^{\rm ba}$.

If transition a↔b and b↔c have similar decay rates and decoherence rates and the population is fixed in the intermediate state, $\sigma_{\rm bb} = 1$, the maximum real part of susceptibility is achieved when the probe field is tuned to the middle of c↔a transition and the frequency separation between a↔b and b↔c transitions is twice the linewidth. The real and imaginary parts of the susceptibility for this case are plotted as a function of δ_2 in Fig. 4.2. There is a problem with this system though, near to the frequency of the probe field corresponding to the maximum refractive index with vanishing absorption lies a region of gain. It means that high refractive index can not be practically realized in this system due to super fluorescent depletion of an intermediate level.

To get rid of regions of gain we need the absorption due to transition b↔c to be larger, i.e. taking $\gamma_{\rm r}^{\rm cb}/\gamma_{\rm cb} > \gamma_{\rm r}^{\rm ba}/\gamma_{\rm ba}$, as well as being wider in frequency, i.e. $\gamma_{\rm cb} > \gamma_{\rm ba}$. Tuning the peak of the gain to the side of the absorption profile one can compensate absorption, keeping resonant enhancement of the refractive index

at the absorbing transition in the absence of any gain regions as shown in Fig. 4.3. Maximum RI at vanishing absorption in the absence of regions of gain is achieved when maximum gain compensates the absorption, with the detuning between amplifying resonance and absorbing resonances equal to a half line width of the absorbing transition, i.e. $\gamma_{\rm r}^{\rm ba}/\gamma_{\rm ba} = 2\gamma_{\rm r}^{\rm cb}/\gamma_{\rm cb}$ at $\omega_{\rm cb} - \omega_{\rm ba} = \gamma_{\rm cb}/2$. This maximum of χ' is equal to the maximum susceptibility of the absorbing two-level medium b$\leftrightarrow$c, $\chi' = (3/16\pi^2)N\lambda_{\rm pr}^3 l\gamma_{\rm r}^{\rm cb}/\gamma_{\rm cb}$ (as seen in Fig. 4.3).

It is worthwhile to note that the frequencies of the amplifying and ESA transitions can be changed by electric or magnetic fields via Stark or Zeeman effects or by composition, allowing for proper tuning of an amplifying resonance to the maximum of the refractive index at the ESA transition. The amplitudes of the ESA and the amplification resonances can be properly matched by choosing the incoherent pumping to appropriately modify the population differences of the corresponding transitions. Much more efficient control of the refractive index may be provided via coherent control of ESA as it is shown in Section 4.3.

4.3 Control of refractive index via coherent driving of the adjacent transition

The previously discussed ladder system is restrictive in the sense we need $\omega_{\rm cb} - \omega_{\rm ba}$ to have a specific value, as well as having restrictions on decay and decoherence rates to prevent regions of gain. We need a way to control the response of at least one of the two level transitions in order to provide a flexible tuning of the system to the optimal regime. Using coherent control we can manipulate the amplitude and frequency of the transitions. If $\gamma_{\rm r}^{\rm cb} > \gamma_{\rm r}^{\rm ba}$ and $\gamma_{\rm cb} > \gamma_{\rm ba}$ than it is appropriate to use a strong control field to make a far detuned lambda scheme using the ESA transition as discussed in Section 4.7. Here we will consider the case when the two transitions are of similar strength $\gamma_{\rm cb}^{\rm r} \leq \gamma_{\rm ba}^{\rm r}$ since we want the absorption provided by the ESA transition to be stronger and wider than the gain provided by the lower system; while our far detuned two photon response will be narrower and weaker than the original

transition. Therefore we add to the ladder system an auxiliary level $|\mathrm{d}\rangle$ coupled to the ground state $|\mathrm{a}\rangle$ by a coherent driving field and forming together a V system (see the Fig. 4.1(b)). This coherent driving allows for efficient control of the properties of the gain resonance and hence the refractive index of the total system.

We start with the steady state density matrix equations for the four level system, using the dipole approximation as well as the rotating wave approximation and assuming the probe field is much weaker than the control field similar to what was done in Section 2, we obtain:

$$0 = \delta_2\sigma_{\mathrm{cb}} - i\gamma_{\mathrm{cb}}\sigma_{\mathrm{cb}} + \alpha_2(\sigma_{\mathrm{cc}} - \sigma_{\mathrm{bb}}), \tag{4.2}$$

$$0 = (\delta_1 + \Delta)\sigma_{\mathrm{ba}} - i\gamma_{\mathrm{ba}}\sigma_{\mathrm{ba}} + \alpha_1(\sigma_{\mathrm{bb}} - \sigma_{\mathrm{aa}}) + \Omega\sigma_{\mathrm{bd}}, \tag{4.3}$$

$$0 = \delta_1\sigma_{\mathrm{bd}} - i\gamma_{\mathrm{bd}}\sigma_{\mathrm{bd}} + \Omega\sigma_{\mathrm{ba}} - \alpha_1\sigma_{\mathrm{ad}}, \tag{4.4}$$

$$0 = \Delta\sigma_{\mathrm{da}} - i\gamma_{\mathrm{da}}\sigma_{\mathrm{da}} - \Omega(\sigma_{\mathrm{aa}} - \sigma_{\mathrm{dd}}), \tag{4.5}$$

Solving these equations gives us the two coherences probed:

$$\sigma_{\mathrm{cb}} = \frac{\alpha_2(\sigma_{\mathrm{bb}} - \sigma_{\mathrm{cc}})}{\delta_2 - i\gamma_{\mathrm{cb}}}, \tag{4.6}$$

$$\sigma_{\mathrm{ba}} = \frac{-\alpha_1(\sigma_{\mathrm{bb}} - \sigma_{\mathrm{aa}})(\delta_1 - i\gamma_{\mathrm{bd}})}{(\Delta + \delta_1 - i\gamma_{\mathrm{ba}})(\delta_1 - i\gamma_{\mathrm{bd}}) - \Omega^2} + \frac{-\alpha\Omega^2(\sigma_{\mathrm{aa}} - \sigma_{\mathrm{dd}})}{(\Delta + i\gamma_{\mathrm{bb}})[(\Delta + \delta_1 - i\gamma_{\mathrm{ba}})(\delta_1 - i\gamma_{\mathrm{bd}}) - \Omega^2]}; \tag{4.7}$$

where Ω is the Rabi frequency of the control field, and the detuning of the control field is given by $\Delta = \omega_{\mathrm{da}} - \omega_{\mathrm{dr}}$. The one photon detuning of the lower transition is $\Delta + \delta_1 = \omega_{\mathrm{ba}} - \omega_{\mathrm{pr}}$, such that δ_1 is the two photon detuning. The one photon detuning of the upper transition is given by $\delta_2 = \omega_{\mathrm{cb}} - \omega_{\mathrm{pr}}$. Since the same probe field is probing both transitions, δ_1 and δ_2 are not independent, they are related by $\delta_2 = \delta_1 + \omega_{\mathrm{cb}} - \omega_{\mathrm{ba}} + \Delta$. Although the Eq. (4.6) and Eq. (4.7) were obtained for homogeneously broadened transitions, they remain approximately valid for inhomogeneously broadened transitions (with γ_{ij} denoting the total linewidth as discussed

in Section 2.6) when Δ greatly exceeds the inhomogeneous broadening. The total susceptibility for the system is given in terms of Eq. (4.6) and Eq. (4.7) as:

$$\chi = \frac{3N\lambda_{\mathrm{pr}}^3 l\gamma_{\mathrm{r}}^{\mathrm{ab}}}{8\pi^2}\frac{\sigma_{\mathrm{ab}}}{\alpha_1} + \frac{3N\lambda_{\mathrm{pr}}^3 l\gamma_{\mathrm{r}}^{\mathrm{cb}}}{8\pi^2}\frac{\sigma_{\mathrm{cb}}}{\alpha_2} \tag{4.8}$$

The influence of coherent driving on realization of resonant index enhancement is the most beneficial when the two-photon coherence, σ_{bd} decays much slower than polarization at the ESA transition: $\gamma_{\mathrm{db}} \ll \gamma_{\mathrm{cb}}$. This condition is typically fulfilled if adjacent level $|\mathrm{d}\rangle$ has the same parity as level $|\mathrm{b}\rangle$. One concern with the far-detuned V system is the system still has gain at the original transition, which can cause depopulation. This is not a problem in the Λ scheme.

4.4 Dressed-state analysis: an effective two-level system

As discussed in Section 4.3, the susceptibility in a V-configuration is inversely proportional to a quadratic polynomial in terms of the two-photon detuning with zeros of this polynomial corresponding to the two resonant contributions to the optical coherence. For the b$\leftrightarrow$a transition, we need to solve for the zeros of the polynomial:

$$0 = (\delta_1 - i\gamma_{\mathrm{db}})(\Delta + \delta_1 - i\gamma_{\mathrm{ba}}) - \Omega^2. \tag{4.9}$$

If we assume $\Delta \gg \Omega, \gamma_{\mathrm{bd}}, \gamma_{\mathrm{ba}}, \gamma_{\mathrm{da}}$; we can expand Eq. (4.7) into its two components:

$$\begin{aligned}\sigma_{\mathrm{ba}} = &\frac{\xi}{1+2\xi}\frac{-\alpha_1\sigma_{\mathrm{bb}}}{\delta_1 - \Delta\xi(1-\xi) - i\gamma_{\mathrm{bd}}(1-\xi) - i\gamma_{\mathrm{ba}}\xi} \\ &+ \frac{1+\xi}{1+2\xi}\frac{-\alpha_1(\sigma_{\mathrm{bb}} - \sigma_{\mathrm{aa}})}{\delta_1 + \Delta(1+\xi-\xi^2) - i\gamma_{\mathrm{ba}}(1-\xi) - i\gamma_{\mathrm{bd}}\xi}.\end{aligned} \tag{4.10}$$

In this work ω_{pr} is tuned to the vicinity of two-photon resonance ($\delta_2 \ll \Delta$) therefore the one photon contribution, the second term in Eq. (4.10), can be neglected when

$\gamma_{\rm ba}/\Delta \ll \xi$. We then have the resonant susceptibility given by the superposition of the upper two level absorption and the lower effective two level gain:

$$\chi_{\rm pr} = \frac{3N\lambda_{\rm pr}^3 l}{8\pi^2}\left[\frac{\gamma_{\rm r}^{\rm cb}}{\delta_2 - i\gamma_{\rm cb}} - \frac{\gamma_{\rm r}^{\rm ba}\sigma_{\rm bb}\xi/(1+2\xi)}{\delta_1 - \Delta\xi(1-\xi) - i\gamma_{\rm bd}(1-\xi) - i\gamma_{\rm ba}\xi}\right]. \qquad (4.11)$$

4.5 Implementation in transition doped crystals

A ladder scheme with intermediate populated level can be naturally realized in transition element doped crystals with excited state absorption. Such crystals were widely studied for the production of solid state-lasers or amplifiers in a wide range of frequencies from IR to VUV. The typical problem preventing lasing in many otherwise promising crystals was the re-absorption of the emitted radiation or the pumping field from an excited metastable laser level to the higher laying energy levels. If the ESA cross-section exceeds the cross-section of the emitting transition, lasing/amplification becomes completely impossible. For example, ESA of emitted radiation made lasing impossible in V^{3+}:$LiAlO_2$, $LiGaO_2$ (at 1400-1800nm) [68], Cr^{4+}:$LiAlO_2$, $LiGaO_2$ (at 1200-1600nm) [69], Ni^{2+}:$MgAl_2O_4$ (at 1100-1300nm) [70], Nd^{3+}:Y_2O_3 (at 1330nm) [71], Ce^{3+}:YAG (at 500nm-600nm) [72], Pr^{3+}:YAG (at 488nm) [73], Pr^{3+}:$LiLuF_4$ (at 255nm) [74] and in many other crystals. In many transition element doped crystals an operating transition is chosen to be a parity forbidden intraconfigurational 4fn-4fn transition. It is easy to produce a population inversion at such a transition since the upper state is metastable. At the same time ESA often occurs at the parity allowed intraconfigurational 4fn-15d-4fn transition. For this reason the ESA cross-section is similar to the cross-section at the emitting transition. Thus such systems are potentially promising for realization of resonant enhancement of refractive index with vanishing absorption in a ladder configuration with excited intermediate state.

Transition element doped crystals are perfect for implementation of our scheme because many have transitions with excited state absorption, and unlike gases, high

densities can be achieved without directly increasing the linewidth. Crystals typically have densities as high as 10^{23}atoms/cm^3, and the amount of doping can be between .001% and 10%, so densities will be between 10^{18}cm^{-3} and 10^{22}cm^{-3}.

With these benefits there are of course also drawbacks. The reason that there is frequently ESA is that nearly every transition in the dopant is allowed due to the admixture of the crystal field with the energy levels, but this also means that the transition dipole moments are weaker than they would be in the free atom. Therefore, oscillator strengths in transition element doped crystals tend to vary from 10^{-6} to 10^{-8}.

The other drawback is that there is always strong inhomogeneous broadening. Since the atoms are held in place by the crystal structure, this is not due to Doppler broadening as it is in gases, rather it is due to disturbances of the crystal field such that each dopant sees a different local environment and therefore has a slightly different transition frequency. Any impurities in the crystal or different isotopes of the constituent atoms will disturb the local environment of the crystal, and this can only be fixed by limiting unwanted impurities and/or by growing crystals from single isotopes [75]. The dopants themselves also disturb the crystal field, as their density increases there can be distortions of the crystal structure, and there will be slight variations of the crystal field each dopant sees based on the random distribution of dopants. This can be reduced by taking low dopings, although that will in turn reduce our RI change. A better option is to choose a dopant where the atomic size closely matches the atom it replaces in the crystal such as Erbium replacing Yttrium, which reduces the strain induced in the crystal with higher doping.

Another major issue with linewidths in transition element doped crystal is that at room temperature the creation of phonons will broaden the transitions by several orders of magnitude. Therefore in order to minimize the linewidth it is necessary to work at low temperature (typically lower than 70K) when phonon broadening is small as compared to inhomogeneous broadening.

Let us estimate the maximum value of RI with zero absorption which could be reached in a transition element doped crystal. As it was shown above the maximum RI with zero absorption is defined by the maximum value of the real part of the RI in the ESA transition:

$$\chi'_{\max} = \frac{3N\lambda_{\rm pr}^3 l}{16\pi^2}\frac{\gamma_{\rm r}}{\gamma}, \tag{4.12}$$

where $\gamma_{\rm r}$ is the radiative decay rate and γ is the total HWHM linewidth. We need to make an estimate for $\gamma_{\rm r}/\gamma$, for forbidden intraconfigurational $4f^n$-$4f^n$ transition the radiative linewidth is of an order of 10Hz-100kHz and the typically inhomogeneous broadening is of an order of 100kHz-10GHz. For parity allowed intraconfigurational $4f^n$-15^d-$4f^n$ transitions the radiative linewidth is of an order 100kHz-1GHz and the inhomogeneous broadening is of an order 1GHz-1THz. For example, with the following reasonable assumptions $\mathrm{N} = 1 \cdot 10^{\ 20}\mathrm{cm}^{-3}$, $n = 1.8$, $\lambda = 600$nm, and $\gamma_{\rm r}/\gamma = 1 \cdot 10^{-5}$ and $\rho = 1$, we get the maximum susceptibility of 7.2 i.e., a RI change of about 1.43. We can see that while solids may have some drawbacks such as needing low temperatures the expected RI is higher than the one we found for gases in Section 3.4.

The intensity of the driving field required for coherent control of the refractive index will be the major limiting factor to deciding which crystals and dopants can be used for our RI enhancement scheme. The intensity will scale with the square of the Rabi frequency and inversely scale with the square of the dipole moment for the a↔d transition:

$$I_{\rm da} = \frac{2\hbar^2 cn\epsilon_0}{d_{\rm ad}^2}\Omega^2 = \frac{16\pi^2\hbar cn}{3\lambda_{\rm c}^3\gamma_{\rm r}^{\rm da}}\Omega^2, \tag{4.13}$$

where c is the speed of light, ϵ_0 is the electric permittivity of free space, and $\lambda_{\rm c}$ is the wavelength of the control field. In order to have achievable intensities, or at least intensities that will not damage the crystal it is important to work with as small a Rabi frequency as possible, although this is less of a concern if we use long pulses instead of a continous wave (CW) beam. At the same time for our

Table 4.1
Measured decoherence for a few transitions

Crystal	Transition	λ	Density	γ
Er^{3+}:$LiYF_4$	$^4I_{15/2} \leftrightarrow ^4I_{13/2}$	1530nm	.1% doping	15MHz [76]
Er^{3+}:Y_2SiO_5	$^4I_{15/2} \leftrightarrow ^4I_{13/2}$	1539nm	.1% doping	150MHz [76]
Er^{3+}:$LiNbO_3$	$^4I_{15/2} \leftrightarrow ^4I_{13/2}$	1532nm	.1% doping	180GHz [76]
Nd^{3+}:YVO_4	$^4I_{9/2} \leftrightarrow ^4F_{3/2}$	880nm	.001% doping	900MHz [76]
Pr^{3+}:YAG	$^3H_4 \leftrightarrow ^1D_2$	610nm	.1% doping	60GHz [76]

two photon feature to have the same susceptibility of the original transition we need $\Omega \gg \Delta^2\gamma_{\rm bd}/\gamma_{\rm ba}$, although we can still get a significant contribution as long as $\Omega \simeq \Delta^2\gamma_{\rm bd}/\gamma_{\rm ba}$. Therefore it is imperative to choose crystals that allow us to have a small one photon detuning Δ. There are two factors that determine Δ.

The first is the general need to stay far detuned, which implies that $\Delta \gg \gamma_{\rm ba}$. This can only be improved by choosing crystals with small inhomogeneous broadening. Unfortunately since the inhomogeneous broadening can only be measured at low temperatures and can be highly different for the same dopant in different crystals or with different densities, it is not something that is recorded for many crystals in the literature and is not easily estimated. In fact no two crystals grown (even with the same amount of doping) will have the exact same decoherence properties. This lack of information is especially true for the higher transitions that are not connected to the ground state, for lower transitions there is interest in the linewidths from groups interested in optical quantum memories, some of which is given in Table 4.1. The key thing to notice is that crystals where Erbium replaces Yttrium are the best bet for getting small inhomogeneous broadening.

The second factor is that for the probe field to address both the lower transition and the two photon effective transition than the one photon detuning of the control field must be chosen to be similar to the difference in transition frequencies between the upper and lower transitions i.e., $\Delta \simeq \omega_{\rm ba} - \omega_{\rm cb}$. This means when we are

Table 4.2
Frequency differences for ESA transitions

Crystal	a↔b Transition	b↔c Transition	λ (nm)	$\omega_{cb} - \omega_{ba}$
Er^{3+}:YAG	$^4I_{15/2} \leftrightarrow ^4I_{9/2}$	$^4I_{9/2} \leftrightarrow ^4G_{9/2}$	813.2nm	-20GHz [77]
Nd^{3+}:YAG	$^4I_{9/2} \leftrightarrow ^4I_{15/2}$	$^4I_{15/2} \leftrightarrow ^4F_{3/2}$	1776.5nm	150GHz [78]
Er^{3+}:YLF	$^4I_{15/2} \leftrightarrow ^4I_{9/2}$	$^4I_{9/2} \leftrightarrow ^4H(2)_{9/2}$	800nm	270GHz [79]
Er^{3+}:YAG	$^4I_{15/2} \leftrightarrow ^4I_{11/2}$	$^4I_{11/2} \leftrightarrow ^4F_{7/2}$	975.1nm	120GHz [77]

looking for an appropriate ESA transition, we need transitions that actually have very closely matched frequencies. Although there are close transitions in Er, Nd, and Pr, the transition frequencies are different for every crystal so only by examining the low temperature spectrum of many crystals can a useful ESA transitions be found. When looking for these transitions it is important to remember that it is okay to use the higher Stark levels, except for level b, where we must use the lowest Stark level so that we can pump the population into the transition effectively. Some of the smaller frequency differences that we have found by studying low temperature spectrum are shown in Table 4.2.

4.6 Physical realization

Therefore the best approach is to choose a crystal that has low inhomogeneous broadening with a closely matched ESA transition. In particular Er^{3+}:YAG or Er^{3+}:YLF combines the two properties we want. As the best possible example consider the $^4I_{15/2} \leftrightarrow ^4I_{9/2} \leftrightarrow ^4G_{9/2}$ transition in Er^{3+}:YAG at 813.2nm where $\omega_{ba} - \omega_{cb} =$ 20GHz. Then we have $\gamma_r^{ba} = 45$Hz and $\gamma_r^{ba} = 15$Hz [40]. The control field can be applied to $^4I_{15/2}$ and $^4S_{3/2}$ which has a stronger dipole moment with $\gamma_r^{da} = 1.16$kHz. At the same time the linewidth between d↔b should not be too large since this is close to not being an allowed transition with $\gamma_r^{db} = .7$Hz. Taking $N = 1.4 \cdot 10^{21}\text{cm}^{-3}$ and low enough temperature to limit phonon broadening we assume with a relatively

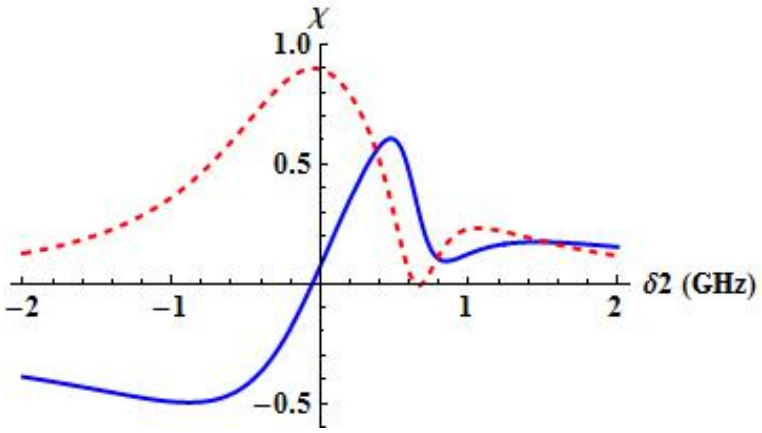

Fig. 4.4. Susceptibility for the implementation in Er^{3+}:YAG as described in the text, where for numerical calculations we assume $\gamma_{da} = 1$GHz. The dashed line red line is Imχ and the solid blue line gives the Reχ.

pure crystal we can have low inhomogeneous broadening $\gamma_{cb} = .8$GHz, $\gamma_{ba} = 0.3$GHz, and $\gamma_{db} = 0.2$GHz.

Normally YAG has a refractive index of $n_{bg} = 1.82$. We take $\Delta = 20.56$GHz and $\Omega = 5.1$GHz, according to Eq. (4.13) in order to get this Rabi frequency we need a control field of intensity $I = 1.34 \cdot 10^5$ W/m^2 at $\lambda_{dr} = 545$nm. Taking these numbers we can implement our scheme for refractive index enhancement as shown in Fig. 4.4 to achieve $\Delta n = .097$.

4.7 Implementation with far-detuned Λ scheme

If the physical system has $\gamma_r^{cb} > \gamma_r^{ba}$ and $\gamma_{cb} > \gamma_{ba}$ or we do not want any regions of gain no matter how far detuned from the probe field, than it is appropriate to use a strong control field to make a far detuned lambda scheme using the ESA transition as shown in Fig. 4.5. In this case the susceptibility is given by:

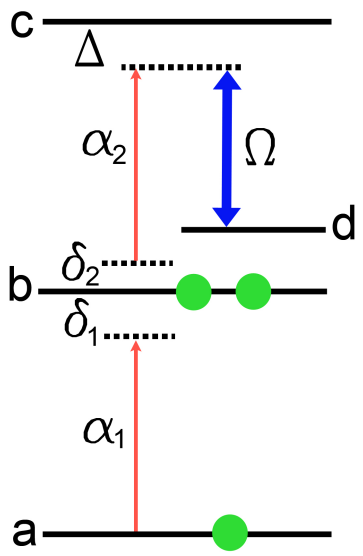

Fig. 4.5. Energy level diagram for the ladder system with absorption controlled by an effective lambda system.

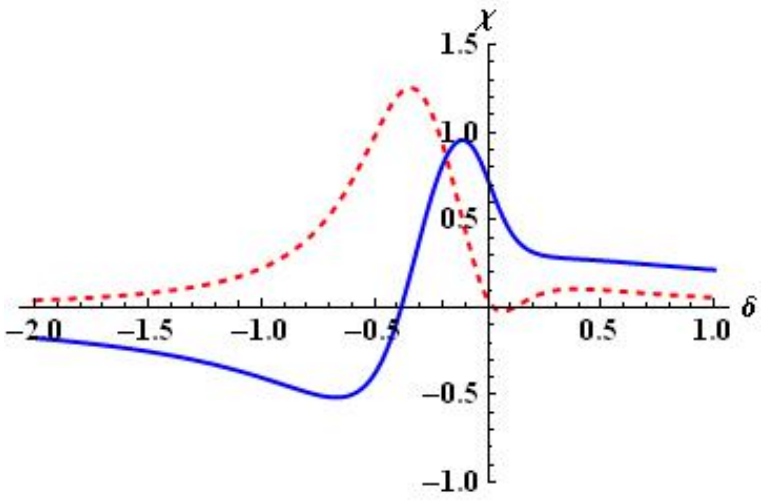

Fig. 4.6. Susceptibility for the implementation in Er^{3+}:YAG at 990nm as described in the text. The dashed line red line is Imχ and the solid blue line gives the Reχ.

$$\chi_{\rm pr} = \frac{3N\lambda_{\rm pr}^3 l}{8\pi^2}\left[\frac{\gamma_{\rm r}^{\rm ba}(\sigma_{\rm bb}-\sigma_{\rm aa})}{\delta_1 - i\gamma_{\rm ba}} - \frac{\gamma_{\rm r}^{\rm cb}\sigma_{\rm bb}\xi/(1+2\xi)}{\delta_2 - \Delta\xi(1-\xi) - i\gamma_{\rm bd}(1-\xi) - i\gamma_{\rm cb}\xi}\right]. \qquad (4.14)$$

When possible, using a far-detuned Λ scheme is a better way to implement refractive index enhancement since now the far-detuned one-photon feature provides absorption instead of gain, therefore unlike the V scheme there is no gain at all in the system. This means there will be no possibility for stimulated emission, making it much easier to keep some population pumped into the intermediate level. Even for the case of similar transition strengths it is also possible to use the far-detuned Λ scheme by using the pumping rate as a free variable to lower the two level gain. While we still need a population inversion, we do not need to pump all of the population to the intermediate level instead we can pump only a small fraction over half, and therefore lowering the gain, but also lowering the total susceptibility that can be achieved. We therefore define the pump parameter p = $(\sigma_{\rm bb} - \sigma_{\rm aa})/\sigma_{22}$.

For implementation of this scheme consider the $^4I_{15/2} \leftrightarrow {}^4I_{11/2} \leftrightarrow {}^4F_{7/2}$ transition in Er^{3+}:YAG at 990nm where $\omega_{cb} - \omega_{ba} = 120$GHz. Then we have $\gamma_r^{ba} = 118.2$Hz and $\gamma_r^{cb} = 67.3$Hz [40]. The control field can be applied to $^4I_{9/2}$ and $^4F_{7/2}$ with $\gamma_r^{da} = 78.3$Hz. At the same time the linewidth between d$\leftrightarrow$b should not be too large since this is close to not being an allowed transition with $\gamma_r^{db} = .5$Hz. Taking $N = 1.4 \cdot 10^{21} \text{cm}^{-3}$ and low enough temperature to limit phonon broadening, we again assume a relatively pure crystal with low inhomogeneous broadening $\gamma_{cb} = 1$GHz and $\gamma_{ba} = \gamma_{db} = 0.2$GHz, and = 0.2GHz. We take $\Delta = 99.1$GHz, $\Omega = 49$GHz, and p = .025. Taking these numbers we can implement our scheme for refractive index enhancement as shown in Fig. 4.6 to achieve $\Delta n = .063$. Although we must point out that since the difference in transition frequencies was large at 120GHz, the control field Rabi frequency also comes out to be very high. With a Rabi frequency that would not be achievable in a CW-regime, but can be achieved in long pulses. In order to implement this scheme with a low intensity control field it would be necessary to find a crystal where the transition frequencies are closer and/or a crystal where the excited state absorption cross-section is much larger than the gain transition cross-section. Such that absorption starts off much stronger and wider, before we create the effective two level system at two-photon resonance which is always weaker and narrower than the original transition.

4.8 Conclusion

A three-level scheme with populated intermediate level coupled to the probe field in the ladder configuration is suggested for realization of the resonant enhancement of the refractive index with zero absorption in the absence of any gain region. It is shown that coherent driving of the auxiliary transition forming together either a far-detuned V or Λ system allows for efficient control of the gain or absorption transition and accordingly allows for the optimization of the parameters of the system. Transition element doped crystals possessing strong ESA at the emission wavelength represent

themselves as natural candidates for practical implementation of such schemes. At low temperature when phonon broadening is negligible, a high density of impurities may result in achievement of high resonantly enhanced refractive index, $\Delta n \simeq 1.4$. We have shown one case where with reasonable drive field intensity Er^{3+}:YAG can be used to achieve $\Delta n = .1$ at 813.2nm.

5. OPTICALLY CONTROLLABLE PHOTONIC STRUCTURES WITH ZERO ABSORPTION

5.1 Introduction

One, two, or three dimensional periodic heterostructures made of two dielectric materials with different refractive indexes, such as distributed Bragg reflectors (DBR), holey fibers, or photonic crystals find many applications, including reflective coatings, distributed feedback lasers, and optical cavities. Different technologies such as photo-lithography, etching, drilling, and self-assembling are used for construction of such structures.

We suggest a method to produce transparent photonic structures in a homogeneous resonant atomic media, such as dielectrics with homogeneously distributed impurities, atomic, or molecular gases, simply by illuminating these materials with standing waves of a laser field. Such optically produced photonic structures could easily be controlled (including switching on/off, changing amplitude and period of modulation) and would be highly selective in frequency, naturally limited by the width of the optical resonance.

In all of the previous proposals [19–22, 44, 57] the RI was uniform in space. Moreover, an enhancement of the RI with vanishing resonant absorption was achieved only at a particular detuning of the probe field from atomic resonance and was accompanied by either absorption or gain at the neighboring detunings. Thus, none of those proposals was suitable for achieving spatial modulation of refractive index with zero absorption. Our proposal [50] is based on spatial modulation of the energy of a populated intermediate state in a nearly degenerate ladder configuration via the ac-Stark effect due to a standing wave field which results in a spatially dependent detuning leading to a periodic resonant increase and decrease of the refractive index in space while simultaneously keeping transparency of the medium.

5.2 A ladder system with optically modulated position of an intermediate state as 1D photonic crystal

Consider the interaction of a probe field with a medium of three level atoms in a ladder configuration such that the probe field interacts with both transitions as illustrated in the inset of Fig. 5.1. The transition frequencies ω_{21} and ω_{32} are close to each other so that the probe field with frequency ω_p interacts simultaneously with both transitions and for a weak probe Rabi frequency $\Omega_p << \gamma_{21}, \gamma_{32}$ the susceptibility is defined as the sum of the susceptibilities of two two-level transitions:

$$\chi = \frac{3N\lambda_{\rm pr}^3 l}{8\pi^2}[\frac{\gamma_{\rm r}^{21}(\rho_1-\rho_2)}{\delta_{21}-i\gamma_{21}} + \frac{\gamma_{\rm r}^{32}(\rho_2-\rho_3)}{\delta_{32}-i\gamma_{32}}]. \tag{5.1}$$

Here N is the atomic density, l is the Lorentz local field correction factor discussed in Section 2.5, the detunings are defined as $\delta_{21} = \omega_{21} - \omega_p$ and $\delta_{32} = \omega_{32} - \omega_p$, $\lambda_{\rm pr}$ is the probe field wavelength in the medium, $\gamma_{\rm r}^{ij}$ is the radiative decay rate for the i$\leftrightarrow$j transition, γ_{ij} is the total decoherence rate, and ρ_i is the population in the i$^{\rm th}$ energy level. We assume that the amplitudes of both transitions are matched but of opposite sign:

$$\gamma_{\rm r}^{21}(\rho_1-\rho_2) = -\gamma_{\rm r}^{32}(\rho_2-\rho_3). \tag{5.2}$$

which means that one of the two transitions is inverted. Let it be transition 2$\leftrightarrow$1 i.e., $\rho_2 - \rho_1 > 0$. We also assume the widths of the transitions are equal $\gamma_{21} = \gamma_{32}$ and the probe field is tuned to two photon resonance, i.e. $\omega_p = \omega_{31}/2$. Thus for arbitrary position of level 2 the blue detuning of the probe field from one of two two-level transitions is equal to the red detuning from the other, i.e. $\delta_{32} = -\delta_{21} = \delta$, leading to the remarkable property that gain at one transition and absorption at

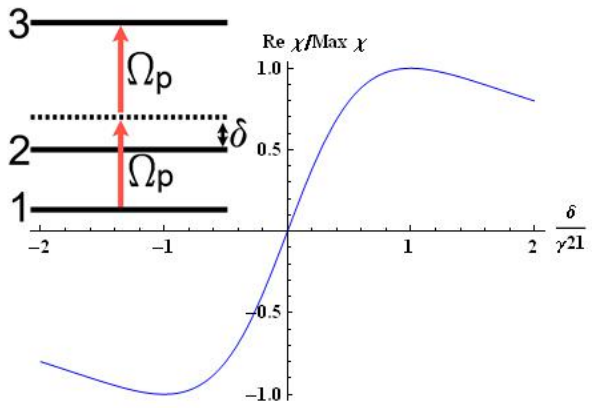

Fig. 5.1. Real part of the susceptibility as a function of the level shift δ. Note that the imaginary part is identically zero. Inset: the energy level diagram for the corresponding three level scheme.

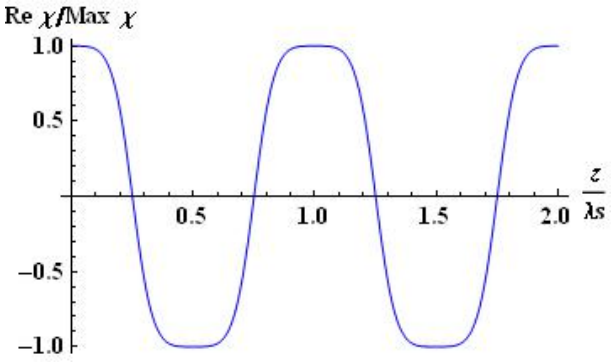

Fig. 5.2. Real part of the susceptibility plotted as a function of position along the optical axis.

another one cancel each other while the real part of susceptibility is doubled. So, the susceptibility is purely real:

$$\chi = \frac{3N\lambda_{\rm pr}^3 l\gamma_{\rm r}^{21}(\rho_1 - \rho_2)}{8\pi^2}\frac{2\delta}{\delta^2 + \gamma_{21}^2}. \tag{5.3}$$

It means that the probe field neither experiences absorption nor gain independently

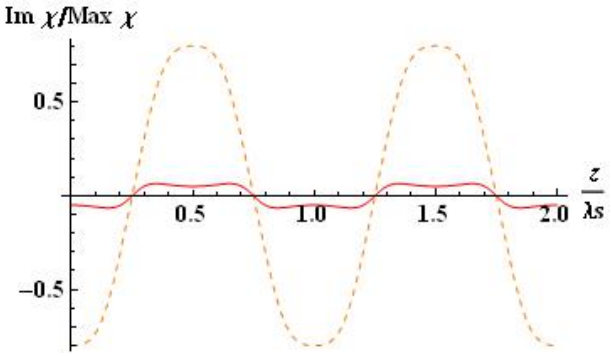

Fig. 5.3. Imaginary part of the susceptibility for a probe field detuned from resonance by $\gamma_{21}/20$ (solid) and γ_{21} (dashed) plotted as a function of position along the optical axis.

of level 2's energy, i.e. for arbitrary values of δ. At the same time the resonant susceptibility varies from the minimum to the maximum value as δ is shifted from $-\gamma$ to γ as shown in Fig. 5.1. If the energy of the intermediate level is modulated in space along the direction of propagation of the probe field, the refractive index is also modulated. Such spatial modulation can be produced along the optical axis via the ac-Stark shift. A control laser field $E_s\cos(\omega_s t)$ applied at the $0\leftrightarrow 2$ transition adjacent to the $1\leftrightarrow 2$ transition and far detuned from this transition $\Delta_s = \omega_s - \omega_{20} >> \gamma_{20}$ would result in a splitting of the intermediate state 2 into two ac-Stark sublevels shifted in frequency by $-|\Omega_s|^2/\Delta_s$ and $\Delta_s + |\Omega_s|^2/\Delta_s$, respectively, where Ω_s is the associated Rabi frequency. The probe field is far out of resonance with the transitions from the second Stark sublevel from both level 1 and level 3 and, therefore its interaction with these transitions is negligible while the first Stark sublevel is slightly shifted from the original level 2 and strongly interacts with the probe field. In other words, the susceptibility at each transition ($2\leftrightarrow 1$ or $2\leftrightarrow 3$), which in general consists of two terms associated with the one-photon and two-photon resonances is reduced to the one-photon contribution and has the same form as given by Eq. (5.3), just with shifted transition frequencies.

If the control field represents itself as a standing wave such that the Rabi frequency is a function of position inside the medium, $\Omega_s(\mathrm{z}) = \Omega_s \cos(k_s \mathrm{z})$, then the ac-Stark shift of level 2 is given by:

$$\Delta E = -\frac{\hbar|\Omega_s|^2}{2\Delta_s} - \frac{\hbar|\Omega_s|^2}{2\Delta_s}\cos(2k_s \mathrm{z}). \tag{5.4}$$

Thus it consists of a constant shift, $|\Omega_s|^2/2\Delta_s$, as well as a sinusoidal modulation, $(|\Omega_s|^2/2\Delta_s)\cos(2k_s \mathrm{z})$. If the difference between the atomic transition frequencies $\omega_{32} - \omega_{21}$ is chosen to be equal to $-|\Omega_s|^2/\Delta_s$ then the susceptibility is described by Eq. (5.3) with $\delta = (|\Omega_s|^2/2\Delta_s)\cos(4\pi \mathrm{z}/\lambda_\mathrm{s})$ (where λ_s is the wavelength of the control field in the medium). Hence the refractive index will be modulated symmetrically with respect to its background value as shown in Fig. 5.2. The spacial period $\lambda_\mathrm{s}/2$ is defined by the wavelength, while the modulation depth $-|\Omega_s|^2/\Delta_s$ is defined by the Rabi frequency of the modulating field Ω_s. To provide the maximum amplitude of refractive index modulation the Rabi frequency of the control field should meet the condition $\Omega_s^2 = 2\gamma\Delta_s$.

With a strong enough index variation a transparent for a particular frequency 1-D photonic crystal can be created with properties that are optically controlled. Similarly a 2-D or 3-D photonic structure can be produced by application of 2 or 3 orthogonal modulating control fields. Even for index variations much smaller than the background RI the medium will behave as a distributed Bragg reflector if $\lambda_\mathrm{s} \simeq \lambda_\mathrm{pr}$ specifically, when the wavelength mismatch is within the width of the Bragg band-gap, $\lambda_\mathrm{s} - \lambda_\mathrm{pr} < \lambda_\mathrm{s}\Delta n/(\pi n_\mathrm{bg})$. Since the medium remains transparent, many periods of spatial RI structures can be used as needed to achieve the required reflection coefficient.

When the probe field is detuned from two-photon resonance with $1 \leftrightarrow 3$ transition it will experience either gain or absorption. The question arises if such gain may result in the building up of a spontaneously amplified field emptying the inverted transition and limiting the propagation length of the probe field in the medium with periodic

refractive index. Fortunately, this is not the case. Indeed, since the position of the intermediate level is periodically modulated in space, then a detuned probe field experiences periodically interchanging regions of gain and absorption suppressing the development of such an instability as can be seen in Fig. 5.3. In fact averaging the absorption over a wavelength λ_s shows that the medium is effectively transparent even when the probe field is detuned from resonance.

5.3 An effective ladder system with optically tunable parameters

The simple model of a ladder system previously discussed assumed the existence of two transitions possessing equal linewidths, equal products of transition strength and population difference, and nearly degenerate (on the scale of the linewidth) frequencies. It is difficult if not impossible to meet these conditions in a real atomic system. However, it is possible to construct an effective ladder system whose upper transition has controllable parameters which could be optically tuned to satisfy these conditions.

It can be accomplished by adding to the original simple ladder system along with the modulating control field E_s coupled to an adjacent transition $0 \leftrightarrow 2$ (as discussed earlier) a second control field E_c coupling the excited state 3 to an additional unpopulated level 4 as shown in Fig. 5.4. This second far-detuned control field ($\Delta_c >> \gamma_r^{32}, \Omega_c$ where $\Delta_c = \omega_{43} - \omega_c$ and Ω_c is the control field Rabi frequency) is chosen to satisfy approximately the two-photon resonance condition: $\omega_c - \omega_{pr} = \omega_{42}$, forming together with the probe field a far-detuned lambda scheme. A strong far-detuned field results in an ac-Stark splitting of level 3 and the response to the probe field consists of two terms representing one-photon (upper Stark sublevel) and two-photon (lower Stark sublevel) contributions in the same way as previously discussed. But now it is the two-photon contribution which plays a dominant role due to the two-photon resonance condition. [44, 54]

We consider a driving field coupling the non-populated levels. Hence this field does not change the population distribution which is provided by incoherent pumping. This field will be chosen such that it is not close to the probe frequencies so it does not act on the other transitions. Since the populations are fixed and the probe field is weak the density matrix equations for the lower two-level system and upper three-level lambda scheme are not coupled to each other. Hence the total susceptibility of the system is the sum of susceptibilities of the corresponding two-level and three-level systems. Considering a steady state solution of the density matrix equations for the four level system, using the dipole approximation as well as the rotating wave approximation and assuming the probe field is much weaker than the control field as derived in Section 2, we obtain:

$$\chi = \frac{3N\lambda_{\rm pr}^3 l}{8\pi^2}\left\{\frac{-\gamma_{\rm r}^{21}}{\delta_1 - i\gamma_{21}} + \frac{\gamma_{\rm r}^{32}(\delta_2 - i\gamma_{42})}{(\Delta_{\rm c} + \delta_2 - i\gamma_{32})(\delta_2 - i\gamma_{42}) - \Omega_{\rm c}^2}\right\}; \tag{5.5}$$

where $\Omega_{\rm c}$ is the Rabi frequency of the control field, and the detuning of the control field is given by $\Delta_{\rm c} = \omega_{34} - \omega_{\rm c}$. The one photon detuning of the lower transition is $\delta_1 = \omega_{21} - \omega_{\rm pr}$. The one photon detuning of the upper transition is given by $\Delta_{\rm c} + \delta_2 = \omega_{32} - \omega_{\rm pr}$, such that the two photon detuning of the upper transition is δ_2. Since the same probe field is probing both transitions, δ_1 and δ_2 are not independent, they are related by $\delta_2 = \delta_1 + \omega_{32} - \omega_{21} - \Delta_{\rm c}$. Though the Eq. (5.5) was obtained for homogeneously broadened transitions it remains approximately valid for inhomogeneously broadened transitions (with $\gamma_{\rm ij}$ denoting the total linewidth as discussed in Section 2.6) when $\Delta_{\rm c}$ greatly exceeds the inhomogeneous broadening.

The influence of coherent driving on realization of resonant index enhancement is the most beneficial when the two-photon coherence, σ_{42} decays much slower than polarization at the ESA transition: $\gamma_{42} \ll \gamma_{32}$. This condition is typically fulfilled if adjacent level $|4\rangle$ has the same parity as level $|2\rangle$.

As discussed in Section 2.7, the susceptibility in a Λ-configuration is inversely proportional to a quadratic polynomial in terms of the two-photon detuning with ze-

ros of this polynomial corresponding to the two resonant contributions to the optical coherence. If we take a further approximation keeping the most necessary terms to keep the position, linewidth, and amplitude accurate up to ξ^2, than we have:

$$\chi_{32}^{2\mathrm{ph}} \simeq \frac{3N\lambda_{\mathrm{pr}}^3 l}{8\pi^2} \frac{(\sigma_{22}-\sigma_{33})\gamma_{\mathrm{r}}^{32}\xi/(1+2\xi)}{\delta_2 - \frac{|\Omega_{\mathrm{c}}|^2}{\Delta_{\mathrm{c}}}(1-\xi) - i[\gamma_{42}(1-\xi)+\gamma_{32}\xi]}, \tag{5.6}$$

$$\chi_{32}^{1\mathrm{ph}} \simeq \frac{3N\lambda_{\mathrm{pr}}^3 l}{8\pi^2} \frac{(\sigma_{22}-\sigma_{33})\gamma_{\mathrm{r}}^{32}(1+\xi)/(1+2\xi)}{\delta_2 + \Delta_{\mathrm{c}} + \frac{|\Omega_{\mathrm{c}}|^2}{\Delta_{\mathrm{c}}}(1-\xi) - i[\gamma_{32}(1-\xi)+\gamma_{42}\xi]}. \tag{5.7}$$

In this work ω_{pr} is tuned to the vicinity of two-photon resonance ($\delta_2 \ll \Delta_{\mathrm{c}}$) therefore the one photon contribution can be neglected when $\gamma_{32}/\Delta \ll \xi$. We then have the resonant susceptibility given by the superposition of the lower two level gain and the upper effective two level absorption:

$$\chi_{32} = \frac{3N\lambda_{\mathrm{pr}}^3 l}{8\pi^2} \left\{ \frac{(\sigma_{11}-\sigma_{22})\gamma_{\mathrm{r}}^{21}}{\delta_1 - i\gamma_{21}} + \frac{(\sigma_{22}-\sigma_{33})\gamma_{\mathrm{r}}^{32}\xi/(1+2\xi)}{\delta_2 + \Delta_{\mathrm{c}} + \frac{|\Omega_{\mathrm{c}}|^2}{\Delta_{\mathrm{c}}}(1-\xi) - i[\gamma_{32}(1-\xi)+\gamma_{42}\xi]} \right\} \tag{5.8}$$

Now if we apply the same modulated field discussed in Section 5.2 we get a similar shift of level 2. As a result, the total five level system under the formulated above conditions is reduced to an effective three-level ladder system with the lower transition 1↔2" and the upper transition 2"↔3'. Its susceptibility takes the form:

$$\chi_{\mathrm{res}} = \frac{3N\lambda_{\mathrm{pr}}^3 l}{8\pi^2} \frac{\gamma_{\mathrm{r}}^{21} p/(2-p)}{\delta_{\mathrm{p}} + \frac{\Omega_s^2}{2\Delta_{\mathrm{s}}} + \delta - i\gamma_{21}} + \frac{3N\lambda_{\mathrm{pr}}^3 l}{8\pi^2} \frac{\xi\gamma_{\mathrm{r}}^{32}/[(2-p)(1+2\xi)]}{\delta_{\mathrm{p}} - \omega_{32} + \omega_{21} - \frac{\Omega_{\mathrm{s}}^2}{2\Delta_{\mathrm{s}}} - \delta + \Delta_{\mathrm{c}}(1+\xi-\xi^2) - i[\gamma_{42}(1-\xi)+\gamma_{32}\xi]}; \tag{5.9}$$

where we assume incoherent pumping (not shown in Fig. 5.4) which provides the necessary population inversion, represented by the pumping factor $p = (\rho_2 - \rho_1)/\rho_2$, while assuming level 3 is empty. Also to avoid confusion we have renamed the one photon detuning of the lower level to $\delta_{\mathrm{p}} = \omega_{21} - \omega_{\mathrm{pr}}$, and replaced the modulation detuning of Section 5.2 with $\delta_{\mathrm{M}} = (|\Omega_s|^2/2\Delta_s)\cos(4\pi z/\lambda_{\mathrm{s}})$.

5.4 Matching the effective absorption to gain

We can now use what we learn from Eq. (5.9) in order to reproduce the results of Section 5.2. The parameters of the effective upper 2"↔3' and lower 1↔2" transitions defined by the control fields can easily be matched.

We choose $\Omega_s = \sqrt{2\gamma_{21}\Delta_s}$ to provide the maximum range of refractive index modulation. Matching the linewidth of 3'↔2" transition to that of 2"↔1 defines the control field parameter ξ:

$$\xi = \frac{\gamma_{21} - \gamma_{42}}{\gamma_{32} - \gamma_{42}}. \tag{5.10}$$

It implies a larger linewidth of the upper 2"↔3' transition as compared to the lower transition 1↔2", $\gamma_{32} > \gamma_{21}$, and relatively slow decay of the coherence at the 4↔2" transition: $\gamma_{42} < \gamma_{32}, \gamma_{21}$. Matching the amplitudes defines the pump parameter as:

$$p = \frac{\gamma_{\mathrm{r}}^{32}}{\gamma_{\mathrm{r}}^{21}} \frac{\xi}{1 + 2\xi}. \tag{5.11}$$

We take the probe field to be resonant with the dressed transition 2"↔1 such that $\delta_{\mathrm{p}} = -\Omega_{\mathrm{s}}^2/2\Delta_{\mathrm{s}}$. Then matching the frequencies of the transitions defines the required detuning of the control field Δ_{c}:

$$\Delta_{\mathrm{c}} = \frac{\omega_{32} - \omega_{21} + 2\gamma_{21}}{1 + \xi - \xi^2}. \tag{5.12}$$

This implies that Δ_{c} will be on the same order as $\omega_{32} - \omega_{21}$. Since $|\Omega_{\mathrm{c}}| = \sqrt{\xi}\Delta_{\mathrm{c}}$ and $\Delta_{\mathrm{c}} \approx \omega_{32} - \omega_{21}$, it is important to have 1↔2 and 2↔3 transitions with close frequencies in order to reduce the required control field intensity. Under the above conditions the susceptibility given by Eq. (5.9) takes the same form as in Eq. (5.3). Thus, it becomes possible to realize resonant modulation of refractive index with zero absorption/gain in the realistic system.

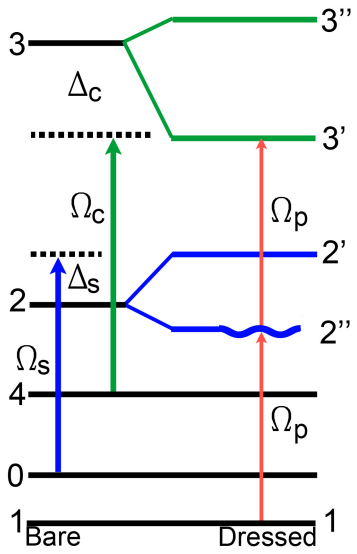

Fig. 5.4. Energy level diagram for the 5-level system coupled with two control fields Ω_s and Ω_c leading in ac-Stark splitting of levels 2 and 3 and resulting in an effective ladder system 1↔2"↔3' in the dressed state basis.

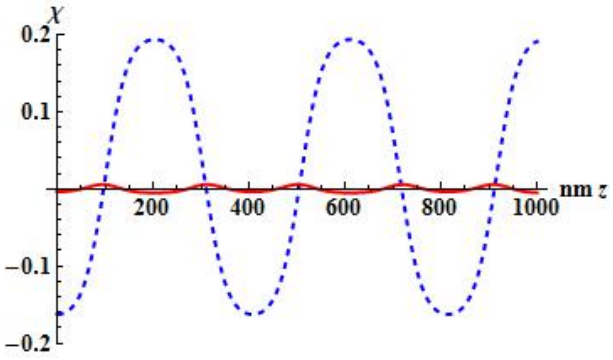

Fig. 5.5. Real (dashed) and imaginary (solid) part of the susceptibility as a function of distance along the optical axis for implementation of a optically controlled distributed Bragg reflector in Er^{3+}:YAG with the parameters listed in the paper.

5.5 Distributed Bragg reflector example

As an example we consider Er^{3+}:YAG ($n_{bg} = 1.82$ so $l = 1.77$) where the ${}^4I_{9/2}$ to ${}^4I_{15/2}$ ($\gamma_r^{21} = 45$Hz) transition at 813.2nm (transition 2-1 in Fig. 5.4) has a closely matched excited state absorption transition (transition 2-3 in Fig. 5.4) from ${}^4I_{9/2}$ to ${}^4G_{9/2}$ ($\gamma_r^{32} = 15$Hz) with $\omega_{32} - \omega_{21} = -20$GHz. [40, 77] Coherent driving of the transition between the next Stark level of the ground state and ${}^4I_{9/2}$ level (transition 2-0 in Fig. 5.4) can be used for modulation of level 2 position, while coherent driving of ${}^4I_{13/2}$ and ${}^4G_{9/2}$ can be used for matching of the parameters of the upper and lower transitions in the effective ladder system. Taking $N = 1.4 \cdot 10^{21}\text{cm}^{-3}$ and low enough temperature to limit phonon broadening we assume $\gamma_{32} = 0.8$GHz, $\gamma_{21} = 0.3$GHz, and $\gamma_{42} = 0.2$GHz. Choosing pump parameter $p = 0.035$ and the following parameters of the driving fields: $\Omega_s = 2.45$GHz, $\Delta_s = -10$GHz, $\Omega_c = 7.449$GHz, and $\Delta_c = -17.893$GHz along with choosing a probe detuning of $\delta_p = .2$GHz, we obtain 5.4% refractive index modulation with respect to background value ($\Delta\chi' = 0.356$) with a periodically modulated practically vanishing absorption ($\max |\chi''| < 0.006$) as shown in Fig. 5.5. This result follows from the numerical analysis of the 5 level system driven with two coherent fields, and is well approximated by the analytical formula in Eq. (5.9).

The refractive index is therefore modulated from $n_{\text{low}} = 1.77$ to $n_{\text{high}} = 1.87$ with a period very close to half of the probe wavelength. This modulation naturally creates a distributed Bragg reflector; one which can be optically manipulated, turning it on and off as well as changing the reflectivity. Since at the probe frequency we have close to complete transparency, the standard equation for the reflectivity of a DBR gives us a good approximation for our scheme:

$$R = \left[\frac{(n_{\text{high}})^{2N_{\text{mod}}} - (n_{\text{low}})^{2N_{\text{mod}}}}{(n_{\text{high}})^{2N_{\text{mod}}} + (n_{\text{low}})^{2N_{\text{mod}}}} \right]^2, \tag{5.13}$$

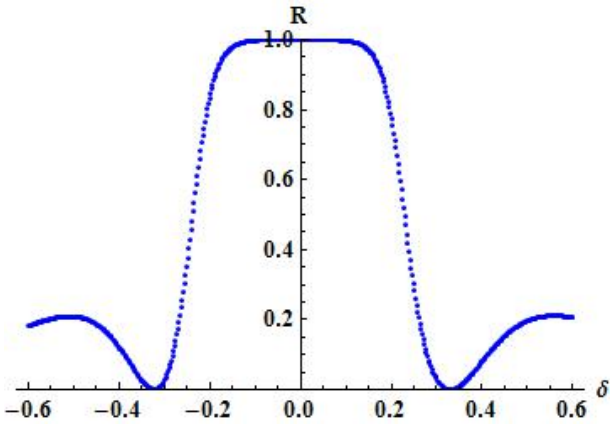

Fig. 5.6. Reflectance as a function of the probe field detuning with $N_{mod} = 122$, plotted with the numbers given for Er^{3+}:YAG.

where the number of periods of modulation of refractive index depends on the length of the interaction, $N_{\rm mod} = 2L/\lambda_s$. As long as the chosen wavelength mismatch, in our case $\lambda_s - \lambda_{pr} = 1.44nm$, is much smaller than the width of a traditional Bragg band-gap, $\lambda_{pr}\Delta n/(\pi n_{bg})$, which in our case is equal to 28nm.

As the probe field is detuned from atomic resonance there will be absorption/gain which alternates on the scale of the wavelength as shown in Fig. 5.3, resulting in zero net absorption/gain. But the combination of this absorption/gain with the fact that only near resonance will there be a significant difference in refractive index leads to a ultra narrow bandwidth of approximately $2\gamma_{21}$.

The bandwidth and reflectivity can be numerically determined by calculating the reflectivity as a function of probe field detuning. We do this by constructing a transport matrix to describe propagation through the medium with changing refractive index. We approximate the index change shown in Fig. 5.5 by repeating modulations of the average index. Then as we move through each section we get boundary effects

going from high to low described by P_{12} and from going from low to high described by P_{21}:

$$\mathrm{P}_{12} = \begin{pmatrix} \frac{1}{z_{12}} & \frac{\mathrm{p}_{12}}{z_{12}} \\ \frac{\mathrm{p}_{12}}{z_{12}} & \frac{1}{z_{12}} \end{pmatrix}, \tag{5.14}$$

$$\mathrm{P}_{21} = \begin{pmatrix} \frac{1}{z_{21}} & \frac{\mathrm{p}_{21}}{z_{21}} \\ \frac{\mathrm{p}_{21}}{z_{21}} & \frac{1}{z_{21}} \end{pmatrix}. \tag{5.15}$$

We also have the effect of propagation through each region of refractive index which can be described by D_1 for propagation through the high refractive index region:

$$D_1 = \begin{pmatrix} e^{-\alpha_{\mathrm{high}}/4} e^{-i\phi_{\mathrm{high}}} & 0 \\ 0 & e^{-\alpha_{\mathrm{high}}/4} e^{i\phi_{\mathrm{high}}} \end{pmatrix}, \tag{5.16}$$

and propagation through the low index region can be described by:

$$D_1 = \begin{pmatrix} e^{-\alpha_{\mathrm{low}}/4} e^{-i\phi_{\mathrm{low}}} & 0 \\ 0 & e^{-\alpha_{\mathrm{low}}/4} e^{i\phi_{\mathrm{low}}} \end{pmatrix}; \tag{5.17}$$

where in these equation we define:

$$z_{12} = \frac{2n_{\mathrm{high}}}{n_{\mathrm{high}} + n_{\mathrm{low}}}, \tag{5.18}$$

$$z_{21} = \frac{2n_{\mathrm{low}}}{n_{\mathrm{high}} + n_{\mathrm{low}}}, \tag{5.19}$$

$$\mathrm{p}_{12} = \frac{n_{\mathrm{high}} - n_{\mathrm{low}}}{n_{\mathrm{high}} + n_{\mathrm{low}}}, \tag{5.20}$$

$$\mathrm{p}_{21} = -\mathrm{p}_{12}. \tag{5.21}$$

The extra phase accumulation of the probe field is given by:

$$\phi_{\mathrm{low}} = \frac{\pi}{2} \frac{n_{\mathrm{low}}}{n} \frac{\lambda_{\mathrm{s}}}{\lambda_{\mathrm{pr}}}, \tag{5.22}$$

$$\phi_{\mathrm{high}} = \frac{\pi}{2} \frac{n_{\mathrm{high}}}{n} \frac{\lambda_{\mathrm{s}}}{\lambda_{\mathrm{pr}}}. \tag{5.23}$$

Notice that the phase accumulation is lowered by the difference in wavelengths but not by much. While the gain or absorption of the probe as it propagates is given by α_{low} and α_{high}. Then we can describe the propagation through one modulation by the transfer matrix:

$$S = \mathrm{P}_{12} \cdot D_2 \cdot \mathrm{P}_{21} \cdot D_1. \tag{5.24}$$

Then we can describe propagation through the entire medium by multiplying out this matrix N_{mod} times giving:

$$S_N = S^{N_{\text{mod}}}. \tag{5.25}$$

From this we can construct the transport matrix:

$$R_N = \mathrm{Re}[S_N \cdot S_N^*], \tag{5.26}$$

and the reflectivity:

$$R = \frac{R_N[1,2]}{R_N[2,2]}. \tag{5.27}$$

Thus we get our reflectance in terms of n_{low}, n_{high}, α_{low}, α_{high}. The next step to determine the bandwidth is to plot the reflectance as a function of probe detuning. Therefore for each detuning we need to solve for R, first by solving for n_{low}, n_{high}, α_{low}, α_{high} at that particular detuning. Then we can numerically solve the optical Bloch equations for the susceptibility of the probe field as a function of the distance through the crystal z at a fixed detuning δ_{p}:

$$n_{\text{high}} = \frac{4}{\lambda_{\text{s}}} \int_{-\lambda_{\text{s}}/8}^{+\lambda_{\text{s}}/8} dz \sqrt{n^2 + \mathrm{Re}\chi(\mathrm{z})}, \tag{5.28}$$

$$n_{\text{low}} = \frac{4}{\lambda_{\text{s}}} \int_{-\lambda_{\text{s}}/8+\lambda_{\text{s}}/4}^{+\lambda_{\text{s}}/8+\lambda_{\text{s}}/4} dz \sqrt{n^2 + \mathrm{Re}\chi(\mathrm{z})}, \tag{5.29}$$

$$\alpha_{\text{high}} = \frac{4}{\lambda_{\text{s}}} \int_{-\lambda_{\text{s}}/8}^{+\lambda_{\text{s}}/8} dz \mathrm{Im}\chi(\mathrm{z}), \tag{5.30}$$

$$\alpha_{\mathrm{low}} = \frac{4}{\lambda_{\mathrm{s}}} \int_{-\lambda_{\mathrm{s}}/8+\lambda_{\mathrm{s}}/4}^{+\lambda_{\mathrm{s}}/8+\lambda_{\mathrm{s}}/4} dz \mathrm{Im}\chi(\mathrm{z}). \tag{5.31}$$

Going through this procedure for a number of different probe field detunings we can get a plot of $\mathrm{R}(\delta_{\mathrm{p}})$ which shows us the bandwidth as shown in Fig. 5.5. Already a relatively thin medium with $L = 50\mu$m (which corresponds to 122 periods of modulation) provides quite high reflection coefficient, $R = 0.9995$. The produced DBR has a very narrow bandwidth of 0.6GHz (defined by the linewidth of atomic resonance) and may be used as a frequency selective reflector.

5.6 Conclusion

In conclusion, we proposed a method to produce periodic modulation of the refractive index while keeping zero net absorption/gain. The method is based on spatial modulation of the energy of the populated intermediate state in effective three level system with matched transition properties by an external strong control field via the ac-Stark effect. Possible implementation of this technique in Er^{3+}:YAG is suggested, where a 5% modulation of refractive index with vanishing absorption is possible. The proposed method may find useful applications for the creation of optically controllable photonic structures such as distributed Bragg reflectors, holey fibers, photonic crystals, etc. A major advantage of these structures as compared to traditional photonic structures is that they can be easily manipulated (including switching on/off, changing the amplitude and period of modulation) by varying the parameters of the optical control fields.

6. OPTICAL FLUORESCENCE AT THE COMBINATIONAL FREQUENCY IN COHERENTLY DRIVEN THREE-LEVEL SYSTEMS

6.1 Introduction

In 3 level systems with a pump and driving field, resonance fluorescence has been mainly studied at transitions directly coupled to one of two applied fields. Fluorescence at the third transition that is not coupled directly to the fields has not been considered since these transitions in atoms are electro-dipole forbidden due to the selection rules. The situation may be different for example, in atomic gases when one of the three transitions is magneto-dipole allowed hyperfine or Zeeman transition driven by a radio frequency field or in molecular gases when the driven transition is chosen between different vibrational or rotational levels. All three transitions may be allowed between the energy levels of rare-earth ions doped into the dielectric crystals due to admixture of the crystal field, or between the dimensional quantization levels in asymmetric quantum wells. In these cases, studying the fluorescence at the transition not coupled to the fields could provide important spectroscopic information.

Recently an interesting counter-intuitive effect, called the "valve" effect, was predicted and experimentally observed in scattering of Mössbauer gamma-ray radiation under the condition of resonant radio frequency (RF) driving of the split excited nuclear state [52, 53]. Namely, it was shown that in the presence of sufficiently strong RF driving field, when the Rabi frequency at the driven transition exceeds the radiative decay at the gamma-ray transition $\Omega_{\rm d} > W_{21}$, the photons prefer to be scattered at the combinational (sum of pump and RF fields frequencies) transition in spite of the fact that the radiative decay rates of the two gamma-ray transitions are the same. This effect looks counter-intuitive. Indeed, naively one could expect that the population of the most upper state 3 in a ladder scheme should not exceed the population of the middle level 2 since the driving field between the two upper levels may only equalize the populations but not provide population inversion between these

levels such that the two-photon transition $3 \leftrightarrow 1$ should be weaker compared to the one-photon transition $2 \leftrightarrow 1$.

The same effect was considered in a three-level system coupled to an optical and a RF field satisfying the two-photon resonance condition in a ladder configuration [81]. An advantage of optical transitions is the possibility of their strong laser excitation resulting in high fluorescence intensity. Since the driven transition in [81] was chosen in the RF range, fluorescence at this transition was not considered and the population decay was neglected. The homogeneous linewidth of all three atomic transitions was also assumed to be caused only by radiative decay and inhomogeneous broadening effects were not considered.

In this section we derive and compare the fluorescence spectra from three-level atomic systems, with all three transitions allowed and coherently coupled with two fields in the cascade and lambda configurations. We show that the total fluorescence intensity at the transition which is not coupled to the fields (which we call for simplicity two-photon fluorescence although it is actually one-photon fluorescence at the combinational frequency) may essentially dominate each of the two one-photon (i.e. directly excited) channels. It is shown that a prevalence of two-photon fluorescence over one-photon fluorescence at the excited transition is due to a counter-intuitive population distribution, namely, higher population in the level from which the two-photon fluorescence originates. In particular, in the lambda scheme it means counter-intuitive population inversion at the driven transition. For this reason the decay rate at the driven transition makes the lambda scheme more favorable as compared with the ladder scheme for realization of the valve effect. We also analyze the influence of additional homogeneous broadening mechanisms (such as collisions in gases, or phonon broadening in solids) and inhomogeneous line broadening (caused by the Doppler effect in gases or fluctuations in the local environment in solids) on the distribution of fluorescence between two-photon and one-photon fluorescence channels. We show that in the case of counter-propagating fields in the ladder scheme and

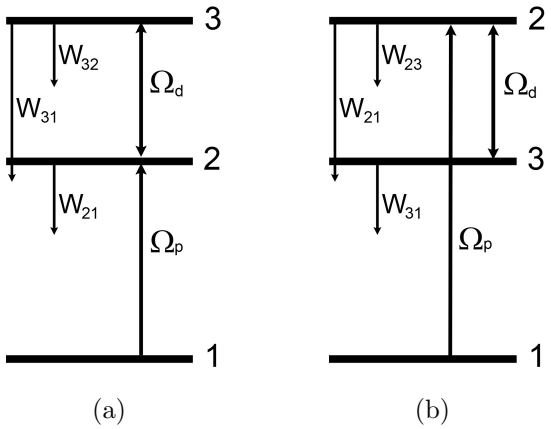

Fig. 6.1. Energy level diagram for the three level (a) cascade scheme and (b) lambda scheme.

co-propagating fields in the lambda scheme Doppler broadening is actually favorable for realization of the valve effect.

6.2 Derivation of the fluorescence spectra

We consider two different configurations of three-level systems, namely the cascade (Ξ) and lambda (Λ) configurations (see Fig. 6.1). In both of these schemes the pumping field couples levels 2 and 1 and the driving field couples levels 3 and 2 so that level 2 is coupled to both fields. The schemes differ from each other only by the relative positions of the energy levels and hence the density matrix equations describing these schemes are essentially the same before the specification of the incoherent transition constants. Although for the different schemes energy levels can change from lower to upper states, the corresponding energy difference just determines which rotating component of the field should be selected in the rotating wave approximation (RWA) in order to provide small detuning of this field from the cor-

responding frequency of the atomic transition. In particular, for the cascade scheme the density matrix equations in RWA take the form:

$$\dot{\sigma}_{21} = -i\delta\sigma_{21} - \gamma_{21}\sigma_{21} - i\Omega_{\rm p}(\sigma_{22} - \sigma_{11}) + i\Omega_{\rm d}^{*}\sigma_{31}, \tag{6.1}$$

$$\dot{\sigma}_{31} = -i(\delta + \Delta)\sigma_{31} - \gamma_{31}\sigma_{31} - i\Omega_{\rm p}\sigma_{32} + i\Omega_{\rm d}\sigma_{21}, \tag{6.2}$$

$$\dot{\sigma}_{32} = -i\Delta\sigma_{32} - \gamma_{32}\sigma_{32} - i\Omega_{\rm d}(\sigma_{33} - \sigma_{22}) - i\Omega_{\rm p}^{*}\sigma_{31}, \tag{6.3}$$

$$\dot{\sigma}_{22} = i\Omega_{\rm p}\sigma_{12} - i\Omega_{\rm p}^{*}\sigma_{21} + i\Omega_{\rm d}^{*}\sigma_{32} - i\Omega_{\rm d}\sigma_{23} - (W_{23} + W_{21})\sigma_{22} + W_{32}\sigma_{33}, \tag{6.4}$$

$$\dot{\sigma}_{33} = i\Omega_{\rm d}\sigma_{23} - i\Omega_{\rm d}^{*}\sigma_{32} - (W_{31} + W_{32})\sigma_{33} + W_{23}\sigma_{22}, \tag{6.5}$$

$$\sigma_{11} = 1 - \sigma_{22} - \sigma_{33}; \tag{6.6}$$

where $\delta = \omega_2 - \omega_1 - \omega_{\rm p}$ is the detuning of the pump and $\Delta = \omega_3 - \omega_2 - \omega_{\rm d}$ is the detuning of the driving field. The population transfer rates are defined such that $\rm W_{ij}$ is the population transfer rate from energy level i to level j, we will take population transfer to be due to radiative decay on the electro-dipole allowed transitions. The equations for the lambda scheme may be obtained from these equations just by the replacement of Δ by -Δ and $\Omega_{\rm d}$ by $\Omega_{\rm d}^{*}$.

For the derivation of the fluorescence spectra we closely follow the classical papers [25, 27]. The set of equations may be rewritten in the compact matrix form:

$$\dot{\hat{\Psi}} = \hat{M}\hat{\Psi} + \hat{L}, \tag{6.7}$$

where $\hat{\Psi} = [\sigma_{12}, \sigma_{13}, \sigma_{23}, \sigma_{22}, \sigma_{33}, \sigma_{21}, \sigma_{31}, \sigma_{32}]^{T}$ and $\hat{M}$ is a 8x8 time independent matrix of the coefficients of Eqs. (6.1-6.6), and the inhomogeneous term $\hat{L}$ is also a column vector, $\hat{L} = [-i\Omega_{\rm p}, 0, 0, 0, 0, i\Omega_{\rm p}^{*}, 0, 0]^{T}$. The formal solution of Eq. (6.7) at steady state is:

$$\hat{\Psi} = -\hat{M}^{-1}\hat{L}. \tag{6.8}$$

The fluorescent spectrum of each of the 3 atomic transitions is defined as the Fourier transform of the correlation function of the polarization at the corresponding transition:

$$S_{\mathrm{ij}}(\vec{r},\omega) = \mathrm{Re}\int_0^\infty \lim_{\hat{t}\to\infty} \langle \hat{P}_{\mathrm{ij}}^{(-)}(\hat{t}+\tau), \hat{P}_{\mathrm{ij}}^{(+)}(\hat{t})\rangle e^{i\omega\tau} d\tau, \tag{6.9}$$

$$\hat{P}_{\mathrm{ij}}^{(+)}(t) = \mu_{\mathrm{ij}}|\mathrm{i}><\mathrm{j}|e^{-i(\omega_{\mathrm{j}}-\omega_{\mathrm{i}})t}. \tag{6.10}$$

According to the quantum regression theorem [82] the two-time atomic correlation functions in Eq. (6.9) can be calculated via one-moment averaging. Then using the formal solution, Eq. (6.8), we obtain the incoherent intensity spectra for each transition. For the Ξ system the fluorescence spectrum is given by:

$$S_{31}^{\Xi}(\omega) = |\mu_{13}|^2 \mathrm{Re}[\hat{N}_{2,2}^{(31)}\Psi_5(\infty) + \hat{N}_{2,1}^{(31)}\Psi_8(\infty) - \sum_{\mathrm{j}=1}^{8} \hat{N}_{2,\mathrm{j}}^{(31)}\Psi_{\mathrm{j}}(\infty)\Psi_7(\infty)], \tag{6.11}$$

$$S_{21}^{\Xi}(\omega) = |\mu_{12}|^2 [\hat{N}_{1,2}^{(21)}\Psi_3(\infty) + \hat{N}_{1,1}^{(21)}\Psi_4(\infty) - \sum_{\mathrm{j}=1}^{8} \hat{N}_{1,\mathrm{j}}^{(21)}\Psi_{\mathrm{j}}(\infty)\Psi_6(\infty)], \tag{6.12}$$

$$\begin{aligned} S_{32}^{\Xi}(\omega) &= |\mu_{23}|^2 \mathrm{Re}[\hat{N}_{3,6}^{(32)}\Psi_7(\infty) + \hat{N}_{3,3}^{(32)}\Psi_5(\infty) + \hat{N}_{3,4}^{(32)}\Psi_8(\infty) \\ &- \sum_{\mathrm{j}=1}^{8} \hat{N}_{3,\mathrm{j}}^{(32)}\Psi_{\mathrm{j}}(\infty)\Psi_8(\infty)]. \end{aligned} \tag{6.13}$$

For the Λ system the spectrum components are the same for S_{31} and S_{21} only the spectrum for S_{23} is different:

$$\begin{aligned} S_{23}^{\Lambda}(\omega) &= |\mu_{32}|^2 \mathrm{Re}[\hat{N}_{8,7}^{(32)}\Psi_6(\infty) + \hat{N}_{8,5}^{(32)}\Psi_3(\infty) + \hat{N}_{8,8}^{(32)}\Psi_4(\infty) \\ &- \sum_{\mathrm{j}=1}^{8} \hat{N}_{8,\mathrm{j}}^{(32)}\Psi_{\mathrm{j}}(\infty)\Psi_3(\infty)]. \end{aligned} \tag{6.14}$$

In Eqs. (6.11-6.14), the matrix functions take the form:

$$\hat{N}^{\mathrm{ij}}(\omega) = \frac{1}{i(\omega - z_{\mathrm{ij}})\hat{I} - \hat{M}}. \tag{6.15}$$

The center frequency of the fluorescence spectrum is given by z_{ij} where $z_{21} = \omega_{\mathrm{p}}$, $z_{32} = \omega_{\mathrm{d}}$ and for the cascade scheme $z_{31} = \omega_{\mathrm{p}} + \omega_{\mathrm{d}}$ while for the lambda scheme $z_{31} = \omega_{\mathrm{p}} - \omega_{\mathrm{d}}$. $\hat{I}$ is the 8x8 identity matrix and $\hat{\Psi}(\infty)$ is the steady state solution of the matrix Eq. (6.7).

To find the total incoherent fluorescence intensity we just need to integrate the spectrum over frequency:

$$I_{\mathrm{ij}}(\mathrm{r}) = \frac{\mathrm{N}\gamma\hbar\omega}{4\pi^2\mathrm{r}^2}\int_{-\infty}^{+\infty}\lim_{\hat{t}\to\infty} S_{\mathrm{ij}}(\mathrm{r},\omega)d\omega; \tag{6.16}$$

where N is the number of atoms, γ is the population decay rate for the transition, ω is the frequency of the transition and r is the distance from the detector. In the case of resonant fields ($\delta = 0$, $\Delta = 0$) the total intensity may be simply expressed via the difference between the steady state population of the upper level in the fluorescence channel and the corresponding coherence:

$$I_{\mathrm{ij}}(\mathrm{r}) = \frac{\mathrm{N}\gamma\hbar\omega}{4\pi\mathrm{r}^2}(\sigma_{\mathrm{ii}} - \sigma_{\mathrm{ij}}\sigma_{\mathrm{ji}}). \tag{6.17}$$

We are looking for situations where the the total fluorescence for the two-photon channel 3↔1 is larger than the one-photon 2↔1, so we will be interested in the ratio of total fluorescence intensities, I_{31}/I_{21}. Since the main contribution to the fluorescence spectrum is due to the population terms we can get a better insight into the valve effect by deriving an analytic expression for the ratio of populations:

$$\frac{\sigma_{33}}{\sigma_{22}} = \frac{(2\gamma_{31} + W_{21})\Omega_{\mathrm{d}}^2 + W_{23}(\gamma_{31}\gamma_{32} + \Omega_{\mathrm{p}}^2)}{(\gamma_{31}\gamma_{32} + \Omega_{\mathrm{p}}^2)(W_{32} + W_{31}) + (2\gamma_{31} - W_{31})\Omega_{\mathrm{d}}^2}. \tag{6.18}$$

Here for the cascade case $W_{23} = 0$, for the lambda case $W_{32} = 0$, and for the RF driving case $W_{32} = W_{23} = 0$.

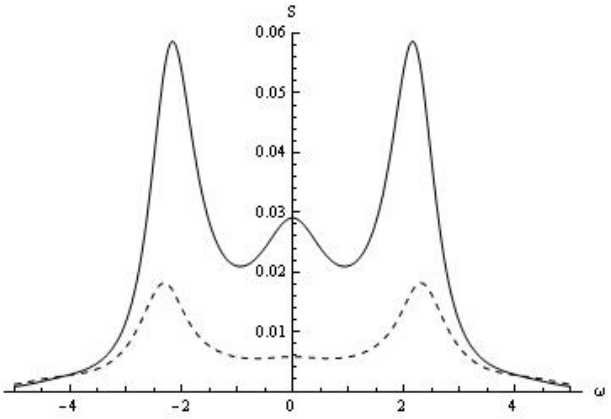

Fig. 6.2. Fluorescence spectrum for the cascade and lambda scheme with RF driving field in arbitrary units. For convenient comparison the position of two-photon spectrum is shifted from it's original position $\omega - \omega_{31}$ to be centered at the same frequency as one-photon spectrum $\omega - \omega_{21}$. The solid line corresponds to the two-photon channel, S_{31}, and the dashed line corresponds to the one photon channel, S_{21}. Both are plotted with $\Omega_{\rm p} = 1$, $\Omega_{\rm d} = 2$, $W_{31} = W_{21} = 1$, $W_{32} = W_{23} = 0$.

6.3 RF-driving

Let us consider the case where the driven transition is in the radio frequency range. It can correspond to the hyperfine or Zeeman sublevels in a gas of alkali atoms or a transition element doped crystal. The population relaxation rates between the hyperfine or Zeeman sublevels are defined in a gas by the interaction time with the light beams while in solids they are defined by the spin-lattice interaction, so that $W_{32} = W_{23} = W_{\rm d}$. Typically, they are much smaller then the spontaneous decay rates at the optical transitions, $W_{\rm d} \ll W_{21}, W_{31}$. Since both optical transitions are dipole allowed and have very close frequencies, we take the decay rates at optical transitions to be equal, $W_{21} = W_{31} = W_{\rm p}$. We assume also that the homogeneous linewidths are defined by the decay rates of population from the corresponding levels: $\gamma_{\rm ij} = \sum(W_{\rm ik} + W_{\rm jk})/2$. In the case of a gaseous medium it corresponds to the situation

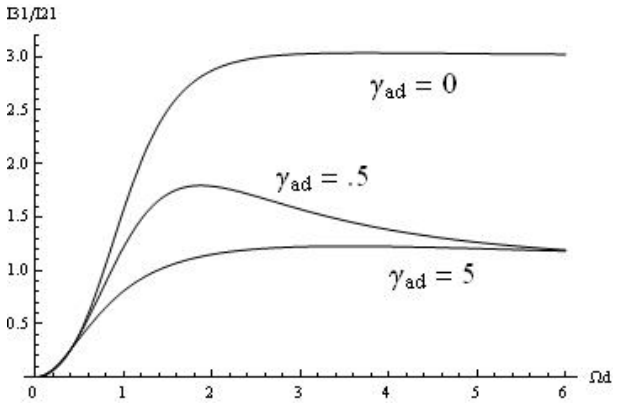

Fig. 6.3. The intensity ratio I_{31}/I_{21} for the RF driven scheme as a function of driving Rabi frequency. With $\gamma_{31} = .5 + \gamma_{31}^{\rm ad}$ and $\gamma_{21} = .5 + \gamma_{21}^{\rm ad}$. Otherwise the same values of parameters as Fig. 6.2.

where atomic collisions are negligible i.e., either in an atomic beam or a cell of low atomic density. In solids it corresponds to cryogenic temperatures where phonon broadening is negligible. Thus taking $W_{\rm d} = 0$, $\gamma_{21} = \gamma_{31} = W_{\rm p}/2$ and $\gamma_{32} = W_{\rm p}$.

Since the expressions for the fluorescence spectra at the one-photon $2 \leftrightarrow 1$ and two-photon $3 \leftrightarrow 1$ transitions are the same for the lambda and cascade systems and the steady-state solution of the density matrix equations for these systems in the case of RF driving also coincide due to the symmetry of the decay rates, $W_{32} = W_{23} = 0$, all results for the cascade and lambda schemes become identical to each other.

The typical two-photon and one-photon fluorescence spectra for these schemes are shown in Fig. 6.2. The reason for the pronounced peaks in the two-photon fluorescence spectrum is the same as in the one-photon fluorescence spectrum namely, the ac-ac-Stark splitting of only the upper levels in case of the strong driving and weak pumping field (resulting in two peaks with positions determined by $\Omega_{\rm d}$) or both upper levels and ground state in the case of strong driving and pumping fields (resulting in three or five peaks) with positions determined by the intensities of both driving and pumping fields (as it was explained in [25, 27] for one-photon fluorescence). For

relatively high intensity of the driving field, $\Omega_d > W_p$, the total two-photon fluorescence intensity may essentially surpass the one-photon fluorescence, see Fig. 6.2 and Fig. 6.3, as it was noticed earlier and termed the valve effect [52,53,81]. Here and for the rest of the paper all magnitudes possessing frequency units will be normalized by the radiative decay rate, W_{21}. The valve effect is clearly due to a population inversion between levels 3 and 2. This is due to a dip in the population of level 2 caused by the Stark splitting of this level while level 3 is maximally populated under the condition of two-photon resonance. It is worth while to note that with strong driving $\Omega_d >> \Omega_p$ both the one-photon and two-photon fluorescence intensities decrease as Ω_p^4/Ω_d^4 while their ratio essentially saturates at $\Omega_d \geq 2\Omega_p$.

Let us assume now that the total polarization decay rate at both optical transitions is defined as $\gamma_{ij} = \sum(W_{ik} + W_{jk})/2 + \gamma_{ij}^{ad}$ where γ_{ij}^{ad} takes into account additional phase destroying processes (such as collisional line broadening in gases or phonon broadening in solids) on the valve effect. As one would expect additional decoherence on the two photon transition decreases the intensity ratio until $I_{31}/I_{21} = 1$, slowly destroying the valve effect as shown in Fig. 6.3. While having $\gamma_{21}^{ad} > 0$ is beneficial since it broadens the one photon transition while not affecting the two photon transition. When there is additional decoherence on both transitions the decay of $3 \leftrightarrow 1$ coherence supersedes any benefit from decreased $2 \leftrightarrow 1$ coherence also destroying the valve effect.

6.4 Optical driving

Let us now consider the situation where the frequency of the driven transition is comparable to the other two atomic frequencies. Such a situation may be realized either in molecular gases when the driven transition is chosen between different vibrational or rotational levels, or in rare-earth doped crystals or asymmetric quantum wells. In this case radiative decay at the driven transition $3 \leftrightarrow 2$ may be comparable to W_p and should be taken into account. It results in depletion of level 3's population

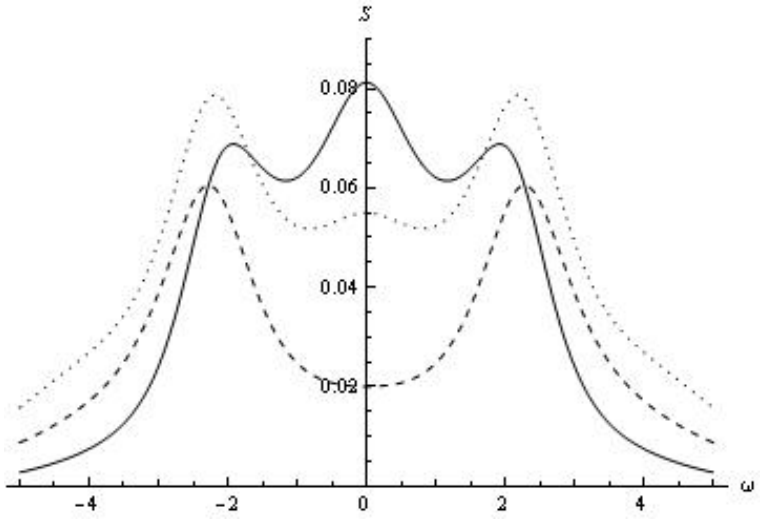

Fig. 6.4. Fluorescence spectra for the optically driven cascade scheme and at the two photon transition S_{31} (solid line), one-photon pumped transition S_{21} (dashed line), and one-photon driven transition S_{32} (the dotted line). All spectra are shifted to the origin for convenient comparison. With $W_{32} = 1$, $W_{23} = 0$. All other parameters are the same as in Fig. 6.2.

in the cascade scheme (due to a additional decay channel W_{32}), and an increase of its population in the lambda scheme (due to W_{23}) as can be seen in Eq. (6.18). Thus the lambda scheme becomes more favorable for the realization of the valve effect (i.e. $I_{31}/I_{21} > 1$ at $W_{31} = W_{21}$) while in the cascade scheme the effect is reduced with increase of W_{32} as illustrated by Fig. 6.4 and Fig. 6.5. At the same time, the radiative decay at 3-2 results in the appearance of fluorescence at the driven transition. For both cases the two-photon fluorescence may dominate fluorescence at the driven transition $I_{31}/I_{32} > 1$ as shown in Fig. 6.6 and Fig. 6.7. For the cascade case since the population of an upper level for transitions $3 \leftrightarrow 1$ and $3 \leftrightarrow 2$ is the same the higher intensity of fluorescence in the two-photon channel is due to a smaller polarization induced at this transition, see Eq. (6.17), and consequently only happens for small driving Rabi frequencies. While for the lambda case since both one photon

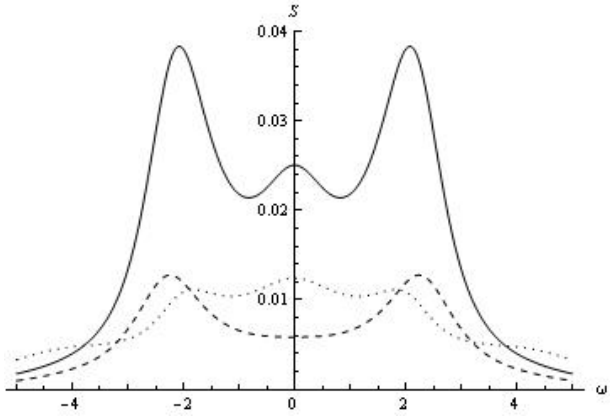

Fig. 6.5. Fluorescence spectra for the optically driven lambda scheme at the two photon transition S_{31} (solid line), one-photon pumped transition S_{21} (dashed line), and one-photon driven transition S_{32} (the dotted line). All spectra are shifted to the origin for convenient comparison. With $W_{23} = 1$, $W_{32} = 0$. All other parameters are the same as in Fig. 6.3.

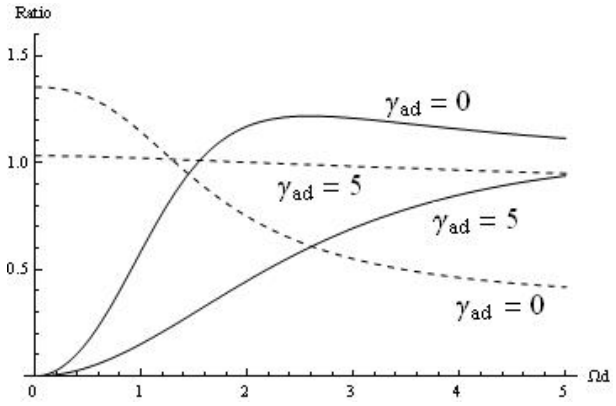

Fig. 6.6. Intensity ratio, I_{31}/I_{21}, (solid line) and intensity ratio I_{31}/I_{32} (dashed line) as a function of Ω_d for the cascade scheme. All other parameters are the same as in Fig. 6.2.

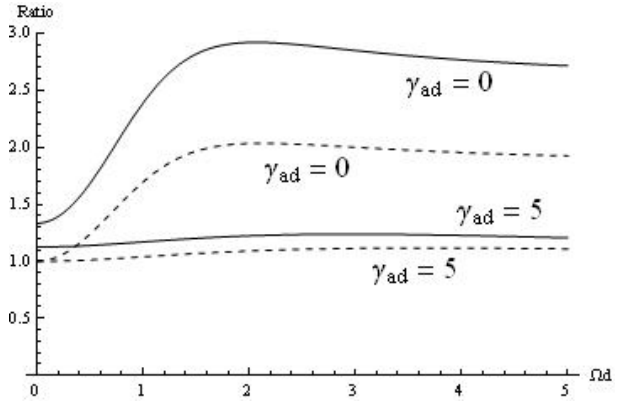

Fig. 6.7. Intensity ratio, I_{31}/I_{21}, (solid line) and intensity ratio I_{31}/I_{32} (dashed line) as a function of Ω_d for the lambda scheme. All other parameters are the same as in Fig. 6.3.

transitions originate from level 2, the higher population in level 3 ensures for strong driving that $I_{31} > I_{32}, I_{21}$.

It is interesting to consider the specific case when the total decay rate from the most upper level is equal to the decay rate from the intermediate state. Indeed, in this case the populations of these two excited states are expected to be equal, according to the balance approach, neglecting the coherences. In the cascade case it would lead to $I_{31} + I_{32} = I_{21}$, implying that $I_{31} < I_{21}$. But it turns out that two-photon fluorescence, excited with both strong pumping and driving fields, $\Omega_p \geq W_{21}$, $\Omega_d \geq \Omega_p$, dominates one-photon fluorescence in both the $2 \leftrightarrow 1$ and $3 \leftrightarrow 2$ channels $I_{31} > I_{21}, I_{32}$, which may be called a generalized valve effect. Similarly in the lambda scheme two-photon fluorescence dominates one-photon fluorescence in both $2 \leftrightarrow 1$ and $3 \leftrightarrow 2$ channels, $I_{31} > I_{21}, I_{32}$, when $W_{21} + W_{23} = W_{31}$ and $\Omega_p \geq W_{21}$, $\Omega_d \geq \Omega_p$. Like in the RF case additional decoherence at the two photon transition is especially harmful for two-photon fluorescence. On the other hand, Doppler broadening under certain conditions increases the ratio $I_{31}/I_{21}, I_{31}/I_{32}$ as discussed in the next section.

6.5 Inhomogeneous broadening

The situation considered above when the linewidths are homogeneously broadened may be realized experimentally either in atomic beams propagating perpendicular to the external fields as well as to the direction of observation or in an ensemble of very cold atoms in an optical trap. In the case of hot and sufficiently dilute (when collisional broadening is negligible) atomic or molecular gas in a cell and in the case of rare-earth doped crystals at cryogenic temperature (when phonon broadening is negligible) inhomogeneous line broadening should be taken into account.

Many systems experience inhomogeneous broadening of energy levels due to each atom being in a different environment. Such as hot gases where each atom has a different velocity or in doped crystals where each atom sees a different part of the surrounding crystal lattice. Thus it is important to study the influence of inhomogeneous broadening on fluorescence in different channels and in particular on the possibility of experimental realization of the valve effect.

For equal inhomogeneous broadening of all three transitions, the effect of the fluorescence intensity is similar to the effect of including extra homogeneous broadening as previously discussed. The more interesting case for the valve effect is when the inhomogeneous broadening mechanism can decrease one photon emission but does not have a significant impact on the two photon fluorescence channel.

For example lets consider a Doppler broadened gas where the atoms are traveling with velocities, ν, given by a Maxwell distribution. Due to the Doppler effect the frequency of the pump and driving field, as seen by each atom, will be slightly different, $\omega_{\rm d}(\nu_{\rm y}) = \omega_{\rm d} \pm \nu_{\rm y}/c$ and $\omega_{\rm p}(\nu) = \omega_{\rm p} \pm \nu_{\rm y}/c$; where c is the speed of light and $\nu_{\rm y}$ is the velocity component propagating with the field. The positive sign means the field is counter propagating with respect to the velocity and the negative sign means it is co-propagating. Since the shift in both fields are due to the same velocity, in the density matrix we can define the detunings such that $\delta(\nu) = \delta + \delta_{\rm D}$ and $\Delta(\nu) = \Delta \pm (\omega_{\rm d}/\omega_{\rm p})\delta_{\rm D}$ where $\delta_{\rm D} = \omega_{\rm p}\nu/c$. When the atom traveling at a

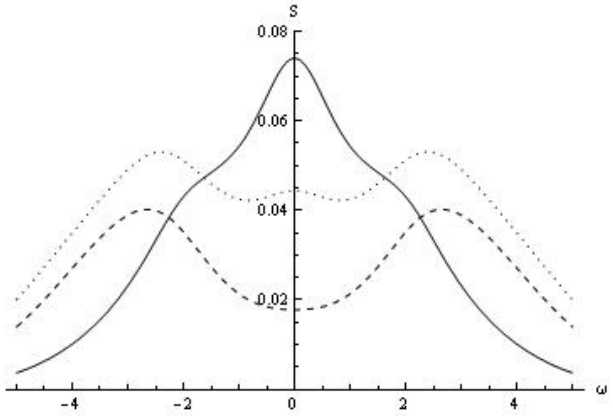

Fig. 6.8. Doppler broadened fluorescence spectra at the two photon transition S_{31} (solid line), one-photon pumped transition S_{21} (dashed line), and one-photon driven transition S_{32} (dotted line) in the cascade scheme with counter-propagating fields. All spectra are shifted to the origin for convenient comparison. The HWHM of the Doppler linewidth is $\Gamma = 2$, and $\omega_{\rm d} = \omega_{\rm p}$. For simplicity the detector is taken to be perpendicular to the beam, $\theta = 0^{\rm o}$. All other parameters are the same as in Fig. 6.4.

velocity ν emits a photon it has a Doppler shifted frequency, as discussed in [83] the spectrum will depend on the angle θ in the x-y plane our detector is positioned since in Eq. (6.15) we need to change $z_{\rm ij}$ to $z_{\rm ij}+\delta_{\rm D}-\delta\omega$ where $\delta\omega = (\nu_{\rm y}cos(\theta)+\nu_{\rm x}sin(\theta))\delta_{\rm D}/\nu_{\rm y}$. We can then integrate $S_{\rm ij}(\omega,\delta_{\rm D})$ over a Gaussian distribution with a HWHM of Γ to give the Doppler broadened spectrum:

$$S_{\rm ij}^{\rm inh}(\omega) = \int_{-\infty}^{+\infty} S_{\rm ij}(\omega,\delta_{\rm D})\frac{1}{\sqrt{2\pi\Gamma ln2}}e^{\frac{-(\delta_{\rm D}-\delta_{\rm p})^2}{2ln2\Gamma^2}}d\delta_{\rm D}. \qquad (6.19)$$

Therefore Doppler broadening under this condition is favorable for the valve effect. Even in situations when the two-photon fluorescence is weaker then one-photon fluorescence, with an increase of the Doppler broadening the two-photon channel starts to dominate both one-photon channels.

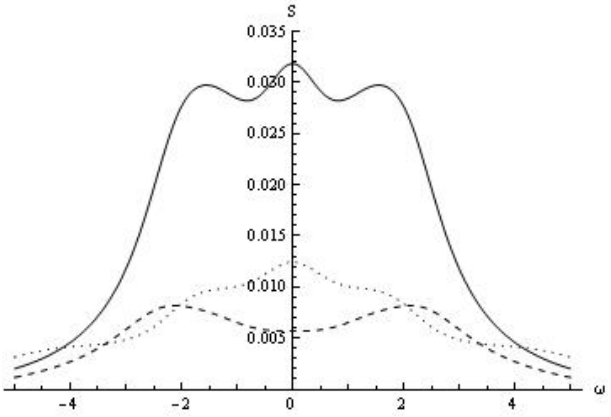

Fig. 6.9. Doppler broadened fluorescence spectra at the two photon transition S_{31} (solid line), one-photon pumped transition S_{21} (dashed line), and one-photon driven transition S_{32} (dotted line) in the lambda scheme with co-propagating fields. All spectra are shifted to the origin for convenient comparison. The HWHM of the Doppler linewidth is $\Gamma = 2$, and $\omega_{\rm d} = \omega_{\rm p}$. For simplicity the detector is taken to be perpendicular to the beam, $\theta = 0^{\rm o}$. All other parameters are the same as in Fig. 6.5.

Apparently, large Doppler broadening washes out the Stark structure both in the one-photon fluorescence and two-photon fluorescence. However in the case of driving and pumping fields of close frequencies $\omega_{\rm d}/\omega_{\rm p} \simeq 1$ the Doppler frequency shifts for counter-propagating fields in a cascade and co-propagating fields in a lambda configuration compensate each other. Thus the ratio I_{31}/I_{21} is enhanced under conditions of Doppler broadening due to less efficient excitation of level 2 by the pumping field as compared to level 3 (since the last one is excited in all the atoms while the first one only in a fraction of atoms of an order of $\gamma_{21}/\gamma_{21}^{\rm inh}$) as it is illustrated by Fig. 6.8 and Fig. 6.9.

Though it is not feasible to have all three transitions allowed in a atomic gas with $\omega_{\rm d}/\omega_{\rm p} \approx 1$ because of the selection rules, the enhancement of the valve effect by the Doppler broadening may be realized in molecular gases using a combination of electronic, vibrational, or rotational transitions so that $\omega_{\rm d}/\omega_{\rm p} \sim 1$.

Inhomogeneous broadening in solids in the case $\omega_d/\omega_p \sim 1$ could also result in relative enhancement of two-photon fluorescence channel with respect to one-photon ones when this broadening at the two-photon transitions is essentially smaller then at the one-photon transitions (resulting again in more efficient excitation of level 3). In solids this effect certainly does not depend on the relative direction of propagation (co- or counter- propagation) of the pumping and driving fields, since the transitions are uniformally broadend in this case.

Since in the case of RF driving the ratio $\omega_d/\omega_p \ll 1$ inhomogeneous broadening effects the two-photon transition in the same manner as one-photon transitions resulting in additional decoherence of these transitions destroying the valve effect.

6.6 Conclusion

We considered the physical situations where all three transitions in a 3-level medium coupled with two fields in the cascade and lambda configuration are allowed and derived the fluorescence spectra at all three transitions. Specific attention is given to the analysis of fluorescence spectra at the transition adjacent to the coupled ones which is excited by a joint action of two fields (two-photon fluorescence) and to its comparison with fluorescence at the driven transitions. It is found that under the two-photon resonance condition the two-photon fluorescence intensity may essentially exceed fluorescence simultaneously in each one-photon channel.

Our analysis was limited by the simplest case of a quantum system with three nondegenerate energy levels which could be realized in practice by using a strong magnetic field to lift the Zeeman degeneracy or under certain conditions by choosing an appropriate circular polarization of the applied fields. It would be interesting to extend this work to the case of degenerate levels to describe the angular dependence of combinational frequency fluorescence (as it was done previously for the calculation of fluorescence at the driven transitions [84, 85]). Since the valve effect deals with the integral fluorescence intensity and is based essentially on the counter-intuitive

population distribution one could expect that it would take place also in the case of degenerate levels.

We have also considered decoherence mechanisms additional to radiative decay (such as collisions in gases or phonon broadening in solids) which lead to suppression of two-photon with respect to one-photon fluorescence. On the other hand, Doppler broadening for counter-propagating pumping and driving fields in a cascade and co-propagating fields in a lambda configuration in the case of similar frequencies of the fields leads to enhancement of two-photon with respect to one-photon fluorescence due to reduction of Doppler broadening in the two-photon absorption. It would be interesting in the future to study the statistics of the two-photon fluorescence in particular, looking for quantum coherence effects such as production of squeezed states, line narrowing, and fluorescence inhibition effects which were observed earlier in one-photon fluorescence spectra.

7. CONCLUSION

We have presented three different applications of coherent control of optical processes in resonant mediums. We gave two schemes that use an effective two-level system with linewidth, amplitude, and frequency that we control, to compensate resonant absorption with gain in order to manipulate the refractive index while maintaining transparency and avoiding nearby regions of gain. We then discussed how such systems could be used to create optically controlled photonic structures in homogeneous media. Finally, we have discussed resonant fluorescence of three-level atoms, in particular we derived the fluorescence spectrum for all three possible transitions in a three-level Λ or V scheme.

We demonstrated the possibility of enhancement and control of the refractive index in a mixture of two three-level atomic species that form a pair of far-detuned lambda schemes under two-photon resonance. Both lambda systems are driven by a corresponding far-detuned coherent field at one atomic transition and probed by a common weak field. By making the absorption transition stronger than the gain transition, we were able to eliminate any regions of gain. We analyze the experimental implementation of such a system in a cell of Rb atoms at natural abundance showing that it is possible to obtain a refractive index enhancement on the order of $\Delta n \simeq 5 \cdot 10^{-3}$. We show that there is a maximum value for the achievable refractive index in such systems since with an increase in density there is also an increase in atomic collisions and dipole-dipole interactions which limit the refractive index in such a system.

We also suggested a three-level nearly degenerate ladder system with populated intermediate state as a promising basic scheme for the resonant enhancement of the refractive index with zero absorption/gain. Coherent driving at an additional transition, either adjacent to the upper absorption transition forming a Λ scheme or adjacent to the lower gain transition forming a V scheme, allows for efficient

control of the parameters of an effective two-level transition. We show that resonantly enhanced refractive index with negligible absorption in a narrow frequency region and with eliminated gain in the nearby frequency range can be achieved. We suggested implementation in transition element doped crystals possessing strong ESA. It was shown that at low temperature when phonon broadening is negligible, a high density of impurities may result in achievement of resonantly enhanced refractive index, for example in Er^{3+}:YAG it is possible to achieve $\Delta n = .1$ at 813.2nm.

We showed how to extend this second scheme for refractive index control to produce periodic spatial variation of the refractive index while keeping zero net absorption/gain. This is the first suggestion of how to optically create photonic structures in a homogeneous medium. The method is based on spatial modulation of the energy of the populated intermediate state in an effective three level system with matched transition properties by an external strong control field via the ac-Stark effect. Possible implementation of this technique in Er^{3+}:YAG is suggested, where a 5% modulation of refractive index with vanishing absorption is possible. We also show how this modulation could be used to produce an optically controlled distributed Bragg reflector. A major advantage of these structures as compared to traditional photonic structures is that they can be easily manipulated (including switching on/off, changing the amplitude and period of modulation) by varying the parameters of the optical control fields.

Finally, we shifted our focus to the coherent control of resonant fluorescence where we derived and compared the optical fluorescence spectra at all three transitions for a three-level systems coherently coupled with two fields in a cascade or lambda configuration. We show that coherent driving can efficiently control the distribution of intensities between the fluorescent channels. In particular, the total intensity of fluorescence at the combinational frequency (sum or difference of the driving fields frequencies in the ladder and lambda systems, accordingly) may essentially exceed the fluorescence intensity at the driven transitions under the condition of two-photon

resonance. This counter-intuitive effect is due to depletion of an intermediate state via atomic interference.

REFERENCES

[1] O. Kocharovskaya, Ya. I. Khanin, Sov. Phys. JETP **63**, 945 (1986).

[2] K. J. Boller, A. Imamoglu, S. E. Harris, Phys. Rev. Lett. **66**, 2593 (1991).

[3] O. Kocharovskaya, Ya. I. Khanin, JETP Lett. **48**, 630 (1998).

[4] S. E. Harris, Phys. Rev. Lett. **62**, 1033 (1989).

[5] M. O. Scully, S. Y. Zhu, A. Gavridiles, Phys. Rev. Lett. **62**, 2813 (1989).

[6] O. Kocharovskaya, Phys. Rep. **219**, 175 (1992).

[7] O. Kocharovskaya, Hyperfine Interactions **107**, 187 (1997).

[8] J. Mompart, R. Corbalán, J. Opt. B **2**, R7 (2000).

[9] E. S. Fry, X. Li, D. Nikonov, G. G. Padmabandu, M. O. Scully, A. V. Smith, F. K. Tittel, C. Wang, S. R. Wilkinson, S. Y. Zhu, Phys. Rev. Lett. **70**, 3235 (1993)

[10] O. Kocharovskaya, R. Kolesov, Y. Rostovtsev, Laser Physics **9**, 745 (1999).

[11] L. V. Hau, S. E. Harris, Z. Dutton, C. H. Behroozi, Nature **397**, 594 (1999).

[12] O. Kocharovskaya, Y. Rostovtsev, M. O. Scully, Phys. Rev. Lett. **86**, 628 (2001).

[13] M. Bajcsy, A. S. Zibrov, M. D. Lukin, Nature **426**, 638 (2003).

[14] D. Strekalov, A. B. Matsko, N. Yu, L. Maleki, Phys. Rev. Lett. **93**, 023601 (2004).

[15] M. Fleischhauer, M. D. Lukin, Phys. Rev. A **65**, 022314 (2002).

[16] M. Fleischhauer, S. F. Yelin, M. D. Lukin, Opt. Comm. **179**, 395 (2000).

[17] R. Kolesov, M. O. Scully, O. Kocharovskaya, Phys. Rev. A **74**, 053820 (2006).

[18] E. Kuznetsova, O. Kocharovskaya, P. Hemmer, M. Scully, Phys. Rev. A **66**, 063802 (2002).

[19] M. O. Scully, Phys. Rev. Lett. **67**, 1855 (1991).

[20] U. Rathe, M. Fleischhauer, S. Y. Zhu, T. W. Hansch, M. O. Scully, Phys. Rev. A **47**, 4994 (1993).

[21] M. Fleischhauer, C. H. Keitel, M. O. Scully, C. Su, B. T. Ulrich, S. Y. Zhu, Phys. Rev. A **46**, 1468 (1992).

[22] M. D. Lukin, S. F. Yelin, A. S. Zibrov, M. O. Scully, Laser Phys. **9**, 759 (1999).

[23] A. S. Zibrov, M. D. Lukin, L. Hollberg, D. E. Nikonov, M. O. Scully, H. G. Robinson, V. L. Velichansky, Phys. Rev. Lett. **76**, 3935 (1996).

[24] D. D. Yavuz, Phys. Rev. Lett. **95**, 223601 (2005).

[25] L. M. Narducci, G. L. Oppo, M. O. Scully, Optics Communications **75**, 111 (1990).

[26] L. M. Narducci, M. O. Scully, G. L. Oppo, P. Ru, J. R. Tredicce, Phys. Rev. A **42**, 1630 (1990).

[27] A. S. Manka, H. M. Doss, L. M. Narducci, P. Ru, G. L. Oppo, Phys. Rev. A **43**, 3748 (1991).

[28] C. H. Keitel, L. M. Narducci, M. O. Scully, Appl. Phys. B **60**, S153 (1995).

[29] E. Paspalakis, C. H. Keitel, P. L. Knight, Phys. Rev. A **58**, 4868 (1998).

[30] S. Y. Zhu, F. L. Li, Phys. Rev. A. **59**, 2330 (1999).

[31] C. H. Keitel, S. Y. Zhu, P. L. Knight, Laser Phy. **9**, 826 (1999).

[32] P. Zhou, S. Swain, Phys. Rev. Lett. **77**, 3995 (1996).

[33] Z. Ficek, B. J. Dalton, P. L. Knight, Phys. Rev. A **51**, 4062 (1995).

[34] S. Y. Gao, F. L. Li, D. L. Cai, J. Phys. B. **40**, 3893 (2007).

[35] S. Gao, O. Kocharovskaya, J. Mod. Optics **56**, 1941 (2009).

[36] A. Kalachev, O. Kocharovskaya, Phys. Rev. A **83**, 053849 (2011).

[37] H. H. Li, J. of Phys. and Chem. Ref. Data **9**, 561 (1980).

[38] J. W. Precker, M. A. da Silva, American J. Phys. **70**, 1150 (2002).

[39] M. Green, K. Keevers, Progress in Photovoltaics **3**, 189 (1995).

[40] D. K. Sardar, C. C. Russell, J. B. Gruber, T. H. Allik, J. Applied. Phys., **97**, 123501 (2005).

[41] M. E. Innocenzi, R. T. Swimm, M. Bass, R. H. French, M. R. Kokta, J. App. Phys. **68**, 1200 (1990).

[42] Y. Kuwano, K. Suda, N. Ishizawa, T. Yamada, J. Crystal Growth **260**, 159 (2004).

[43] J. H. Burnett, J. of Photopolymer Sci. and Tech. **18**, 655 (2005).

[44] C. O'Brien, P. Anisimov, Y. Rostovtsev, O. Kocharovskaya, submitted to Phys. Rev. A.

[45] C. O'Brien, O. Kocharovskaya, J. Mod. Opt. **56**, 1933 (2009).

[46] N. A. Proite, B. E. Unks, J. T. Green, D. D. Yavuz, Phys. Rev. Lett. **101**, 147401 (2008).

[47] M. E. Crenshaw, C. M. Bowden, M. O. Scully, J. Mod. Opt. **50**, 2551 (2003).

[48] H. Qiong-Yi, W. Tie-Jun, G. Jun-Yue, Chinese Phys., **15**, 1798 (2006).

[49] H. F. Zhang, J. H. Wu, X. M. Su, J. Y. Gao, Phys. Rev. A **66**, 053816 (2002).

[50] C. O'Brien, O. Kocharovskaya, Phys. Rev. Lett. **107**, 137401 (2011).

[51] C. O'Brien, S. Gao, O. Kocharovskaya, J. Mod. Opt., DOI:10.1080/09500340.2011.606626 (2011).

[52] É. K. Sadykov, V. V. Arinin, G. I. Petrov, A. V. Pyataev, F. G. Vagizov, O. Kocharovskaya, Hyperfine Interact **167**, 893 (2006).

[53] É. K. Sadykov, V. V. Arinin, F. G. Vagizov, O. Kocharovskaya, Laser Phys. **17**, 727 (2007).

[54] P. Anisimov, O. Kocharovskaya, J. Mod. Opt., **55**, 3159 (2008).

[55] C. M. Bowden, J. P. Dowling, Phys. Rev. A, **47**, 1247 (1993).

[56] J. D. Jackson, *Classical Electrodynamics,* 3rd ed. (Wiley, New York, 1999), Chap. 4.

[57] J. P. Dowling, C. M. Bowden, Phys. Rev. Lett. **70**, 1421 (1993).

[58] H. Kampen, V. A. Sautenkov, C. J. C. Smeets, E. R. Eliel, J. P. Woerdman, Phys. Rev. A **59**, 271 (1999).

[59] M. Born, E. Wolf, *Principles of Optics*, 6th ed. (Pergamon Press, Oxford, 1991).

[60] M. E. Crenshaw, C. M. Bowden, Phys. Rev. A **53**, 1139 (1996).

[61] E. L. Lewis, Physics Reports **58**, 1 (1980).

[62] M. Gorris-Neveux, P. Monnot, M. Fichet, M. Ducloy, R. Barb`e, J.C. Keller, *Opt. Comm.* **134**, 85 (1997).

[63] J. J. Maki, M. S. Malcuit, J. E. Sipe, R. W. Boyd, Phys. Rev. Lett. **67**, 972 (1991).

[64] J. E. Thomas, W. W. Quivers, Phys. Rev. A **22**, 2115 (1980).

[65] M. Shuker, O. Firstenberg, Y. Sagi, A. Ben-kish, N. Davidson, A. Ron, Phys. Rev. A **78**, 063818 (2008).

[66] M. D. Rotondaro, G. P. Perram, J. Quant. Spectrosc. Radiat. Transfer **57**, 497 (1997).

[67] I. Novikova, A. V. Gorshkov, D. F. Phillips, Y. Xiao, M. Klein, R. L. Walsworth, Proc. of SPIE **6482**, 64820M (2007).

[68] S. Kück, P. Jander, Optic. Matt. **13**, 299 (1999).

[69] S. Kück, S. Hartung, Chem. Phys. **240**, 387 (1999).

[70] N. V. Kuleshov, V. G. Shcherbitsky, V. P. Mikhailov, S. K*ü*ck, J. Koetke, K. Petermann, G. Huber, J. Lumin. **71**, 265 (1997).

[71] S. Kück, L. Fornasiero, E. Mix, G. Huber, Appl. Phys. B **67**, 151 (1998).

[72] D. S. Hamilton, S. K. Gayen, G. J. Pogatshnik, R. D. Ghen, Phys. Rev. B **39**, 8807 (1989).

[73] Y. M. Cheung, S. K. Gayen, Phys. Rev. B **49**, 14827 (1994).

[74] S. Nicolas, et. al. Opt. Mat. **22**, 139 (2003).

[75] N. I. Agladze, M. N. Popova, G. N. Zhizhin, V. S. Egorov, M. A. Petrova, Phys. Rev. Lett. **66**, 447 (1991).

[76] A. K. Rebane, C. W. Thiel, R. K. Mohan, R. L. Cone, Bull. Russ. Acad. of Sci. Phys. **74**, 891 (2010).

[77] J. B. Gruber, J. R. Quagliano, M. F. Reid, F. S. Richardson, M. E. Hills, M. D. Seltzer, S.B. Stevens, C.A. Morrison, T.H. Allik, Phys. Rev. B **48**, 15561 (1993).

[78] G. W. Burdick, C. K. Jayasankar, F. S. Richardson, M. F. Reid, Phys. Rev. B **50**, 16309 (1994).

[79] K. Heyde, K. Binnemans, C. Görller-Walrand, J. Chem. Soc. Faraday Trans. **94**, 843 (1998).

[80] E. Kuznetsova, O. Kocharovskaya, P. Hemmer, M. O. Scully, Phys. Rev. A **66**, 063802 (2002).

[81] S. Y. Gao, O. Kocharovskaya, J. Mod. Optics **56**, 1941 (2009).

[82] M. Lax, Phys. Rev. **129**, 2342 (1963).

[83] D. Z. Wang, J. Y. Gao, Phys. Lett. A **228**, 25 (1997).

[84] J. Cooper, R. J. Ballagh, K. Burnett, Phys. Rev. A. **22**, 535 (1980).

[85] P. D. Kleiber, K. Burnett, J. Cooper, Phys. Lett. **84A**, 182 (1981).

VITA

Christopher Michael O'Brien

Doctorate of Philosophy, Physics (Dec. 2011)

Texas A&M University, College Station

Advisor: Dr. Olga Kocharovskaya,

Thesis: Coherent Control of Optical Processes in a Resonant Medium

Bachelor of Science, Physics and Mathematics (May 2006)

Texas A&M University, College Station

Email

cobrien.physics@gmail.com

Contact

Chris O'Brien

27 Applewood Dr.

Cabot, AR 72023